chemical analysis in this test because the cell was the instrumented one. The test was continued for a total period of 1,298 h. At the end of processing, the soil was divided into three layers for analysis; top, middle, and bottom. Each layer was divided into longitudinal and transverse sections, as described in Section 5.11, and analyzed.

The second pilot-scale test (PST2) was conducted on kaolinite loaded with lead at a concentration of 1,533 µg/g and at a pH of 4.5. The processing time for this test is 2,952h. At the end of processing, the soil was divided into horizontal layers at five depths for analysis. Each layer was then divided into 1ongitudinaI and transverse sections and analyzed for final lead concentration and pH (Figure 5.8). The first set of soil samples was taken for chemical analysis after one month of processing. These samples displayed significant amounts of lead transport across the specimen. Since one objective of the study was to compare the transport in the pilot-scale test with predictons of the theoretical model, it was found necessary to conduct a third pilot-scale test (PST3) with more frequent sampling within the first month. A kaolinite/sand mixture was used in this third test instead of only Kaolinite. This change was made in order to minimize the volume change expected during processing. Excessive volume changes lead to development of cracks and disfunctioning of the tensiometers. PST3 was used for comparison of the predictions of the theoretical model with thc results of the experiment. The specific results of this test also support accomplishment of the primary project objectives; however, these results associated with PST3 are documented in the next Section and Appendix D since this test was specifically used to assess and evaluate the theoretical model.

6.2 Catholyte and Anolyte pH

It is essential to measure and predict the pH changes across the soil since pH is a master variable in chemical equilibria and dissolution/precipitation, aqueous phase and sorption reactions in the pore fluid. Zeta potential of the clay and electroosmotic coefficient of permeability across the soil may be affected by the changes in pH (Daniel and Eykholt 1994) while the fabric of the soil and engineering characteristics such as hydraulic conductivity also will be influenced by pH (MitchelI 1993). Since variations in pH imply changes in concentration of H+ ions, pH is also a strong indicator of the electrical conductivity which affects electrical conductance and species transport in the soil pore fluid under electrical fields.

In all cases, it was essential to scrutinize the changes in the pH of the catholyte, anolyte, and the soil. Changes in the anolyte and catholyte pH values in time are displayed in Figure 6.1 for BSTl and BST2, Figure 6.2 for PST1 and PST2. Similar trends were noted. Electrolysis reactions at the electrodes were expected to cause oxidization of the anolyte, decreasing its pH, and reduction in the catholyte, increasing its pH. The results of all bench-scale and pilot scale tests demonstrate an initial increase in the pH to about 10-11 and a decrease in the anolyte pH to less than 2. .

The H+ concentration in the catholyte of Cell B was almost a reflection of that in Cell A which displayed repeatability. Electrolysis reactions at the electrodes caused oxidation at the anode which decreased the pH in the anolyte to less than 2 and reduction at the cathode which increased the pH in the catholyte to about 11.0-11.5. Most of the changes in the catholyte and the anolyte pH were realized within the first 100-200 hours of processing. The magnitude of the pH and its rate was predicted through Faraday's Law of equivalence of mass and charge (Acar et al. 1980; Acar et al. 1990). If it is assumed that all charge is used in generation of the hydrogen and the hydroxyl ion under steady state conditions and neglecting all other chemical reactions, one Faraday of charge (96,500 As) will generate one mole of H+ at the anode and 1 mole of OH- at the cathode (Acar et al. 1989; Acar et al. 1990). The current of 0.85 A across each cell in PST2 will produce 32 x IO-2 moles of OH- every hour in the two cathode compartments. In the anode compartment, the H+ production will be twice that amount or 6.4 x 10^{-2} moles/h owing to having one anode and two cathode compartments. Considering a 70-2L volume of liquid in each compartment, the rates of increase in OH- and H+ concentrations will be approximately equal to 4.6 x 10^{-4} mole/Lh and 9.1 x 10^{-4} mole/Lh, respectively. The H+ concentration estimated using this rate of increase agreed with each ather only within the first 50 h . Subsequently, the H+ concentration at the anode and the OH- concentration at the cathode fell short of the values predicted only by the electrolysis reactions. The differences were due to 1) prevailing secondary electrolysis, 2) transport of hydrogen and hydroxyl ions across the specimen towards respective counter electrodes and the aqueous phase reactions associated with their transport (Alshawabkeh and Acar 1996), and 3) the dilution of the species to a larger volume due to transport

One factor that may have affected changes in the catholyte and anolyte pH includes the water auto-ionization reaction and electrodeposition reactions. Some of the H- and OH- generated by electrolysis reactions at the electrodes reacted to produce water in the soil pores, in accordance

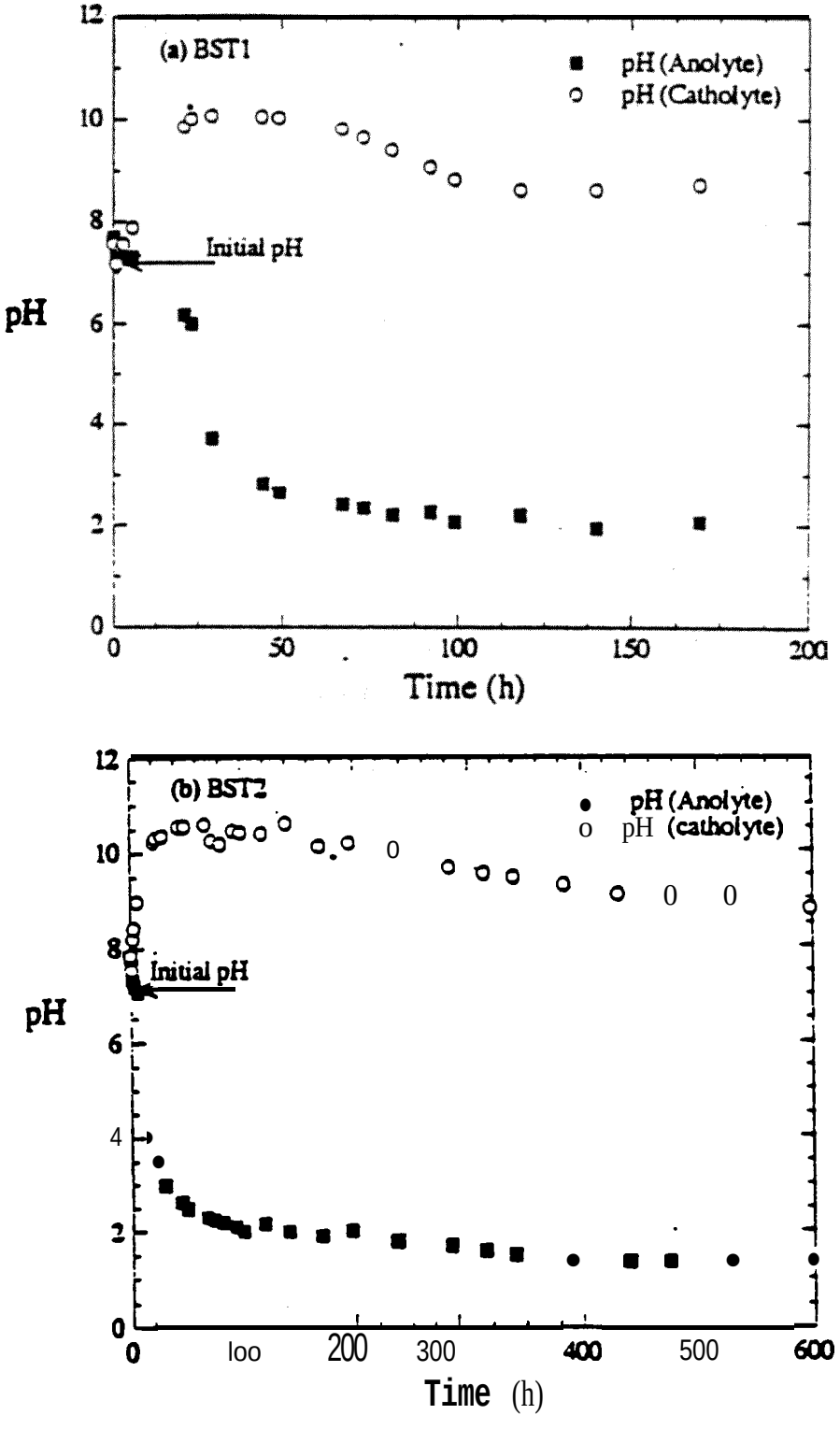

Figure 6.1: Catholyte **and Anolyte** pH Changes with Time in (a) BSTl and (b) BST2

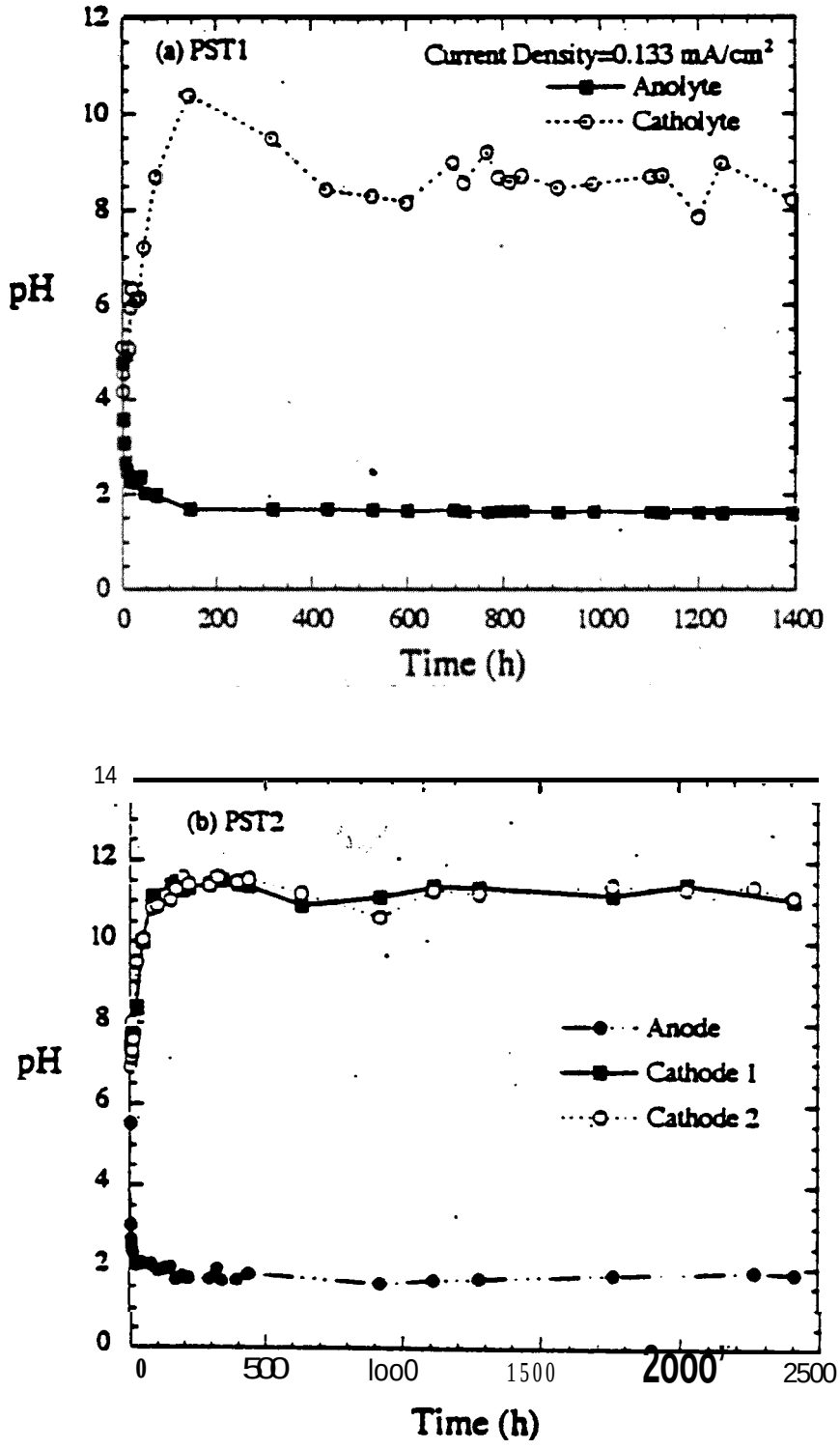

Figure 6.2: Catholyte and Anolyte pH Changes with Time in (a) PST1 and (b) PST2

with the mass equilibrium of the water auto-ionization reaction ($c_H c_{OH} = K_w$). Increase of the concentration of lead in the cathode compartment, as a result of transport processes, caused the following competitive electrodeposition reaction

$$Pb^{2+} + 2e^- \rightarrow Pb(s) \qquad E^0 = 0.126 \qquad (6.1)$$

The results of BST2 displayed that around 44% of initial lead is found precipitated and/or electodeposited on the cathode, while in PST2 less than 1% is found on the cathode (the results of final lead distributions are presented in Section 6.6). The main procedural difference between the two tests was the placement of the cathode. The electrodeposition reaction must have affected the catholyte pH in bench-scale tests when the electrodes were held in contact with the soil specimen. This effect may have been the cause of the gradual decrease in catholyte pH in BSTl and BST2 after 100 h of processing. The final catholyte pH recorded in these tests was around 9. On the other hand, concentrations of Pb^{2+} in the catholyte in pilot-scale tests Were not high enough to stimulate any electrodeposition of lead on the electrodes. Therefore, for unenhanced applications the water auto-ionization reaction and/or lead electrodeposition reaction may have affected the efficiencies of electrolysis reactions when the pH of the effluent increased to around 11. When the pH of the catholyte remained within 7 to 11, **then the** electrolysis reaction were expected to be mainly water reduction.

6 . 3 Soil pH

Distributions of pH across the soil at the end of processing BSTI and BST2 illustrated the advance of the acid front developed at the anode towards the cathode (Figure 6.3). The anode region showed a soil pH of less than 2 while the cathode region showed a final pH of 4 to 5, which was in the range of the initial soil pH (the terms anode and cathode regions are used in the manuscript to represent the region between the electrodes and midsection of the soil specimen).

The final pH distributions across the pilot-scale soil specimens are shown in Figure 6.4 for the middle layer in PST1, Figures 6.5 and 6.6 for Cell A and Cell B of the middle layer in PST2 (layer 3). Data for final pH distributions in all bench-scale tests and pilot-scale tests are presented in Appendix D. One-dimensional pH profiles across the soil specimen were similar and they did not display significant changes with depth. The results also displayed that the pH within the anode

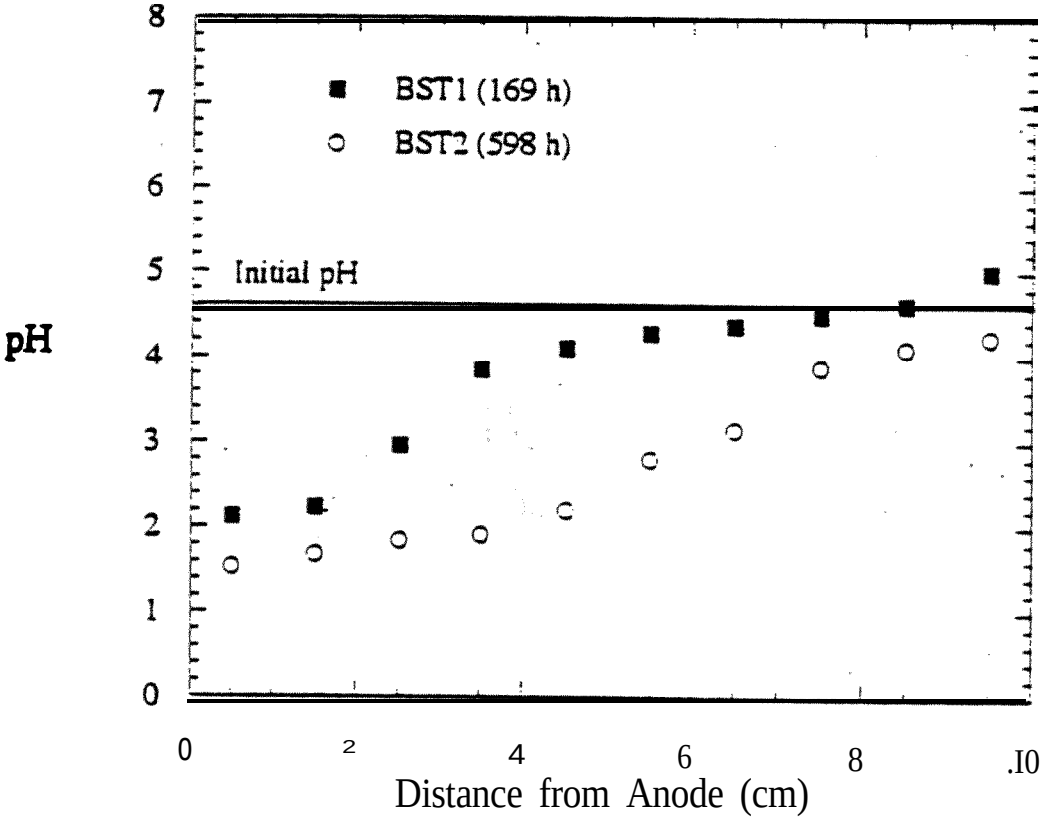

Figure 6.3 Final pH Distributions across Bench-Scale Specimens at a Current Density of 127 $\mu A/cm^2$

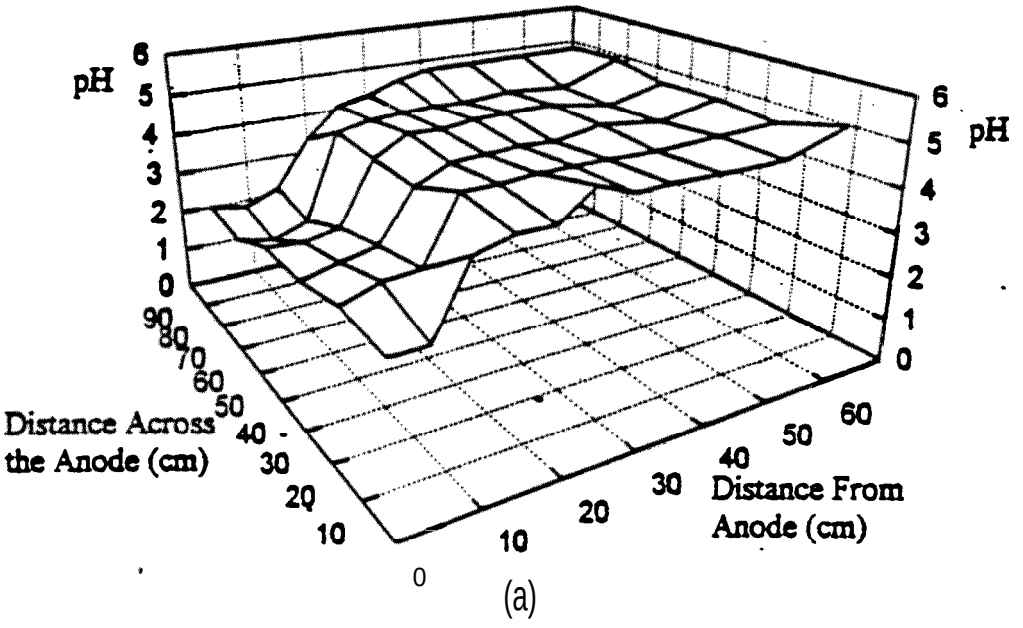

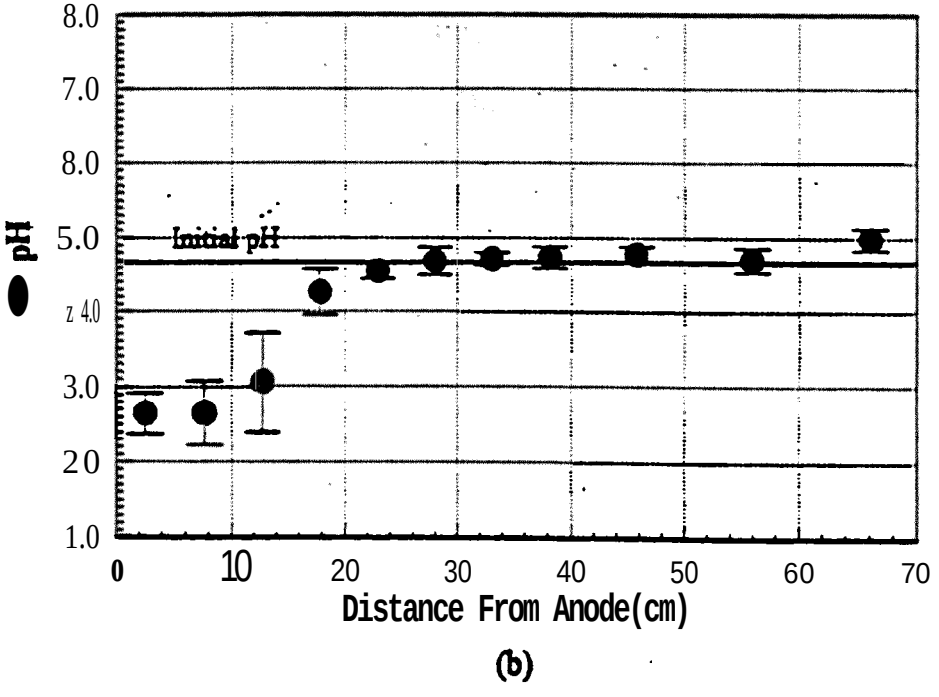

Figure 6.4: Final pH Distribution across the Middle Layer of PST1 (a) 3-D Contour Diagram and (b) Mean and Standard Deviation

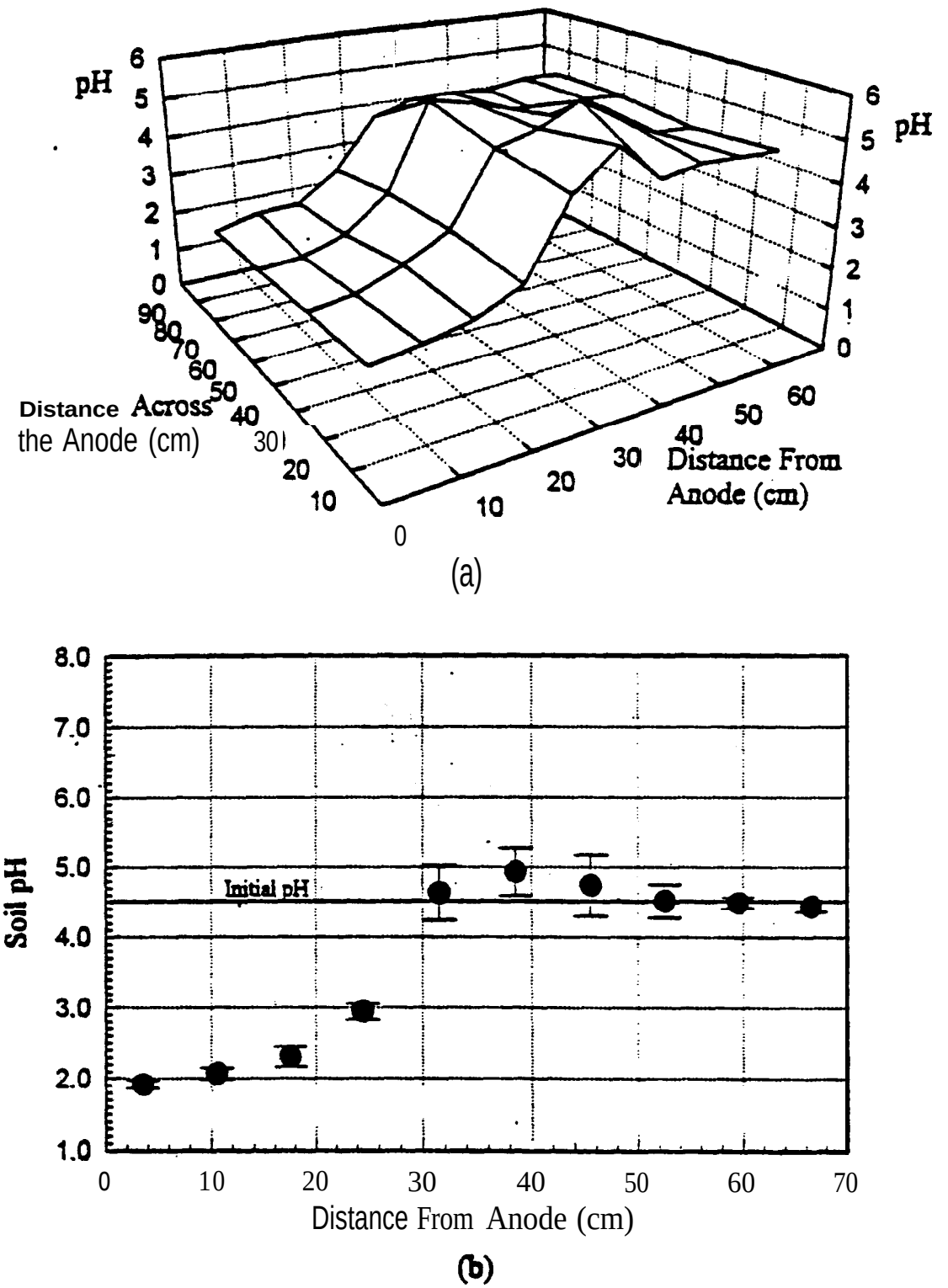

Figure 6.5 Final pH Distributions across Cell A in the Middle Layer (Layer 3) of PST2 (a) 3-D Contour Diagram and (b) Mean and Standard Deviation

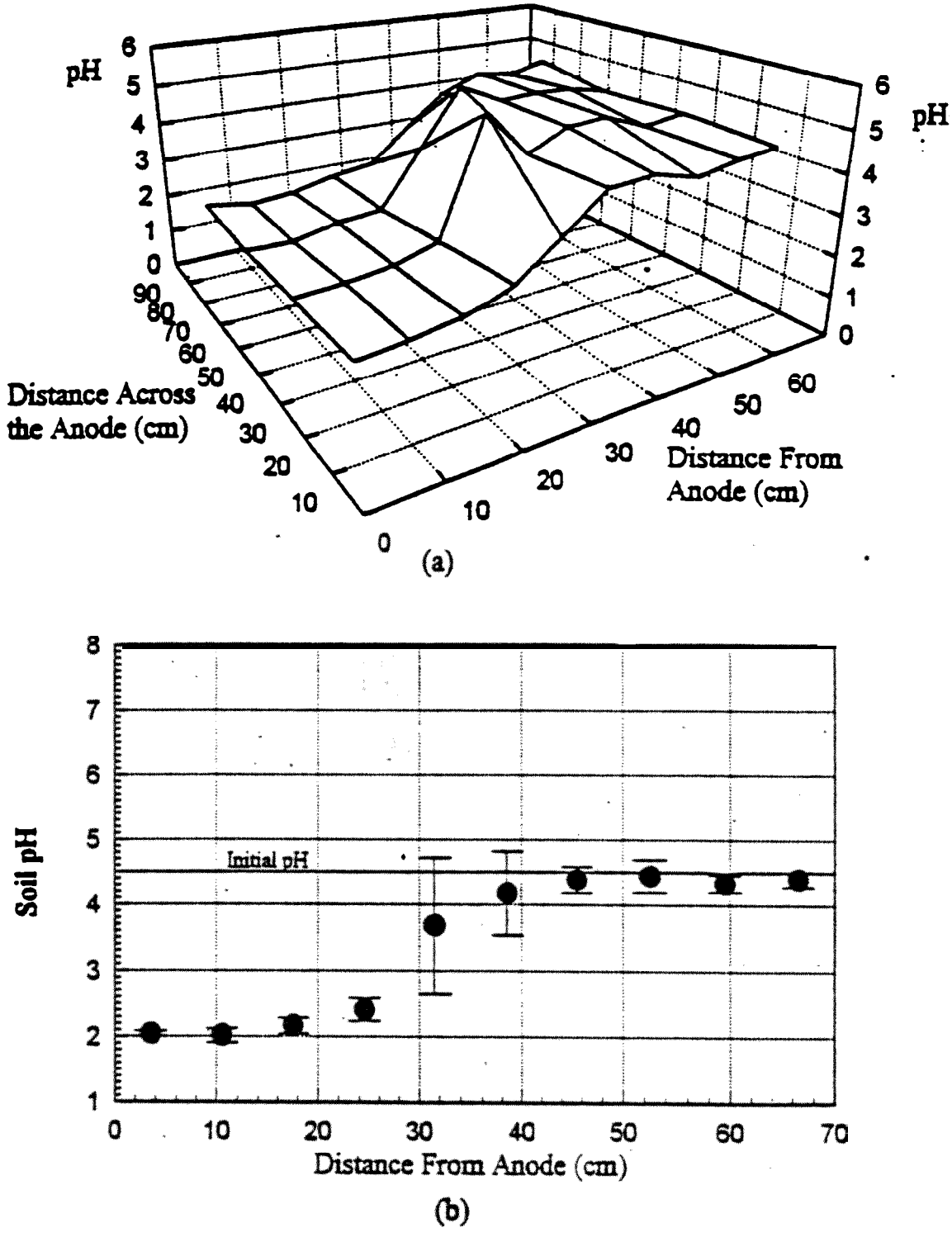

Figure 6.6: Final pH Distributions across Cell B in the Middle Layer (Layer 3) of PST2 (a) 3-D Contour Diagram and (b) Mean and Standard Deviation

region decreased to about 2.5 in PST1 and to 1.5 in PST2, while the cathode region the pH stayed within the initial value in both tests (4.7 in PSTI and 4.5 in PST2). Slight differences at the anode region between the two tests could be related to the differences in processing (2950 h for PST2 and 1298 h for PSTI). Mean and standard deviation of pH distributions across the two cells in PST2 are displayed in Figure 6.7. The acid front was depicted at a distance of 30 to 35 cm from the anode in PST2 after 2950 h. For PSTl, the acid front was at a distance of 16 to 18 cm from the anode after 1298 h.

The rate of advance of H+ towards the cathode was evaluated using measured pH changes across the specimen with time. The results from PST3 were used for this purpose. pH changes in time in PST3 were plotted for certain points along the specimen (5 cm, 15 cm, and 25 cm from the anode). The time required to reach a specific pH value in these points was recorded as shown in Figure 6.8a. A pH value of 3 was taken as the reference value because it is equal to 50% of the chage in the anode pH. The two points selected in the soil were at distance of 5 cm and 15 cm from the anode. The time required for these points to reach a pH of 3 was 5 days for the first point and 15-16 days for the second point (Figure 6.8a). Figure 6.8b shows the relation between the distance from the anode and the time required to reach a pH of 3. The slope of the line was approximately 1.0 cm/d and WaS a good estimate for the rate of advance of the acid front in this test. The molecular ionic mobility of H+ at infinite dilution was 313 cm^2/Vd (Table 3.3). When an **average** tortuosity of 0.45 and **a** porosity of 0.56 were used, the theoretical value of effective ionic mobility was 79 cm^2/Vd. Considering an average voltage gradient of 0.1 V/cm recorded in the anode section of the cell, the rate of advance of the acid front was 8.0 cm/d (if there was no retardation due to sorption, autoionization, and/or aqueous phase reactions). It was noted that the calculated rate of transport under ionic migration over estimates the measured value. Differences between the calculated and measured rates of transport of H+ are discussed further in Section 7.3.

6.4 Electric Potential

Figure 6.9 shows the changes in the total voltage across BSTI and BST2. The total voltage applied across the first specimen increased with time to about 40 V (electric gradient of 4.0 V/cm) after 169 h of processing. In the second specimen, the voltage increased to about 50 V (5.0 V/cm) in the first 150 h and remained within that range. The total voltage applied across the soil specimen

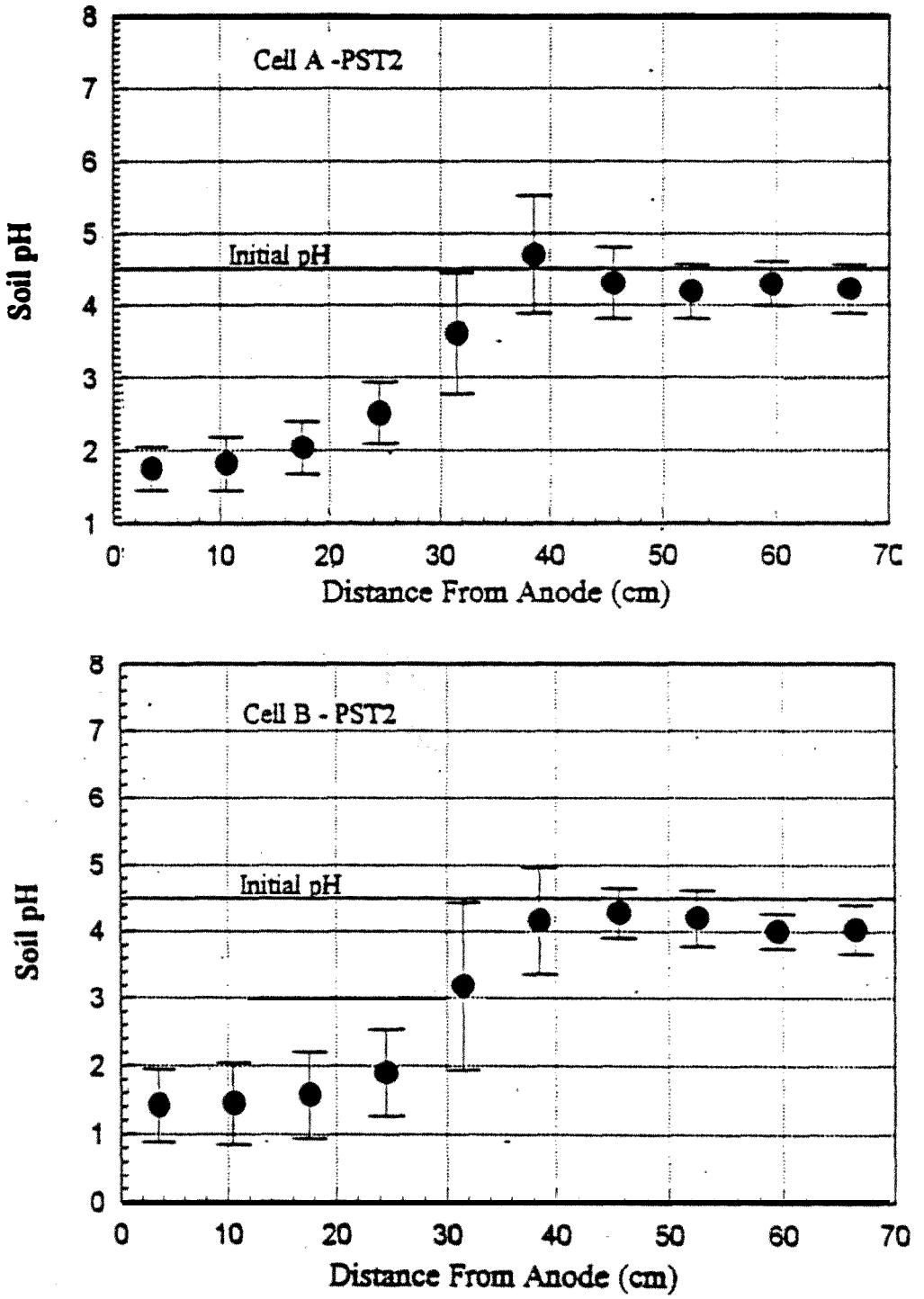

Figure 6.7: Mean and Standard Deviation of Final pH Distribution across all Layers of PST2 (a) Cell A and (b) Cell B

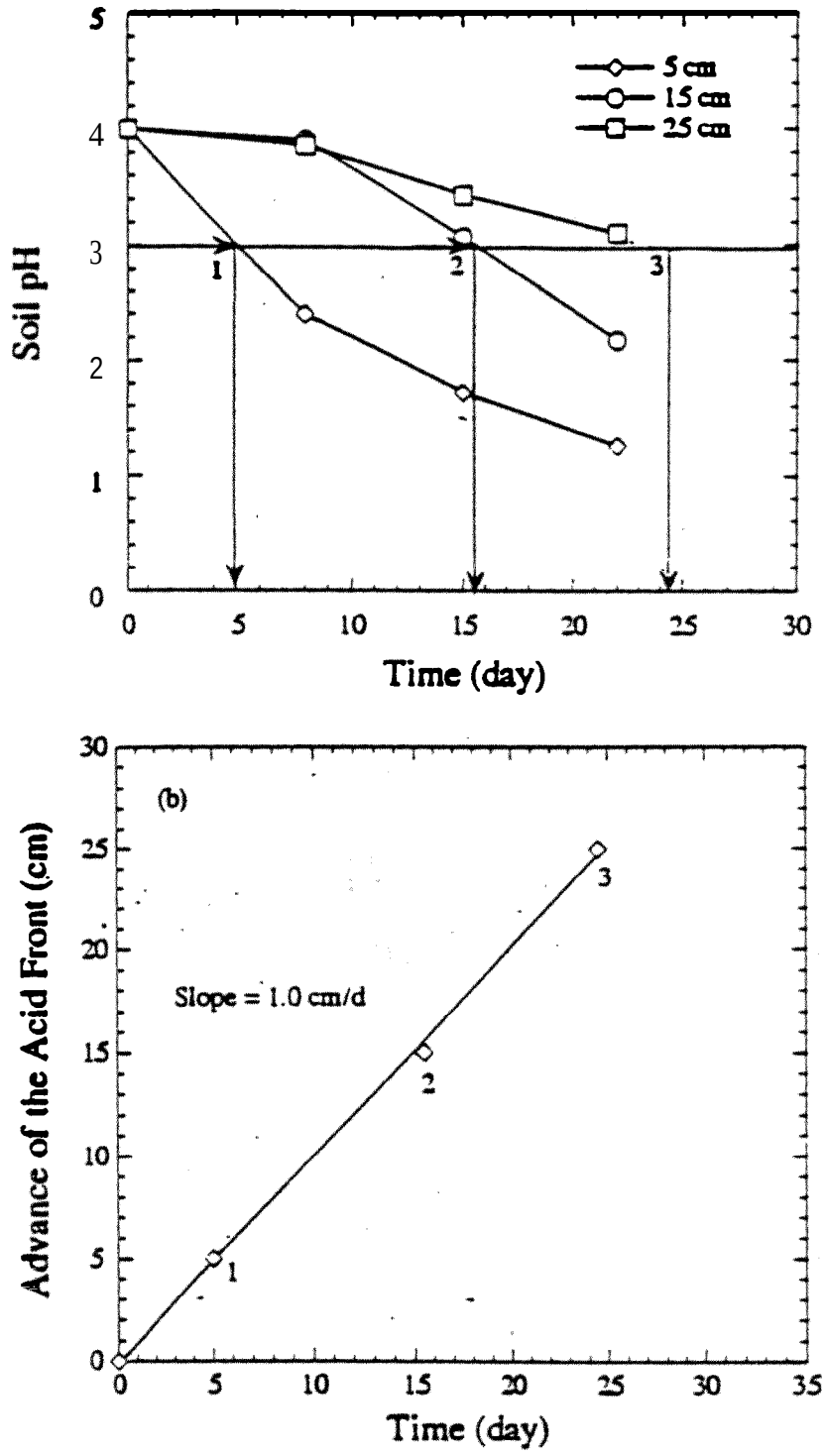

Figure 6.8: Prediction of Rate of Advance of the Acid Front (a) Time Changes in pH at Distance of 5, 15, and 25 cm from the Anode, and (b) Rate of Advance of the Acid Front

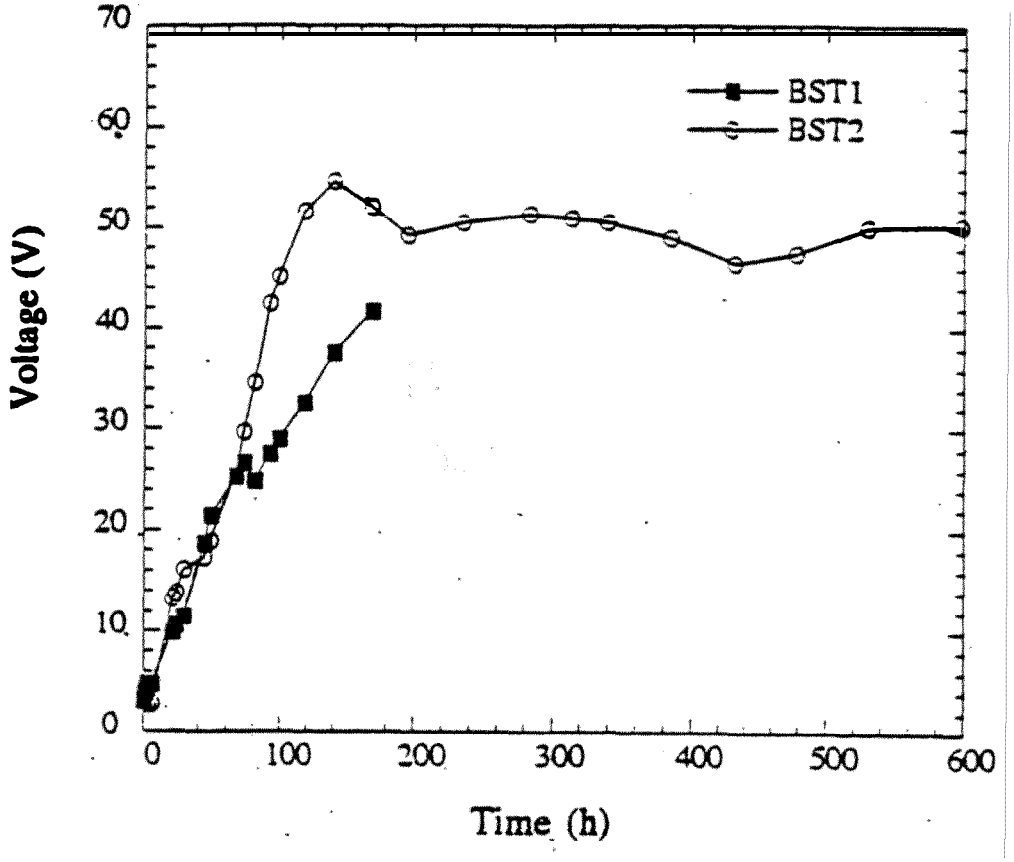

Figure 6.9: Changes in the Total Applied Voltage in (a) BSTI and (b) BST2

in PST1 increased linearly with time to about 180 volts in the first 900 hand then to around 200 volts at the end of the test resulting in a final voltage gradient of 2.9 V/cm (Figure 6.10). The total voltage applied across each cell in PST2 demonstrated changes similar to those of BST2 and **PST1 .** The total applied voltage increased linearly in the first 900 h to about 150 volts (2.1 V/cm) and remained steady around that value. Total voltage in PST3 showed slight differences when compared with PST1 and PST2 For the first 300 h of processing, PST3 did not show an increase in the total voltage. Subsequent to this "induction" period, the voltage increased to about 170V after 1000h and thcn increased slightly to about 200V . Differences in the 300h in PST3 may have been related to differences in the initial pore fluid chemistry.

The total voltage applied across each specimen depended upon the chemistry developed across the medium, since the electric conductivity of the soil was a function of the ionic strength of the soil pore fluid. Generally, the soil pore fluid was composed of a multicomponent solution of different species such as lead, hydrogen, calcium, sodium, nitrate, chloride, and hydroxyl ions. High initial concentrations of these ions resulted in a high ionic strength and a high pore fluid electric conductivity. Initially the soil specimens in both bench-scale and pilot-scale tests had a uniform distribution of the electric conductivity, as there is a uniform distribution of charged species, PH, and ionic strength. However, multispecies transport under the applied electrical gradient redefined the, electric conductivity distribution across the soil. Electric conductivity changed significantly from one position to another depending upon the pH and ionic strength. Therefore, the term "apparent" conductivity, κ_a was used instead of the effective electric conoductivity (Acar et al. 1994). κ_a gave an equivalent conductivity value for the medium across the electrodes that disregarded the discrete changes in conductivity across the soil. In other words, the soil across the electrodes was assumed to behave as a series of resistors and the apparent conductivity represented an equivaient value for all the resistors. The apparent electric conductivity of each sample was evaluated by,

$$\kappa_a = \frac{I_t}{EA} L \quad \frac{I_a}{i_e} \tag{6.2}$$

where E was the voltage applied (V), I_t was the total dectric current (A), L was the specimen length (cm), A is the cross-sectional area of the specimen (cm^2), I_a was the electric current density A/cm^2, i_e was the electric gradient V/cm, and κ_a is the apparent conductivity of the soil in S/cm.

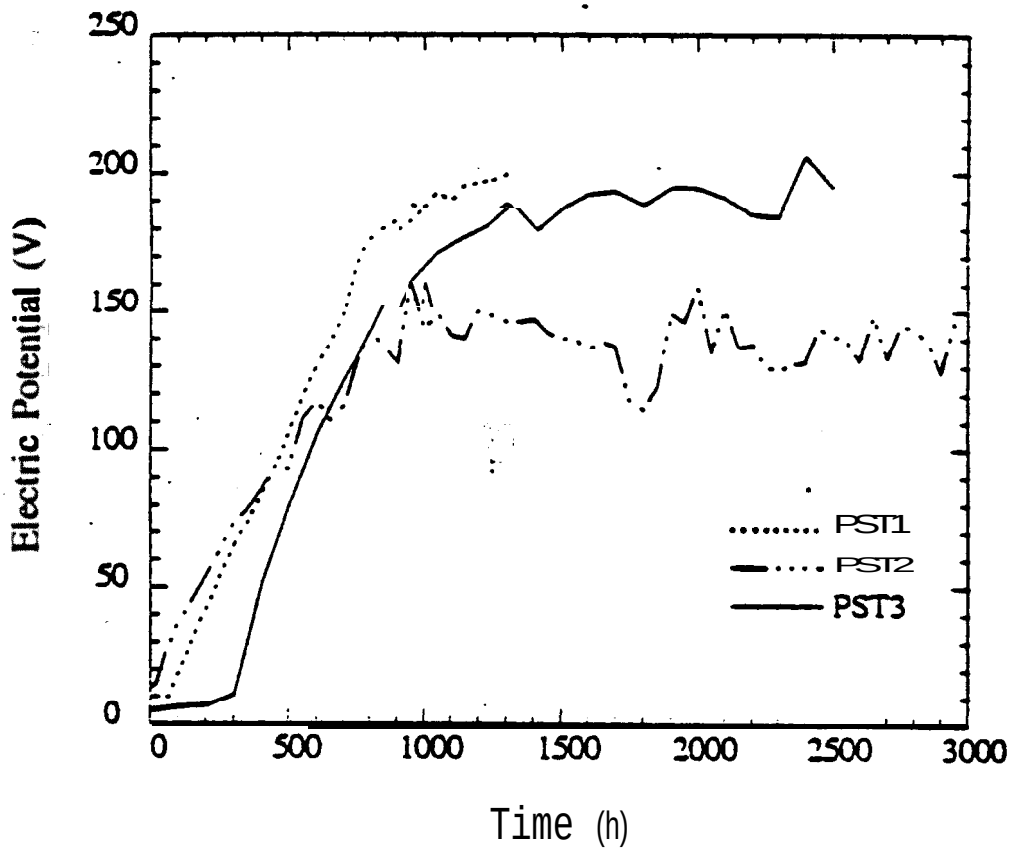

Figure 6.10: Time Changes in the Total Applied Electric Voltage in PST1, PST2, and PST3

Pilot-scale tests showed that the specimens were relatively conductive (greater than 1,000 uS/cm, which is about the maximum conductivity of potable water). Figure 6.11 displays that the apparent conductivity in bench-scale and pilot-scale specimens decreased with time until they reached a constant value (or steady state condition). Similar findings were reported by Hamed et al. (1991). The decrease in apparent electric conductivity occurred in the first 100 h of processing bench-scale tests and within the first 800 h to 1000 h of processing pilot-scale tests. It was noted that the apparent electric conductivity of PST3 was higher than those of PST1 and PST2 in the first 500 h, and decreased sharply after that time. The higher electric conductivity in the first 500 h was the reason for the delayed increase in the total voltage applied across PST3 (Figure 6.10). The high initial lead concentration in the soil pore fluid rendered high ionic strength and electric conductivity. The results displayed that changes in species concentration within the first 500 h of processing PST3 did not have a significant decrease in the electric conductivity of the pore fluid. However, the sharp decrease after this stage may have been directly related to the precipitation of lead at its hydroxide solubility limit or due to the effect of the high pH environment developed near the cathode.

The steady state values of the apparent electric conductivity were around 30 μS/cm in bench-scale tests and around 50-70 μS/cm in pilot-scale tests. Though these values were higher in the pilot-scale tests than the bench-scale tests, they all fell within the same range, which was about the electric conductivity of a good city water.

As the electric current passing through a unit area was constant in time and space, the change in the electric conductivity of the medium was accompanied by the change in the electric gradient in order to maintain a constant current density. Accordingly, the total applied voltage increased with time until it reached a steady state value. At this time, the chemistry across the soil became independent of time. Figure 6.10 displays that most of the voltage increase occurred in the first 1000 hours of processing of pilot-scale tests, with an increase of up to about 190 V in the first test, 150 V in the second and 200 V in the third test. The rate of increase of the total voltage in these tests was almost constant and is within the range of 0.15 to 0.2 V/h. This suggests that the change in total ionic concentration of the soil specimen was constant with time and implied that the rate of depletion of the ionic species from the total soil mass due to transport and removal or due to precipitation or sorption reactions must be constant in time.

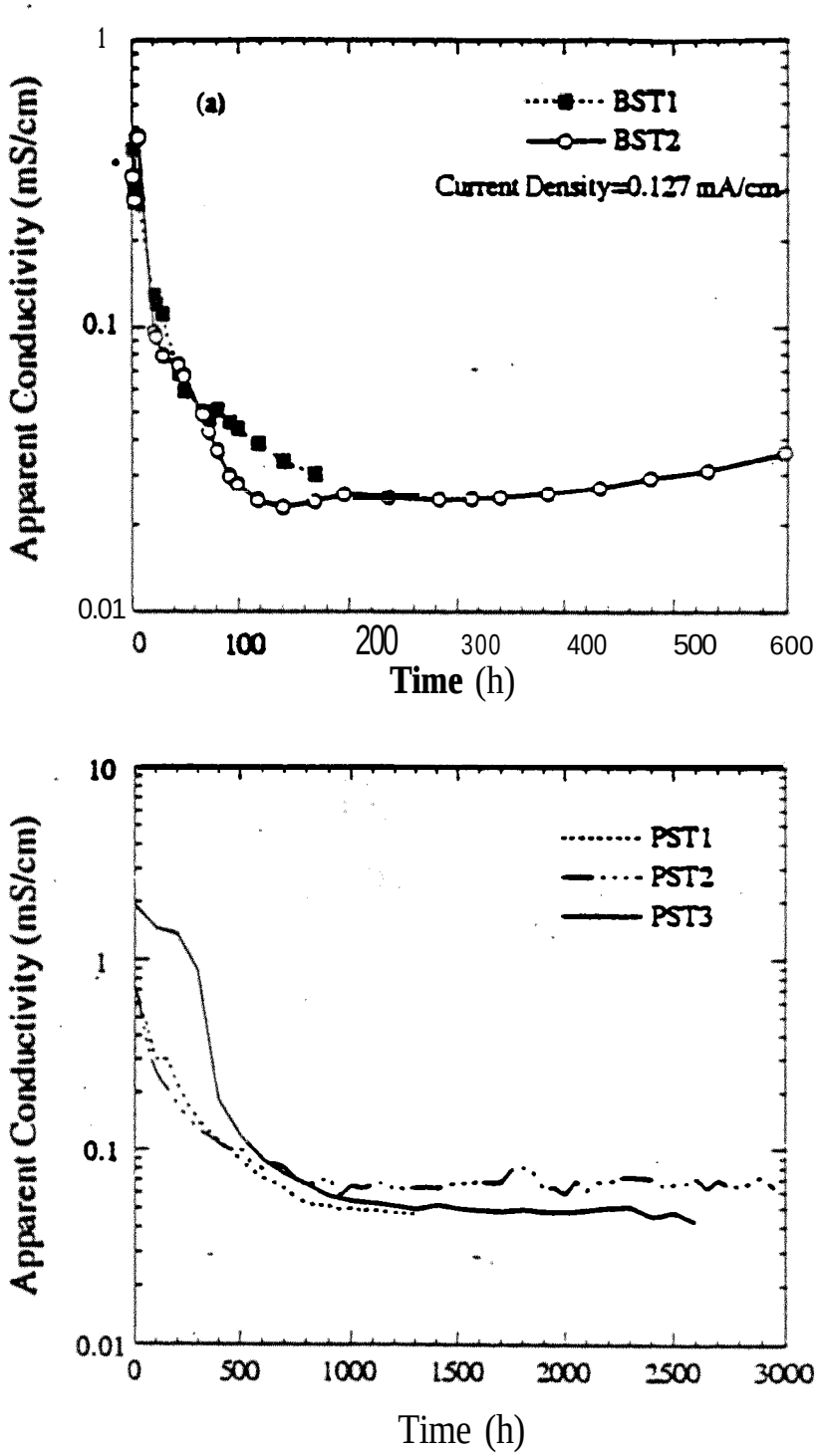

Figure 6.11: Apparent Eletric Conductivities of (a) Bench-Scale Specimens and (b) Pilot-Scale Specimens

Electric conductivity of the soil in bench-scale and pilot-scale tests decreased in time until it reached a steady state value (Figure 6.11). This finding could not be generalized for all types of pore fluid chemistry and soil type. In soil specimens prepared for this study, lead nitrate salt was initially dissolved in a low pH solution (HNO_3 acidified) and then mixed with the clay. For this case, almost all the lead and the other species were present in ionic form in the soil pore fluid and were ready to be transported under electrical gradients resulting in relatively high initial electric conductivities. In naturally contaminated samples, significant amounts of contaminants were expected to be present as salt pracipitates in the soil. In a study of in-situ remediation of heavy metals by electrokinetics, Lageman (1993) reported that some sites with high initial salt concentrations showed an increase in theelectric conductivity after application of the electric fields. When the chemical species were present in the form of salts and the ionic conductivity of the pore fluid was low, the resistance to charge flux was high leading to high voltage gradients. Transport of the acid generated at the anode across the specimen resulted in dissolution of the salts, increased the ionic conductivity in the pore fluid, and decreased the voltage gradient. However, if the process was continued unenhanced until the species in the pore fluid were removed from the soil, the ionic conductivity would again decrease pushing the voltage gradient up again. If enhancement techniques were used, then introduction of chemicals at the cathode or anode compartments would have resulted in species transport into the soil, affecting the electric conductivity of the pore fluid.

6.5 EIectric Potential Distribution

The electrical potential profiles across the specimens are displayed in Figure 6.12 for BSTI and BSl2, Figure 6.13 for PST1 and PST2. All tests demonstrated similar behavior in voltage profiles. First, a relatively linear distribution was developed due to the uniform distribution of charged species across the specimen. In time, the profile became nonlinear. Most of the voltage drop was observed to develop in the soil near the cathode, that implicated development of a zone of high electric resistivity. On the other hand only a small decrease in the voltage was realized within the anode region. Most of the change in the electric potential distributions was observed to occur within the first 100 h of processing in bench-scale specimens and within the first 1000 h of processing in pilot-scale specimens. The electrical potential distribution seemed to reach a steady state condition after this amount of processing.

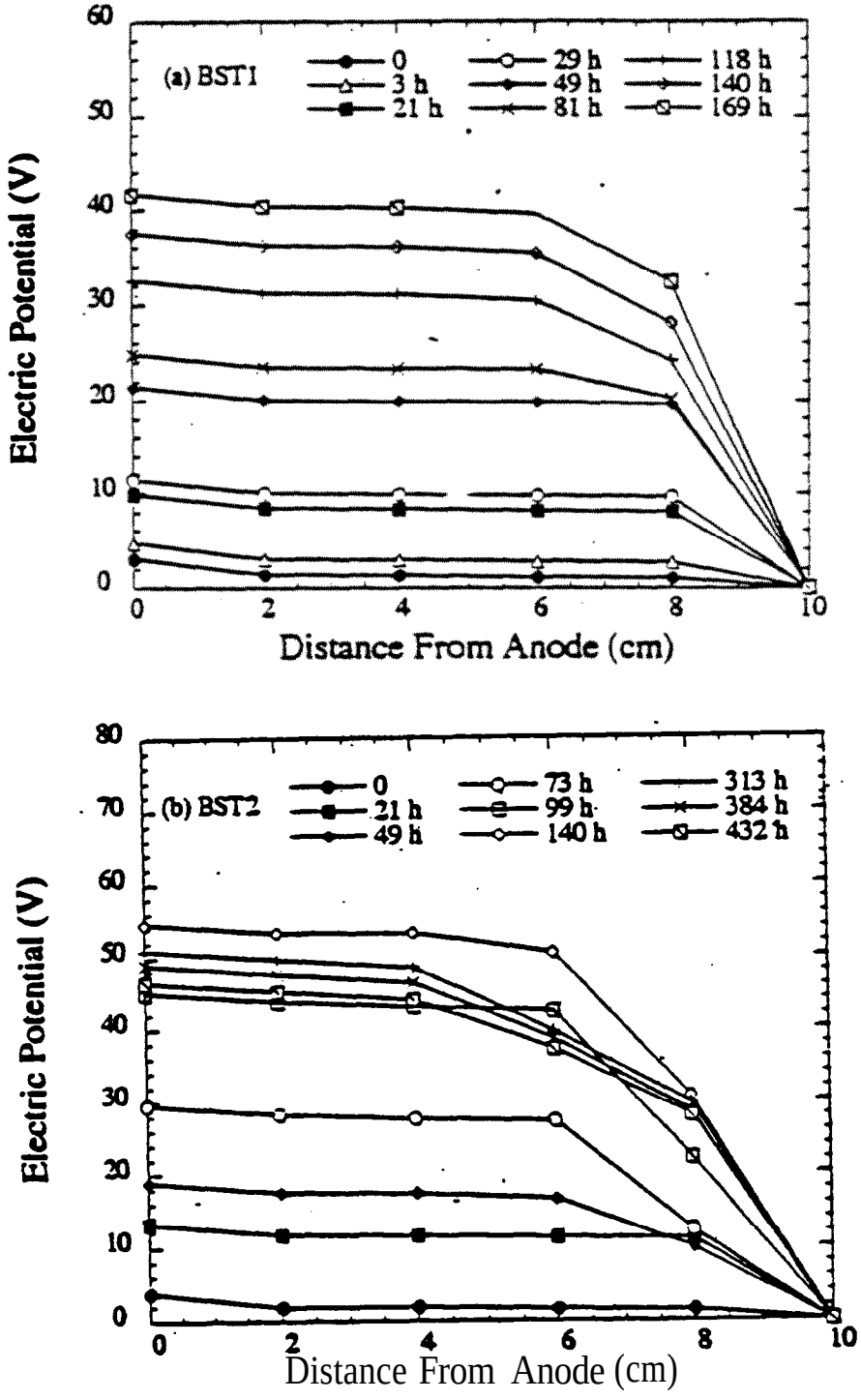

Figure 6.12: Electric Potential Distribution Across (a) BST1 and (b) BST2 (Current Density, I_r= 127 $\mu A/cm^2$)

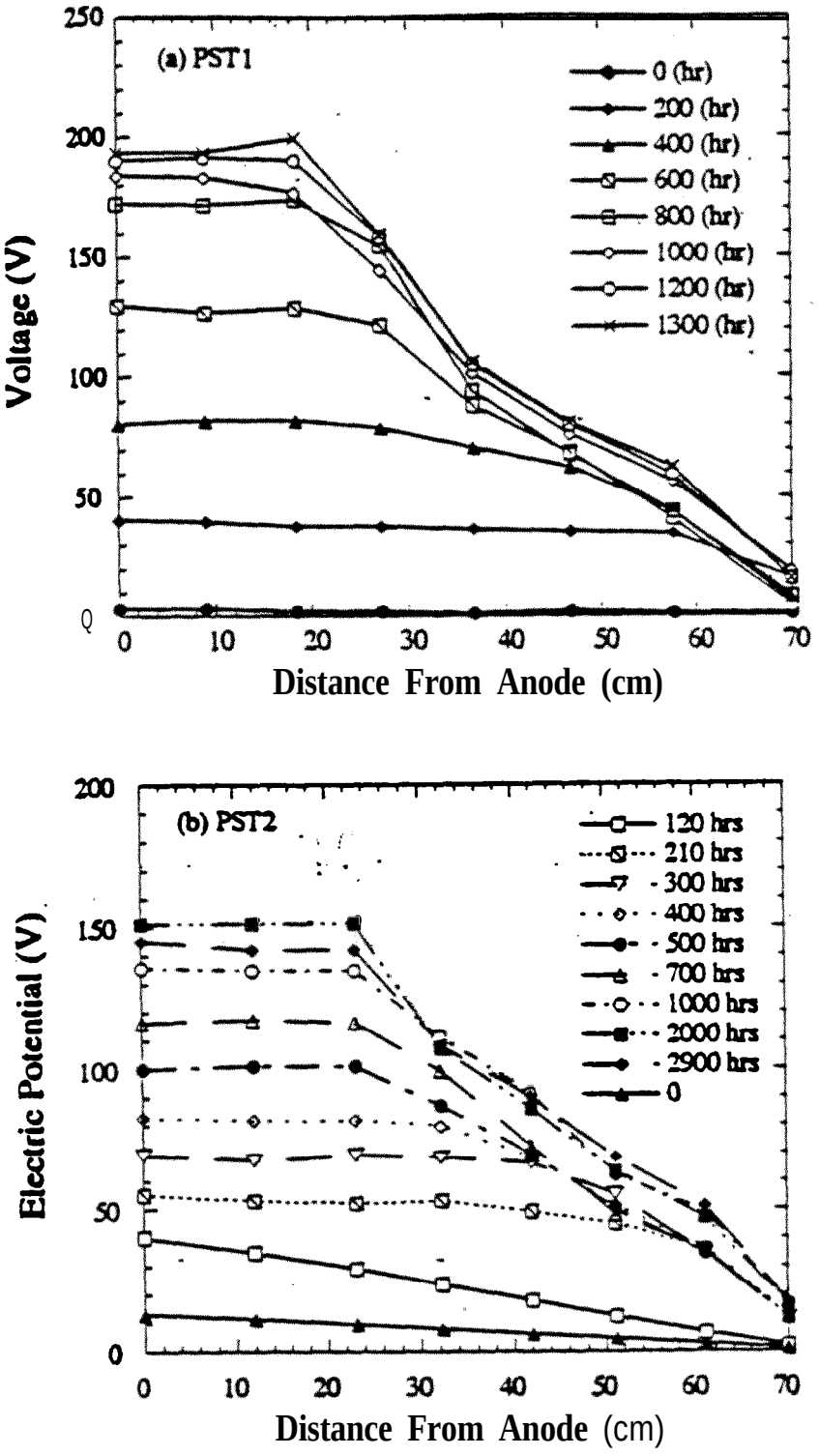

Figure 6.13: Electric Potential Distribution Across the Soil Specimen (a) PST1 and (b) PST2 (I_r= 133 $\mu A/cm^2$)

Changes in the electric conductivity **across** the soil and the corresponding variations in electric voltage distribution were related directly to the electrochemical changes in the soil pore fluid; mainly the ionic strength and pH. The effect of pH on the electric conductivity was quite significant in eletrokinetic soil remediation. The effect of soil pH on the conductivity was evaluated by considering the contribution of only H+ and OH- concentrations on the conductance of the soil medium. The contribution of all other ions was assumed to be negligible. The initial pH of the kaolinite mixture was less than 5 in most cases which indicated that most of the current was carried by the H+ ions. The effective electric conductivity of the soil in this case was then evaluated by,

$$\sigma^* = \frac{F^2}{RT}\left(D^*_H c_H + D^*_{OH} c_{OH}\right) \qquad (6.3)$$

At infinite dilution the value of D^*_{OH} was 0.57 times D^*_H (Tables 3.3 and 3.4),

$$\sigma^* = \frac{F^2 D^*_H}{RT}\left(c_H + 0.57\, c_{OH}\right) \qquad (6.4)$$

Assuming that the initial soil pH was 5 then the initial effective electric conductivity would be,

$$\sigma^* = \frac{F^2 D^*_H}{RT}\left(10^{-5} + 0.57 \bullet 10^{-9}\right) = \frac{F^2 D^*_H}{RT} 10^{-5} \qquad (6.5)$$

For kaolinite with a tortuosity factor of 0.45 and porosity of 0.56, Equation 6.5 rendered an initial electric conductivity of about 1 mS/cm (neglecting presence of other species). The contribution of OH- was neglected because the contribution of H+ on the electric conductivity was four orders of magnitude higher than that of OH-.

Electrolysis reactions increased the H+ concentration at the anode and decreased the soil pH at the region to about 2. Consequently, the electrical conductivity within this region increased up to $= 10^{-2}\,(F^2 D^*_H/RT)$, which was about 3 orders of magnitude higher than the initial conductivity: For example, if the pH at the cathode region increased to 8, the electric conductivity would be,

$$\sigma^* = \frac{F^2 D^*_H}{RT}\left(10^{-8} + 0.57 * 10^{-6}\right) = \frac{F^2 D^*_H}{RT} 5.7 \bullet 10^{-7} \qquad (6.6)$$

which was two orders of magnitude less than the initial conductivity (Equation 6.5).

Furthermore, the increase in cathode pH as a result of electrolysis reactions led to precipitation of most heavy metals and decreased the ionic concentration in the pore fluid. Consequently, the electric conductivity of the soil pore fluid within that zone also decreased. Therefore, the analogy of series resistors may well have been a good representation of the electrical conductance across the soil. Small voltage drops occurred at the lower resistivity zone (anode region) and most of the voltage drop was realized at the interface of the acid/base front (the soil zone near to the cathode).

6.6 Pore Water Pressure

Electroosmosis is pore fluid transport through soil under an electric field. Measurement of electroosmosis requires application of an electric gradient across the soil without any hydraulic head difference (or accounting for any flow under hydraulic or other **gradients). Though no** hydraulic head difference was applied across the electrodes in the pilot-scale tests, negative pore water pressure was developed across the specimen. This negative pore water pressure contributed to the pore fluid flow. Consequently, a coupled hydraulic flow occurred under the applied electric gradient and the generated hydraulic gradient; even though a head difference was not applied across the electrodes. Assessment of the electroosmotic flow across the specimen required investigating the effect of development of negative pore water pressure on the pore fluid flow.

Figure 6.14 shows the development of negative pore pressure across PST2. The first tensiometer located at a distance of 14 cm from the cathode (TEN1 in Figure 5.9) showed an increase in suction to about -70 kPa within the first 150 h. Suction started after about 200 h in TEN2 (28 cm from cathode) and after 300 h in TEN3 (42 cm from cathode). TEN4, which was the nearest to the anode (14 cm from anode) did not display any significant change. It was noted that suction was first developed near the cathode and slid back to the middle parts of the specimen. Dissipation of suction in TEN1 and TEN2 occurred after 500 h of processing and in TEN3 after 1000 h. Data for all tensiometers readings in time are presented in Appendix D.

The electric potential distribution across the soil in PST2 demonstrated that most of the electric potential drop was confined to the soil section close to the cathode (Figure 6.13). The high electric gradient within that zone (up to 10 V/cm) resulted in higher electroosmotic flux than the soil within the anode zone. In kaolinite specimens, the hydraulic conductivity was relatively low (in

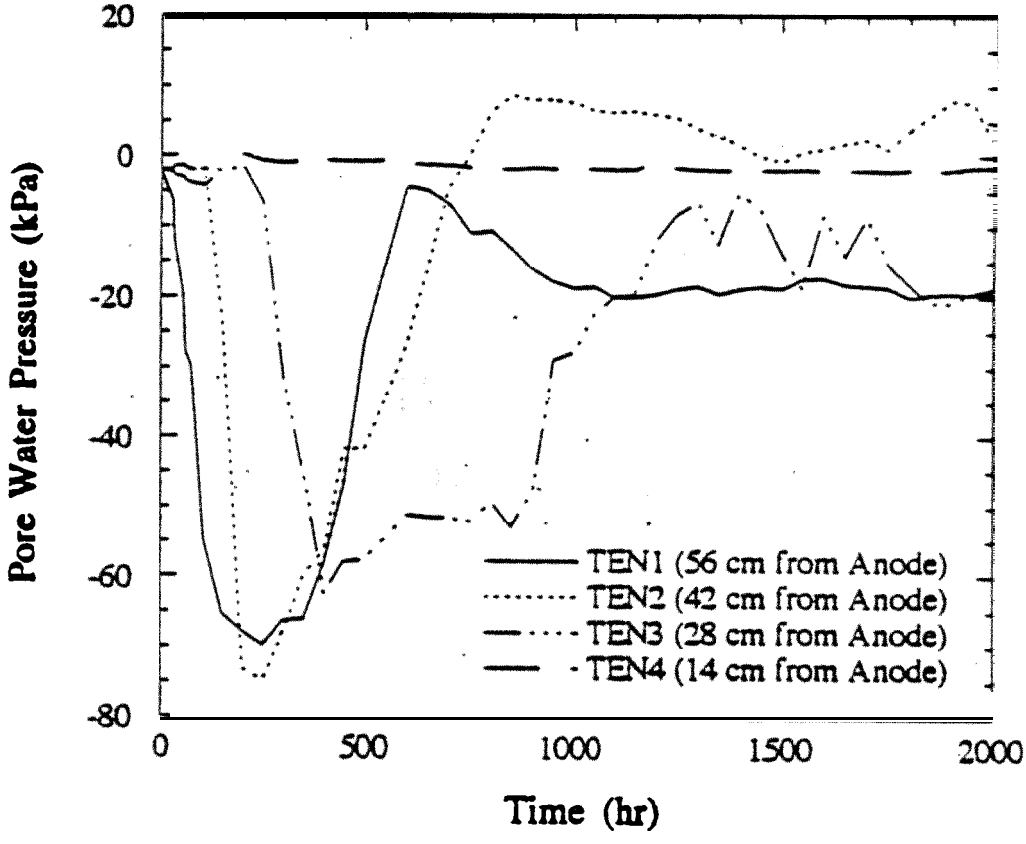

Figure 6.14: Pore Pressure Developed in Tensiometers with Time

The electric gradient distribution ($\partial i_e/\partial x$ where i_e is the electric gradient) and the ratio of the coefficient of electroosmotic permeability to hydraulic conductivity (k_e/k_h).

The soil within the cathode region (up to 42 cm from the cathode) was the section that demonstrated change in the pore water pressure. The electric potential distribution across PST2 (Figure 6.13) showed that most **of the electric** drop occurred within this region. Figure 6.13 also shows that the electric drop occurs first near the cathode and then it advances towards midsections. The electric potential drop was realized withen 10 cm from the cathode after 210 h, 28 cm from the cathode after 300 h, 35 cm from the cathode after 400 h. After 500h the eledtric drop was within 45-50 cm from the cathode and remained at this zone till the end of processing. Figure 6.15 shows a comparison between the dectric potential profile and suction profile across the specimen after 300 h and 500 h. These comparisons clearly demonstrate that the locauons of the highest suction developed was where the drop in electric potential occurred (where $\partial i_3/\partial x$ is the maximum).

6.7 **Pore Fluid Flow**

The first pilot-scale test (PSTl) was the only one that displayed pore fluid flow under the applied electric field among the three pilot-scale tests (Figure 6.16). Electroosmotic pore fluid flux is a function of the coefficient of electroosmotic permeability and the electric gradient; therefore, changes in the electroosmotic flow were expected to be either due to a change in the electric gradient or a change in the coeffcient **of electroosmotic** permeability. However, other factors also were expected to affect measurement of any electroosmotic flow in pilot-scale specimens. These factors included the effect of any generated pore pressures, and boundary effects in the experiment. Differences in the fluid flow between the three pilot-scale tests could have been related to differences in the initial chemistry of the soil pore fluid. Increasing initial lead concentration in the soil above the cation exchange capacity increased the conductivity of the pore fluid and decreased the voltage gradient across the specimen. A decrease in the voltage gradient resulted in a decrease in the electroosmotic flow if the electric current is kept constant.

Ionic strength of the soil pore fluid was expected to have a significant effect on charge transport in the diffuse double layer (or surface current). An increase in the electric conductivity of the pore fluid due to an increase in ionic strength decreased the fraction of the total electric current

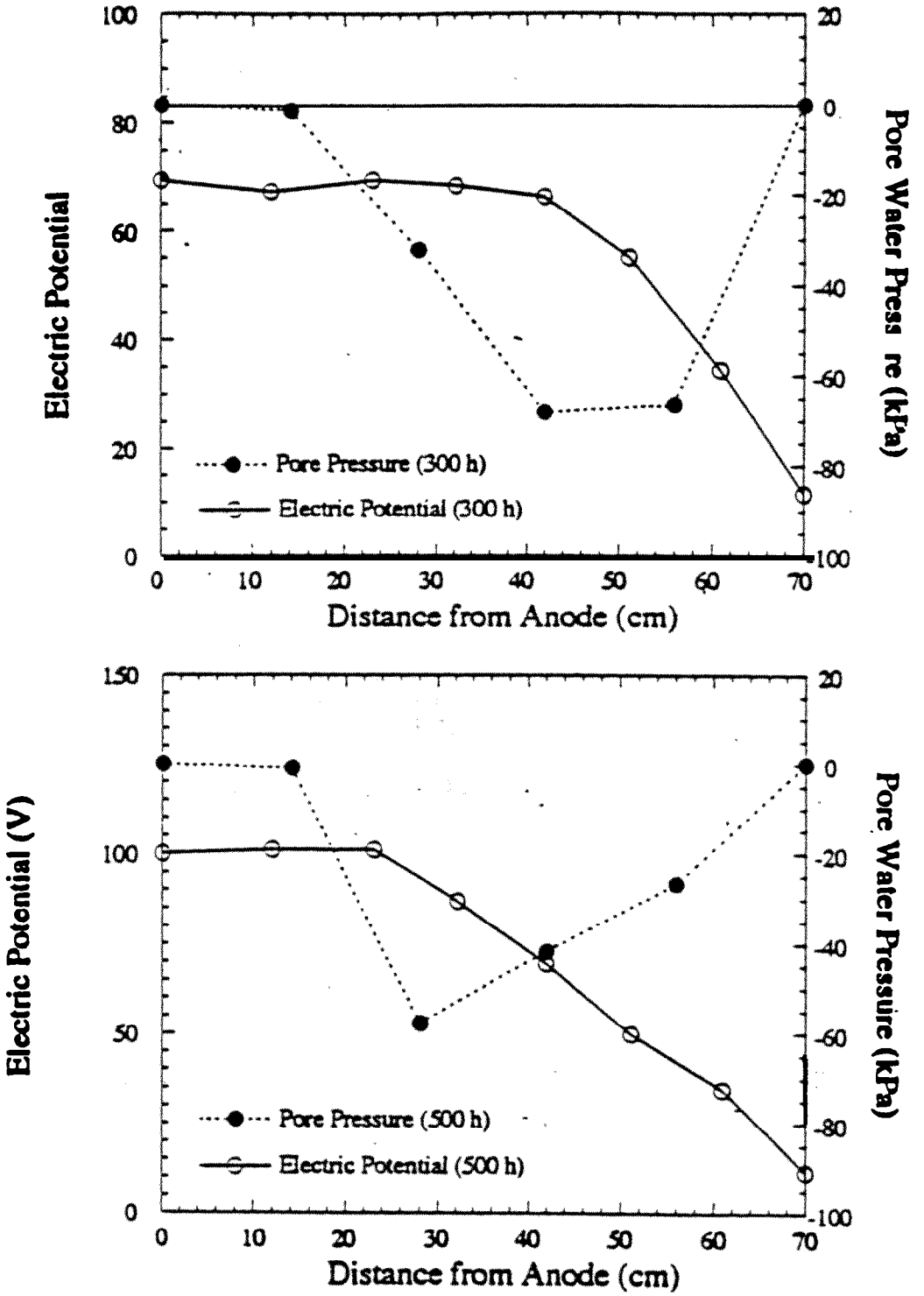

Figure 6.15: Comparison between Electric Potential Profile and Pore Pressure Profile across PST2 after 300h and 500 ***h.***

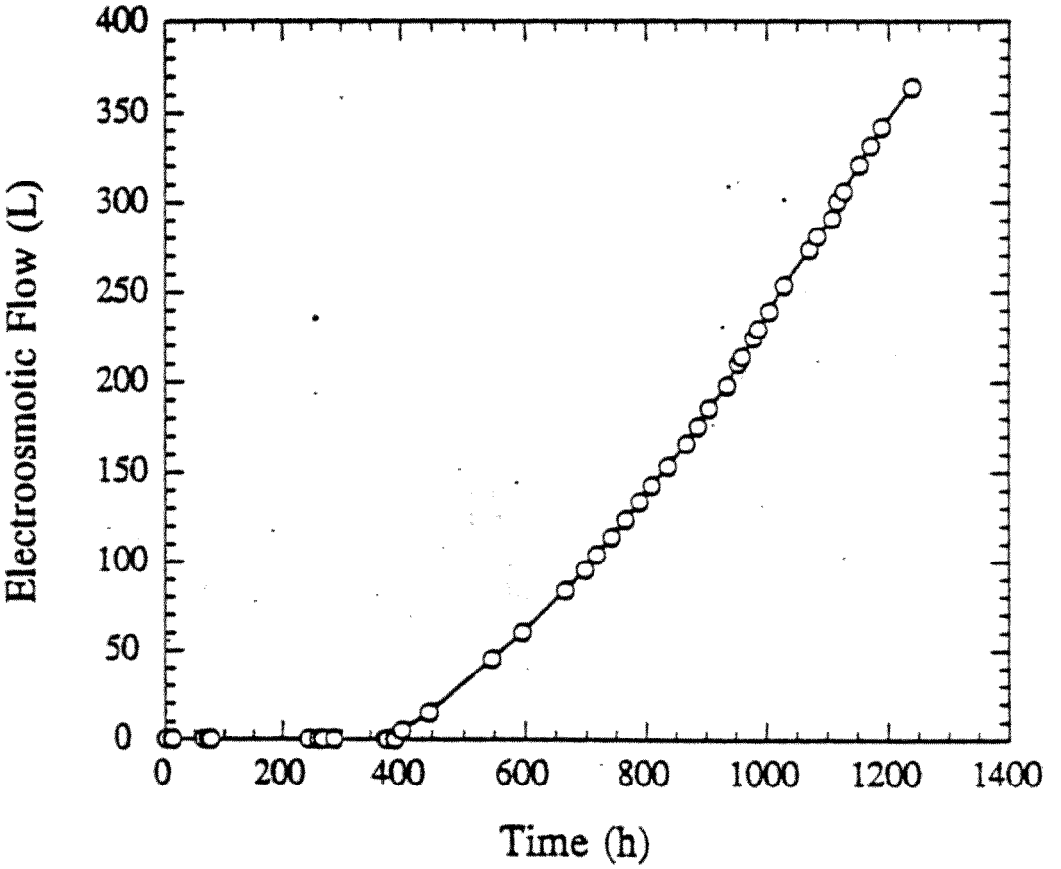

Figure 6.16: Pore Fluid Flow in PST1

that passed through the double layer. Figure 3.5(iii) shows that the soil free pore fluid and soil diffuse double layer could be simulated by two resistors that were connected in parallel. The electric current passing through each resistor depends on the resistivity of each layer, lower the resistivity, higher will be the current. Consequently, having increased the pore fluid ionic strength increased the conductivity, increased the current component passing through the pore fluid, and decreased relatively the current component passing through the double layer, if the surface charge remained a fixed amount. Classical theories of electroosmosis (Hdmholtz-Smoluchowski theory) have postulated that electroosmotic flow is a result of the current passing through the diffuse double layer due to transport of the excess charge. Accordingly, a decrease in the electric current passing through the double layer decreased the electroosmotic flow. Furthermore, decreasing the soil pH and increasing the electrolyte concentration of the soil pore fluid decreased the thickness of the diffuse double layer. This was also expected to decrease the surface charge density of the soil particles, and the zeta potential (Hunter 1981), and consequently the coefficient of electroosmotic permeability.

It should be noted that there are othcr differences between the first pilot-scale (PSTI) and the other pilot-scaIe tests. Differences in the pIacement of electrodes might have also affected the flow. The electrodes were held in separate auger holes in PSTI, while they were held in trenches only in PST2 and PST3. Furthermore, cracks developed in the soil specimen only PST1 and they were not detected in PST1 and PST2. It is not clear how all of these factors have affected the flow.

Furthermore, the developed suction was expected to influence the flow. The equivalent hydraulic head difference generated by the suction caused pore fluid flow towards the section with the highest suction. In other words, pore fluid flow could have occurred from the cathode and the anode compartments towards the section with highest suction but the net flow was towards the cathode. However, for soils with hydraulic conductivity of 10^{-7} cm/s and electroosmotic permeability of 10-6 cm^2/Vs, the hydraulic gradient should have been one order of magnitude higher than the electric gradient in order to affect the flow significantly. Furthermore, the electroosmotic flow depended on the zeta potential, which was a function of the soil pH. The decrease in pH across the soil within the anode zone to less than 2 might have reversed the sign of the zeta potential. In this case, the eletroosmotic flow might have reversed its direction and a flow may have prevailed from the cathode to the anode (Eykholt 1992). All these factors affected the pore fluid collected in the cathode in a complex manner.

The coefficient of electroosmotic water transport efficiency, k_i, formalized the volume of water transported by a unit charge and it was given by

$$k_i = \frac{q}{I} \qquad (6.7)$$

The **value** of k_i was expected to change with time depending upon the value of q if I was constant throughout the process. If the incompressible medium assumption is made and neglecting the effects **of** pore fluid chenmistry and pH on the zeta patential, then k_i will also have a constant **value** across the specimen at any specific time; however, the soil undergoes a consolidation process and the experimental results demonstrate volume change across the specimen. Therefore, the value of k_i is also expected to vary from one position to another at any specific time.

Bench-scale studies reported by Hamed (1990), Eykholt (1992), and Acar et al. (1994) displayed different electroosmotic flow efficiencies. Most of these bench-scale studies were conducted with kaolinite specimens spiked with lead, cadmium, chromium, and copper species at concentrations less than the cation exchange capacity of the soil. The evaluated coefficients of electroosmotic flow for these tests were in the range of 10^{-5} to 10^{-7} cm^2/Vs. Hamed (1990) and Hamed et al. (1991), also demonstrated that for bench-scale tests conducted using 10 cm specimens, there was an electroosmotic fluid flow only within the first 100 hours of processing and this flow decreased with time. Consequently, the coefficient of electroosmotic permeability measured in these tests increased within the first 100 h to about $2x10^{-5}$ cm^2/Vs and then decreased to around $1x10^{-7}$ cm^2/Vs after about 500 h of processing

PST1 showed that k_e increased with time to 10^{-6} cm^2/Vs (Figure 6.17). This contradicting behavior in PST1 compared to the results of Hamed (1990) and Hamed **et al.** (1991) may have been related to the differences in the setup of bench-scale tests and pilot-scale tests. The open surface of the soil specimen may have had a two dimensional effect on the fluid flow. Furthermore, the volume change in PST1 may have resulted in development of cracks across the specimen and also some separation zone appeared between the soil and the liner along the sides near the cathode. These factors may have significantly affected the fluid flow rendering a flow and an apparernt k_e value

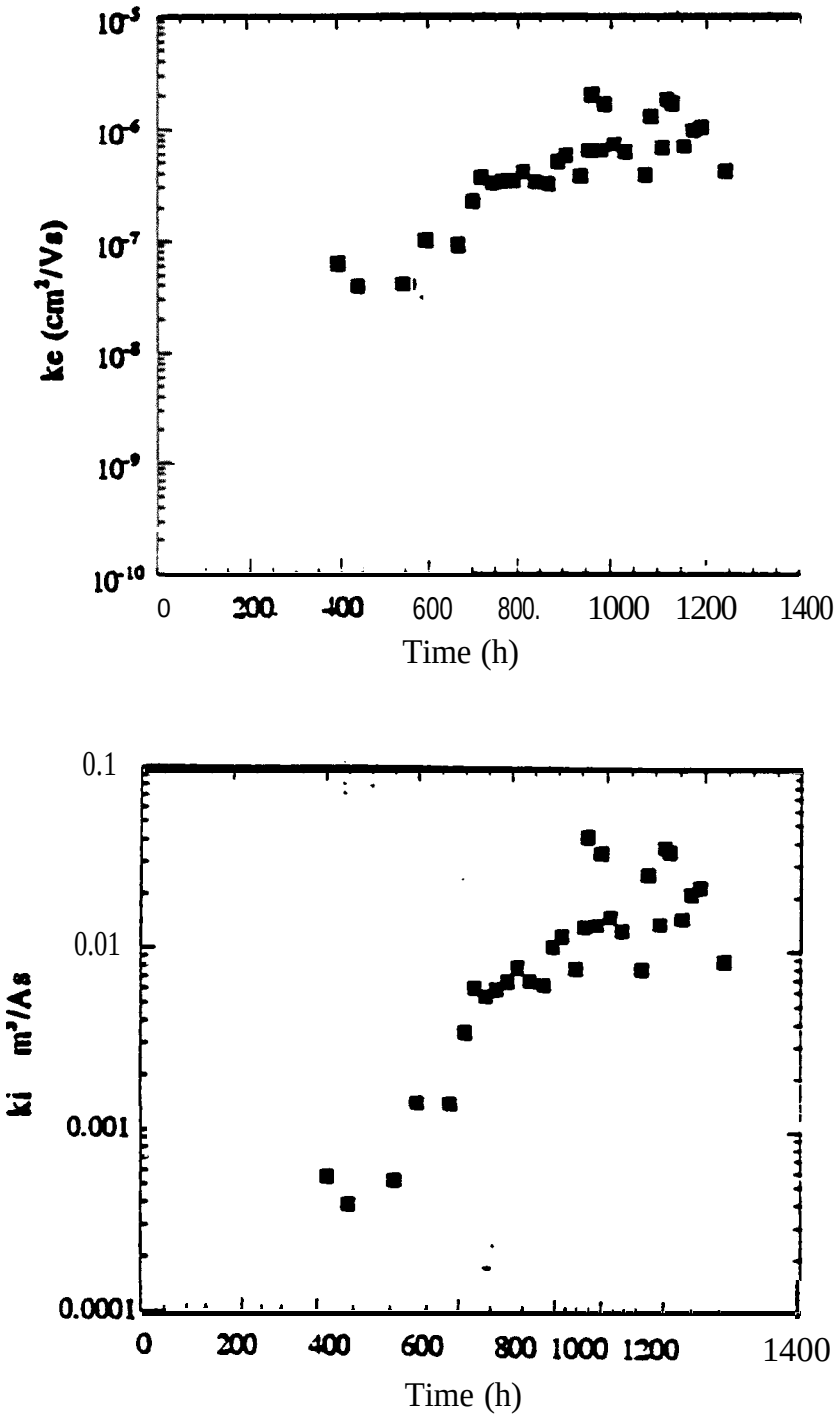

Figure 6.17: Changes in Coefficients of Electroosmotic Permeability and Electroosmotic Water Transport Efficiency in PST1

6. 8 Ionic Migration vs Electroosmosis

The relative contribution of electroosmosis and ion migration to the total mass transport varies for different soil types, pore fluid concentration, and processing conditions. Under electric fields, **Acar** and Alshawabkeh (1993) proposed a dimensionless mass transport number, λ_e

$$\lambda_e = \frac{u_i^*}{k_e} \qquad (6.8)$$

which defined the relative contribution of the migrational mass flux with respect to the electroosmotic mass flux under a unit electric gradient. Figure 6.18 presents the change in transport number, λ_e, for different species. Coefficients of electroosmotic permeability in this figure were obtained from the results **of** Hamed (1990), Hamed **et al.** (1991), and Acar et al (1994). Figure 6.18 demonstrates that the fate of mass transport by ion migration was orders of magnitude higher than that by electroosmosis. Ionic migration was expected to be the primary transport mechanism for ionic species under electric gradients. Furthermore, the results of bench-scale tests and pilot-scale tests conducted in this study at concentrations higher than the cation exchange capacity of the clay demonstrated that there was no electroosmotic flow. In such cases ionic migration would have been the, primary if **not** the only, effective mass transport mechanism.

6.9 Volume Change

Figure 6.19 gives the water content profiles in bench-scale tests. A decrease in water content in mid-parts of the specimens was accompanied by a corresponding increase near the electrodes (swelling). Similar observations were made in the pilot-scale tests (Figures 6.20 and 6.21). Data for final water content distributions in all layers are presented in Appendix D.

The change in water content across the soil was a direct indication of change in pore water pressure and the effective stresses. Since the total stress across the specimen was kept constant, development of suction was accompanied by an increase in the effective stress. Consolidation occurred due to the changes in the effective stresses and release of the generated suction accompanied the consolidation process. The rate of change in suction was dependent on the soil

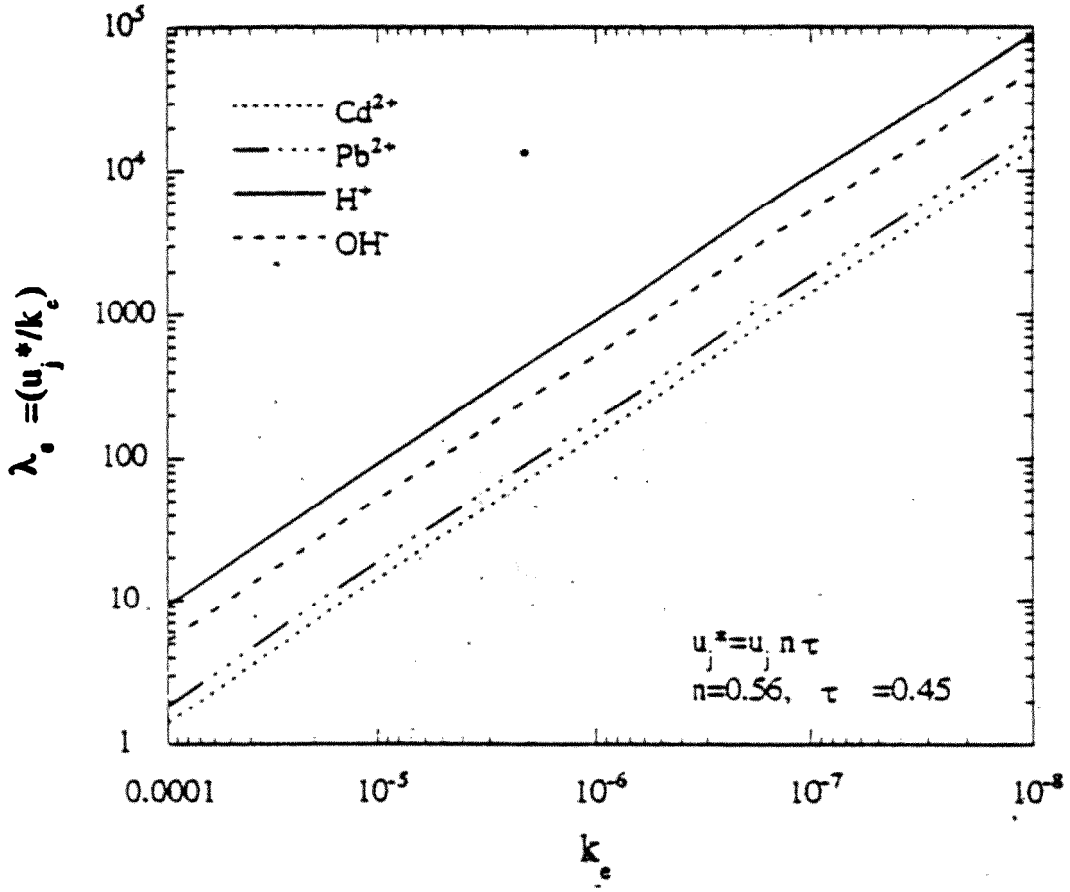

Figure 6.18: Significance of Migration with Respect to Electroosmosis

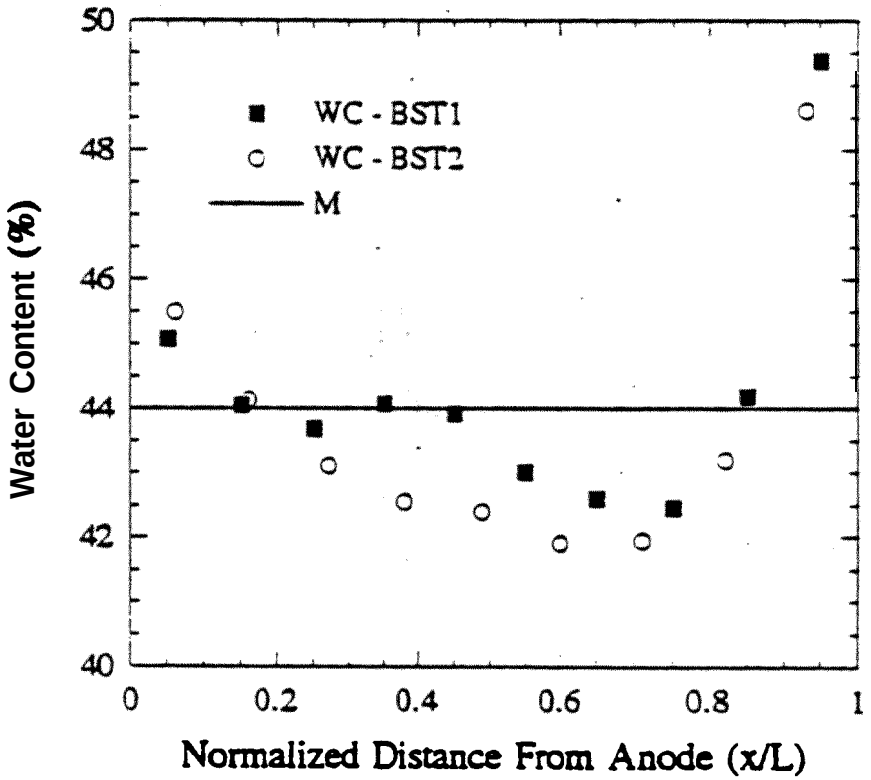

Figure 6.19: Final Water Content Distribution in Bench-Scale Specimens

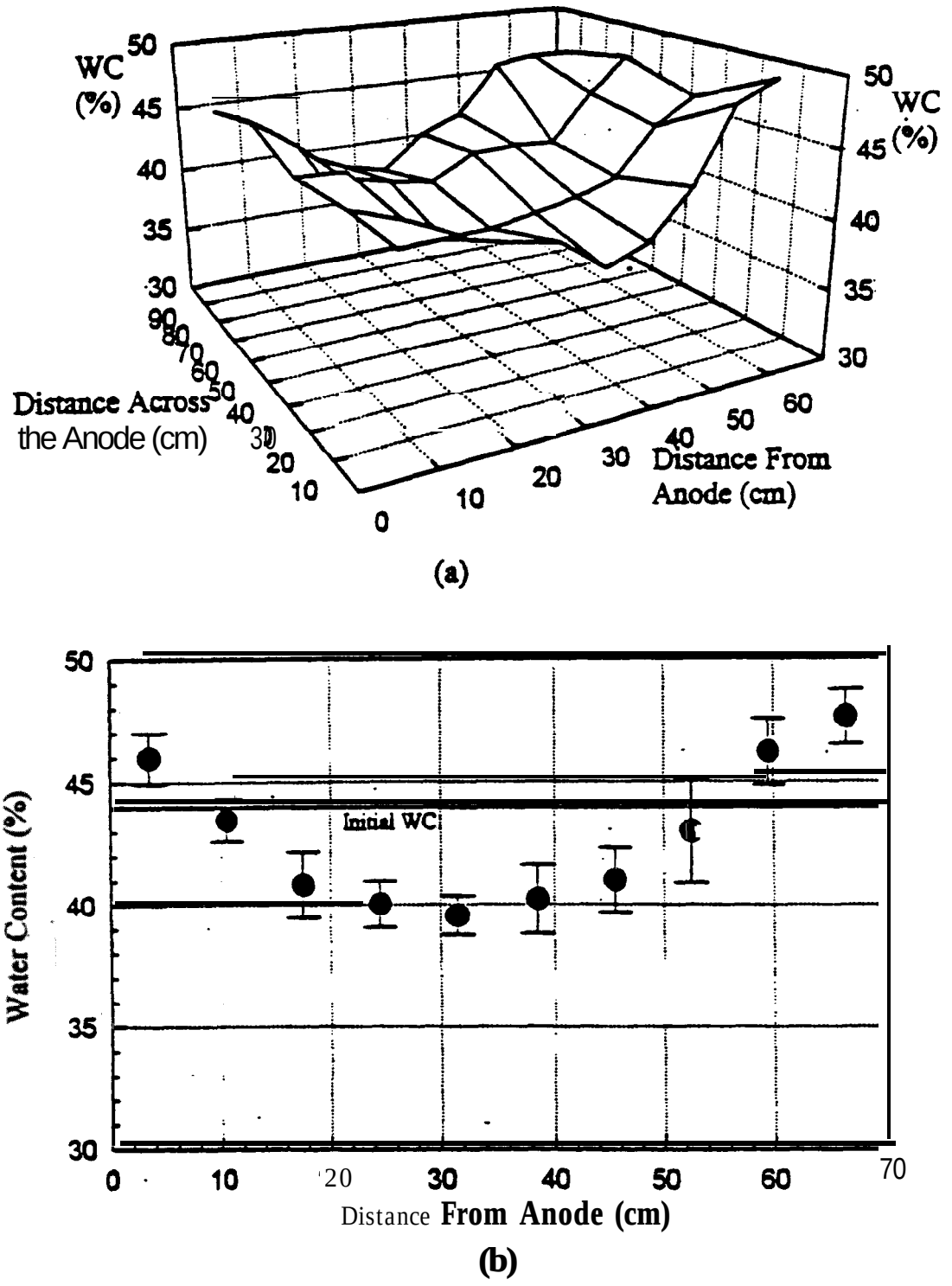

Figure 6.20: **Final** Water Content Distribution in across Cell-A in the Middle Layer (Layer 3) of PST2 (a) 3-D Figure and (b) Mean and Standard Deviation

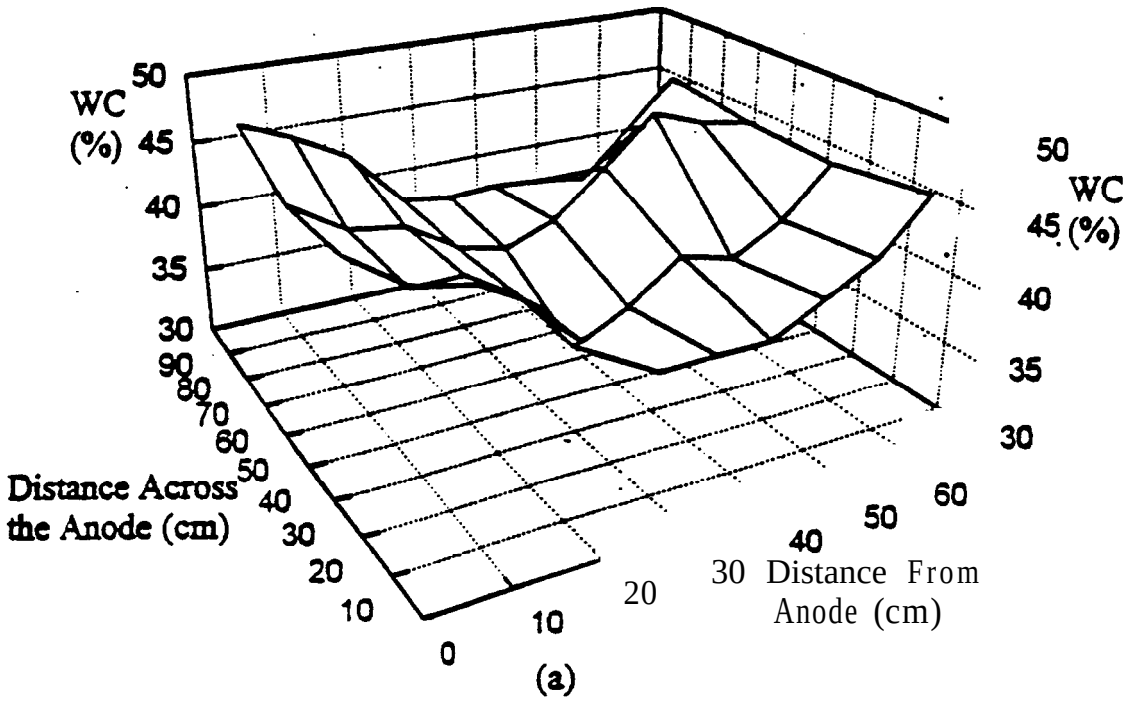

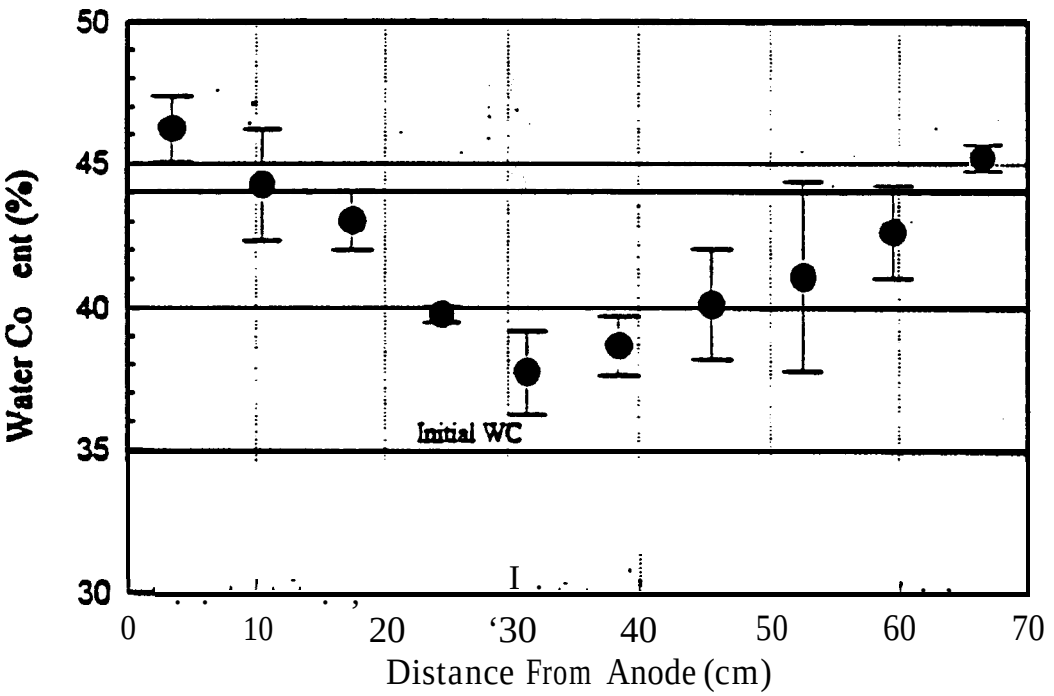

(b)

Figure 6.21 Final Water content Distribution in across Cell B in the Middle Layer (Layer 3) of PST2 (a) 3-D Figure and (b) Mean and Standard Deviation.

hydraulic conductivity, coefficient of electroosmotic permeability, and coefficient of volume compressibility of the soil medium.

Figure 6.19 demonstrates that the decrease in water content in the shorter duration test (BSTl) was less and closer to the cathode than that in BST2. This indicates that more volume change occurred in the longer duration test. Furthermore, volume change progressed from the section close to the cathode to the midsection of the specimen.

Figures 6.20 and 6.21 show that the water content decreased at middle parts of PST2 to about 32% while at the cathode and anode increased to 46-48 %. The increase in water content near the electrodes was observed in all specimens. The support used for the electrodes did not provide. confinement to the soil near the electrodes. The soil was in direct contact with the fluid in the electrode compartments. When intact clay gets in direct contact with water without confinement, clay will disperse into the adjacent water (Mitchell 1993). Swelling will occur as a result of water adsorption by the clay.

Final water content distributions across the soil specimens showed similar patterns in both these bench-scale tests and pilot-scale tests. A decrease in water content was depicted at midsections of all specimens. Since total stress in the soil was constant and did not change with time, the increase in the negative pore water pressure was accompanied by an increase in the effective stress. Consolidation occurred due to the changes in the effective stresses and release of the generated suction accompanied the consolidation process. The rate of change in suction was dependent on the soil hydraulic conductivity, the coefficient of electroosmotic permeability, and the coefficient of volume compressibility of the soil medium.

The changes in water content across the soil and the suction profile recorded across the electrodes could not be rationalized using the conventional theories of electroosmotic consolidation presented by Esrig (1968), Wan et al. (1976), Lewis et al. (1973), Bruch (1976), and Banerjee et al (1980a). These theories assume constant electric potential distribution across the specimen and neglect the effect of electrochemical changes on the electric potential distribution. Consequently, negative pore water pressure is expected to be generated in the zone near the anode only if an impermeable anode is used allowing no water flow from the anode towards the soil. These theories did not predict any pore water pressure if both the anode and the cathode were kept open for water flow and the water head was kept constant at both boundaries.

6.10 Efficiency of Lead Removal

Bench-scale tests at a concentration of 1,439 ug/g displayed transport and removal of lead across the soil specimens. Final lead distributions demonstrated that the longer duration test (BST2)resulted in a higher degree of removal than the shorter duration test (BSTI); however, in both tests significant masses of lead were found precipitated close to the cathodes (Figure 6.22). Mass balances of lead in both tests at the end of processing are presented in Figure 6.23. BSTI demonstrated that about 73% of the initial lead was transported from sections (l-9) and precipitated in the last section near the cathode (section 10). BST2 demonstrated 65% of total lead was removed from the soil sample, 96% of which was from sections 1-9 The greatest fraction of the lead (about 44 %) was found precipitated and/or electrodeposited at the cathode. Differences in the results between the two tests were due to the differences in processing periods; 169 h for the first test and 598 h for the second test, both at a current density of 127 $\mu A/cm^2$. In general, final lead distributions in these tests displayed that the removal efficiencies were similar to those reported by Hamed et al. (1991) and Hamed (1990).

Three layers at different elevations were analyzed for final lead distribution in PSTl. Figure 6.24 presents a 3-D contour diagram and the mean and standard deviation of final lead distribution across the middle layer 6 this test. Data for other layers are presented in Appendix D.

During processing PSTl, the soil at the cathode region showed more consolidation and volume change than the soil at the anode region. At the end of processing (1,300 h), cracks were developed across the soil surface (plate 6.1). These cracks were located at midsections of the specimen and close to the cathode. Development of such cracks was not anticipated. The top Iayer of PST2 and PST3 did not show any cracks such as those developed in PSTl. There is no clear explanation yet for the development of these cracks. It has been hypothesized that cracks might have been generated in PST1 due to the significant volume change at the cathode region together with the loss of support created by the specific electrode support system.

PST1 was the first pilot-scale test conducted. The initial lead concentration in this test was about half that of **PST2** and about 16% of the amount loaded in PST3. It was the only test that displays electroosmotic flow. Hence, it was postulated that the low initial concentration in this test (compared to concentrations in other pilot-scale teats) was the reason for higher electroosmotic flux at the cathode zone, that resulted in development of higher suction values of up to -90 kPa, higher

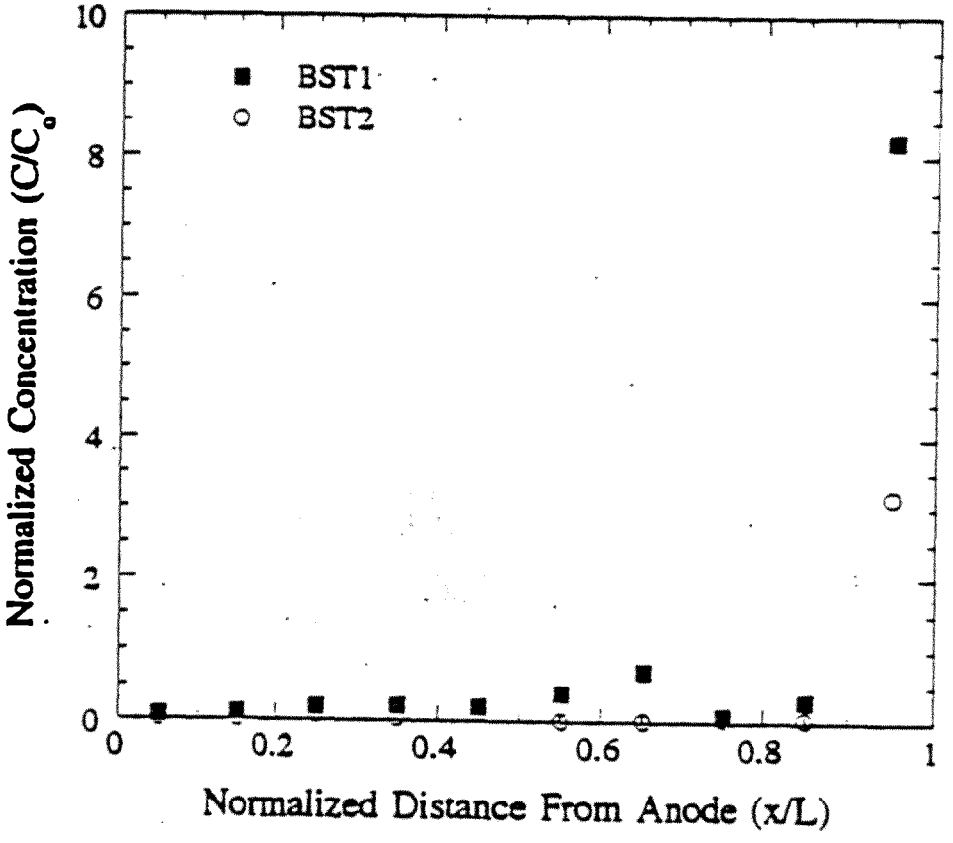

Figure 6.22: Final Lead Concentration across Bench-Scale Soil Specimens

Mass Balance For Bench-Scale Tests(% of Initial Lead)

Section Name	BST1	BST2
Section 10	82.38	32.54
Sections 1 to 9	23.18	3.15
Effluent	0.04	0.04
Electrodes	2.34	44.29
Error	-7.94	19.98

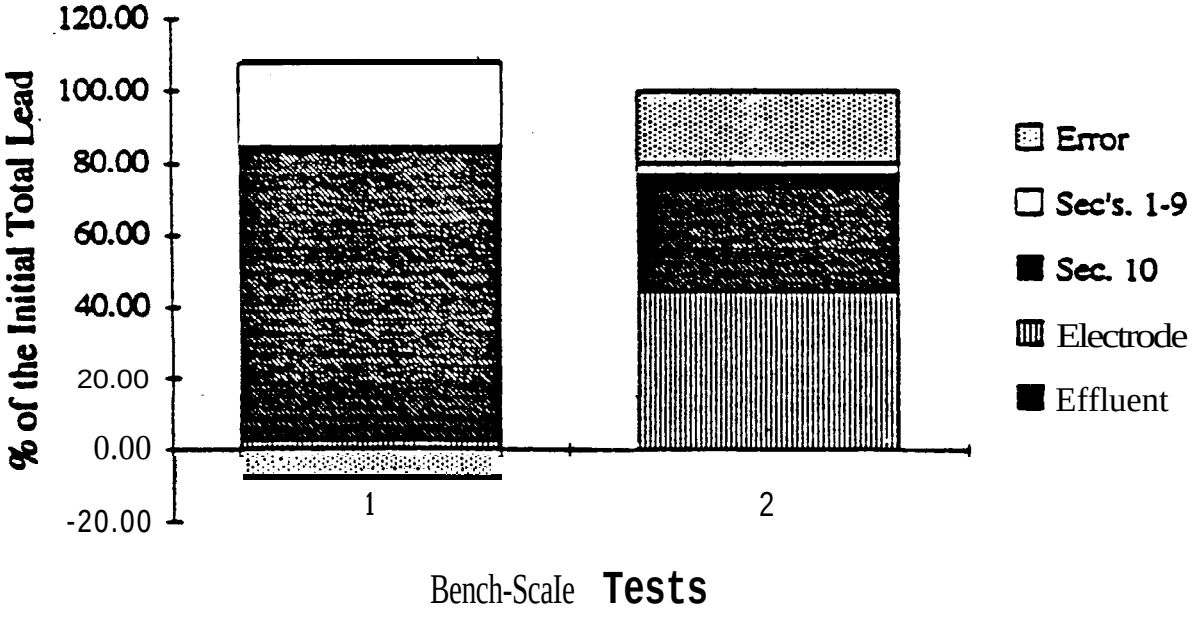

Figure 6.23: Mass Balance for Bench-Scale Tests (BSTl=169 h, BSTt=598 h. I_r= 127 $\mu A/cm^2$ for Both)

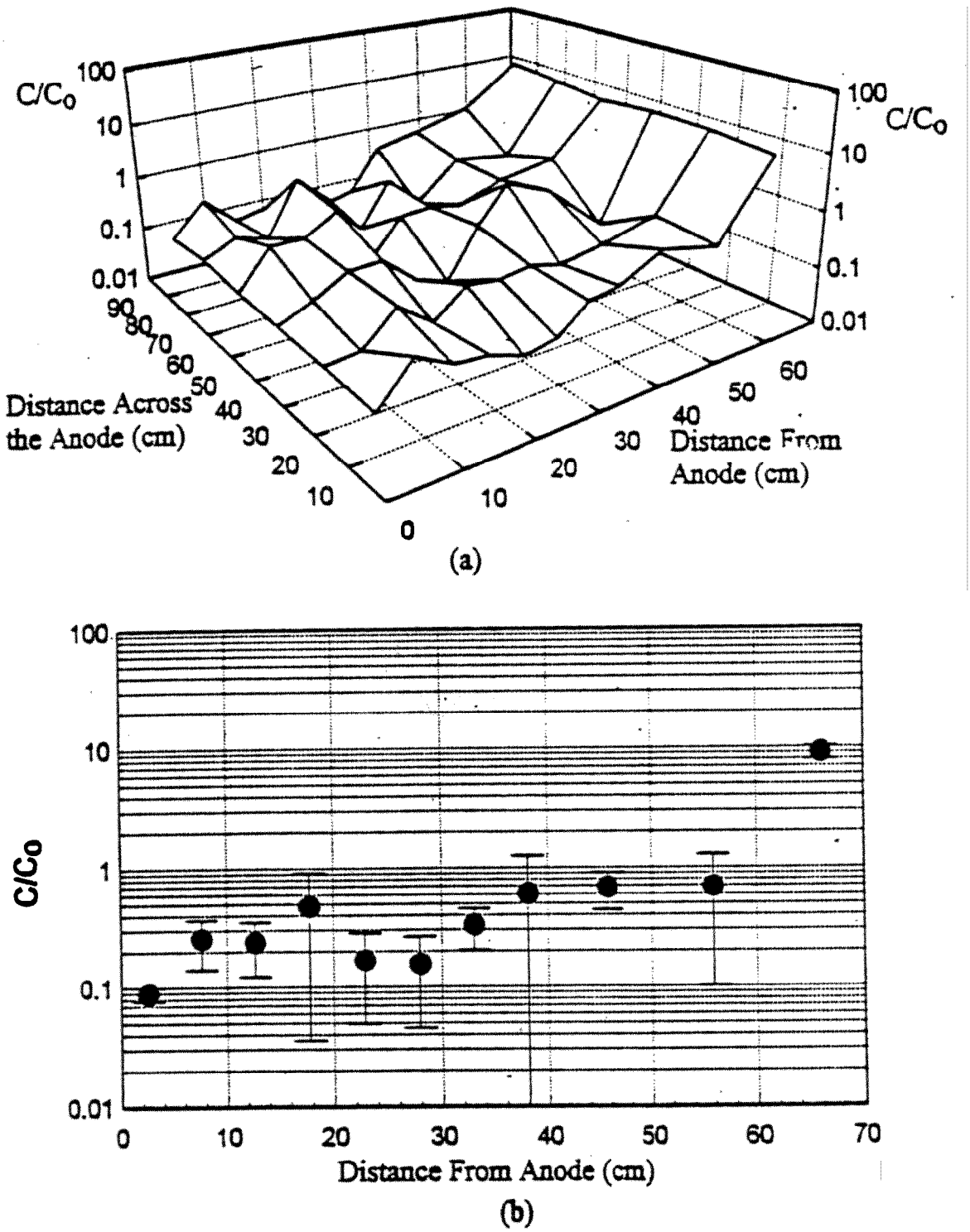

Figure 6.24: Final Lead Concentration across the Middle Layer of PST1 (a) 3-D Contour Diagram and (b) Mean and Standard Deviation

Plate 6. 1 : **Surface of the Soil Specimen on PST1 Depicting Development of Cracks at Midsections and Near Cathode**

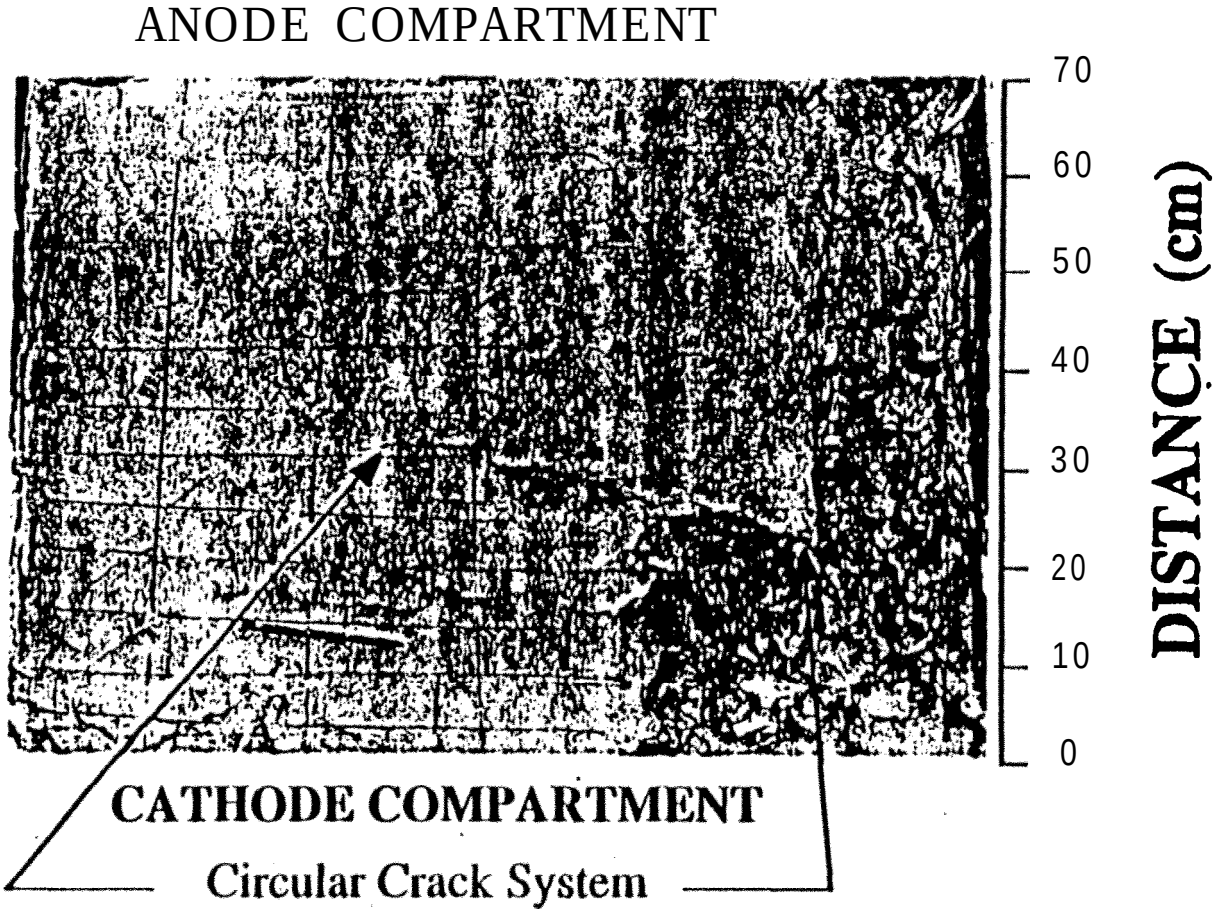

effective stresses and more consolidation within that zone. At the same time, the anode region did not display as much consolidation because less suction was expected to develop at that zone. Consequently, the volume change at the cathode zone due to consolidation was higher than that at the anode zone resulting in development of cracks at the interface (as shown in Plate 6.1). Unfortunately, suction profiles could not be measured in this test due to failure of the tensiometers and limited experience with tensiometers at the time

Final chemical analyses of the soil in PST1 have shown a nonuniform lead distribution across the soil mass. Figures 6.24 and 6.25 demonstrate that different sections of the soil contained less than 0.1% of the initial concentration, while other parts contained high lead concentrations. It is noted that most of the high lead concentrations were found along the cracks. A comparison between final lead distribution in the top layer of PST1 (Figure 6.25) and locations of the cracks at the surface of the specimen (Plate 6.1) clearly demonstrates that the high lead concentrations were cited at same locations of these cracks.

Figure 6.26 displays the mass balance in PSTl. Most of the lead was found precipitated in the last section close to the cathode, which contained about 54% of the initial lead. The soil across the electrodes (excluding the last section) contained around 40% of the initial lead; most of it was found in permetivity of the cracks. Almost no lead was found in the catholyte because of the high pH Approximately l% of the initial lead was electrodeposited and/or precipitated at the electrodes.

The second pilot-scale test (PST2) demonstrated successful removal and transport of lead across the soil specimen from the anode towards the cathode. Figures 6.27 and 6.28 display final concentration profiles across the middle layer of PST2. Most of the soil across the top layer (up to the last 7 cm of the cathode zone) displayed more than 90% removal, with a final concentration of less than 150 µg/g. Most parts of the soil demonstrated a final concentration of less than 50 µg/g, with removal efficiencies up to 98% of the initial lead. Some strips in the middle part of the soil between the electrodes displayed concentrations of about 20% of the initial concentration (or 80% removal). The middle layer of the sample (layer No. 3) demonstrated similar behavior at the top layer and at other layers presented in Appendix D. More than 90% removal (up to 98% in most parts of the layer) was achieved across the specimen. Strips with 80% removal also appeared at certain sections in the middle of the specimen. Comparing the results of layer 3 with the other layers, showed that there were no major differences in the final concentration distributions between

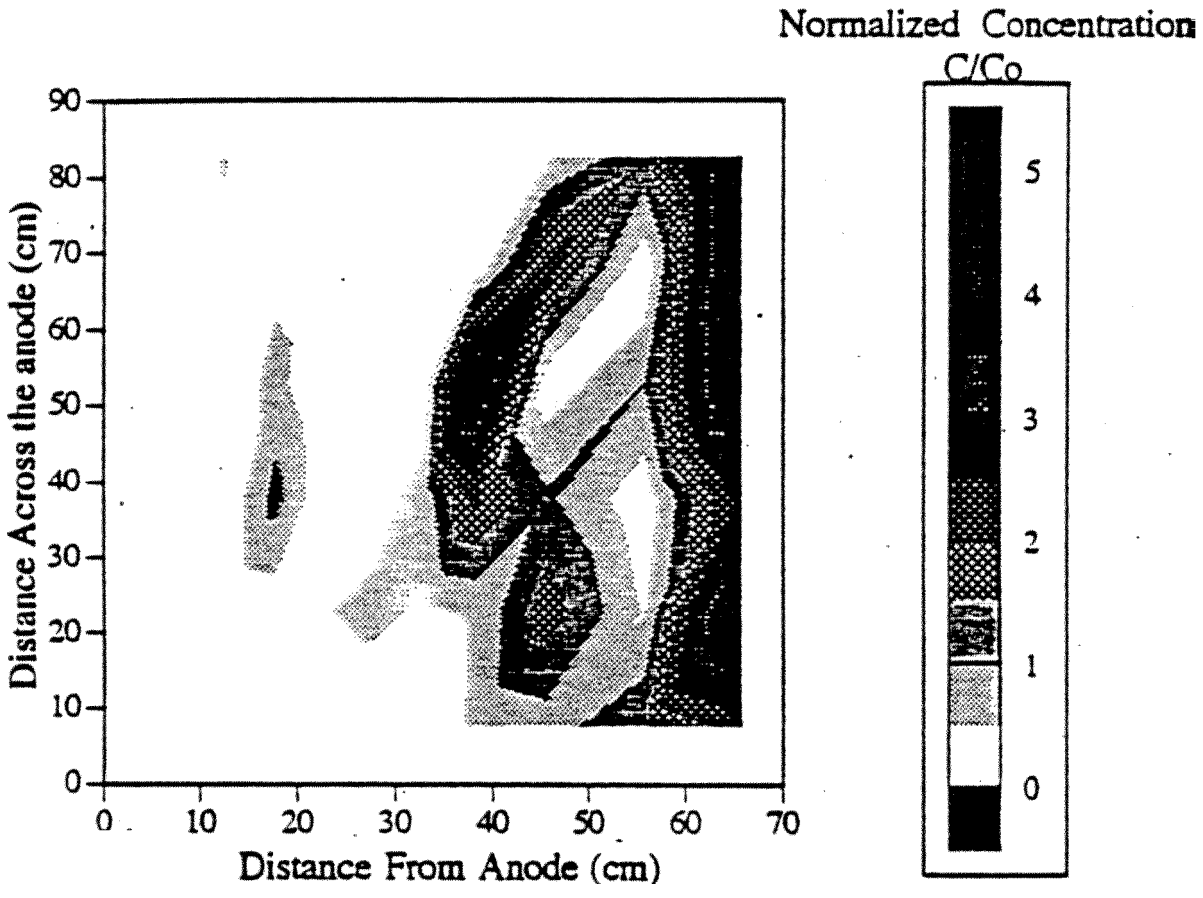

Figure 6.25: Final Lead Distribution across the Top Layer of PST1

Mass Balance For PST1
Initial Concentration = 856 mg/kg
Total Lead = 479 g

Section Name	Lead (g)	% of Lead
Effluent	0.01	0.00
Electrodes	5.67	1.18
Layer 1	66.52	23.1
Layer 2	53.54	38.54
Layer 3	67.04	31.88
Total		94.69
Error		5.31

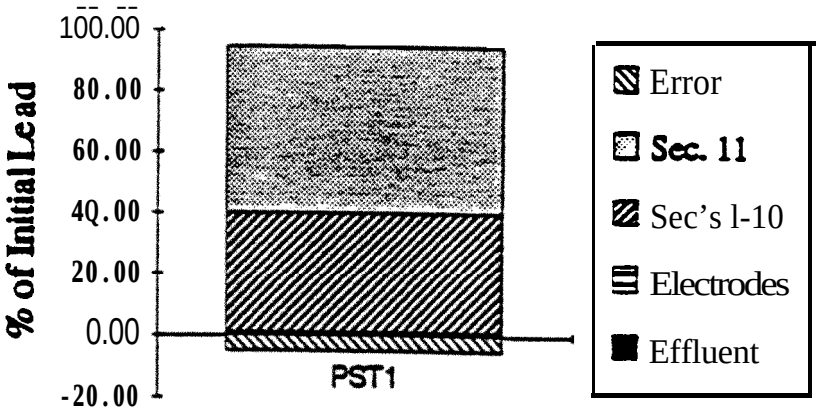

Figure 6.26: Mass Balance for PST1 (Duration=1300 h, $I_o = 133\ \mu A/cm^2$)

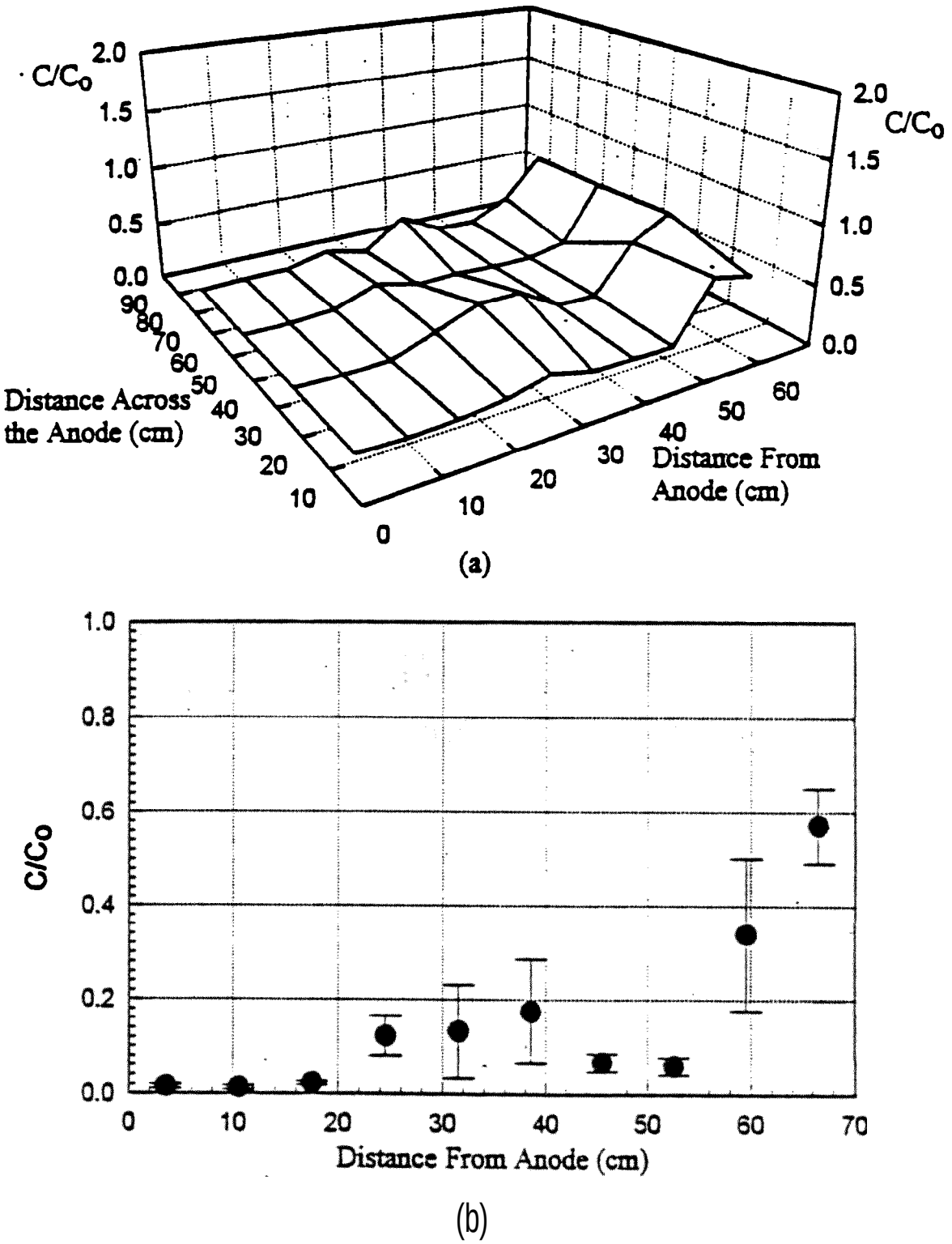

Figure 6.27: Final Lead Concentration across Cell A in the Middle Layer (Layer 3) of PST2 (a) 3-D Contour Diagram and (b) Mean Standard Deviation

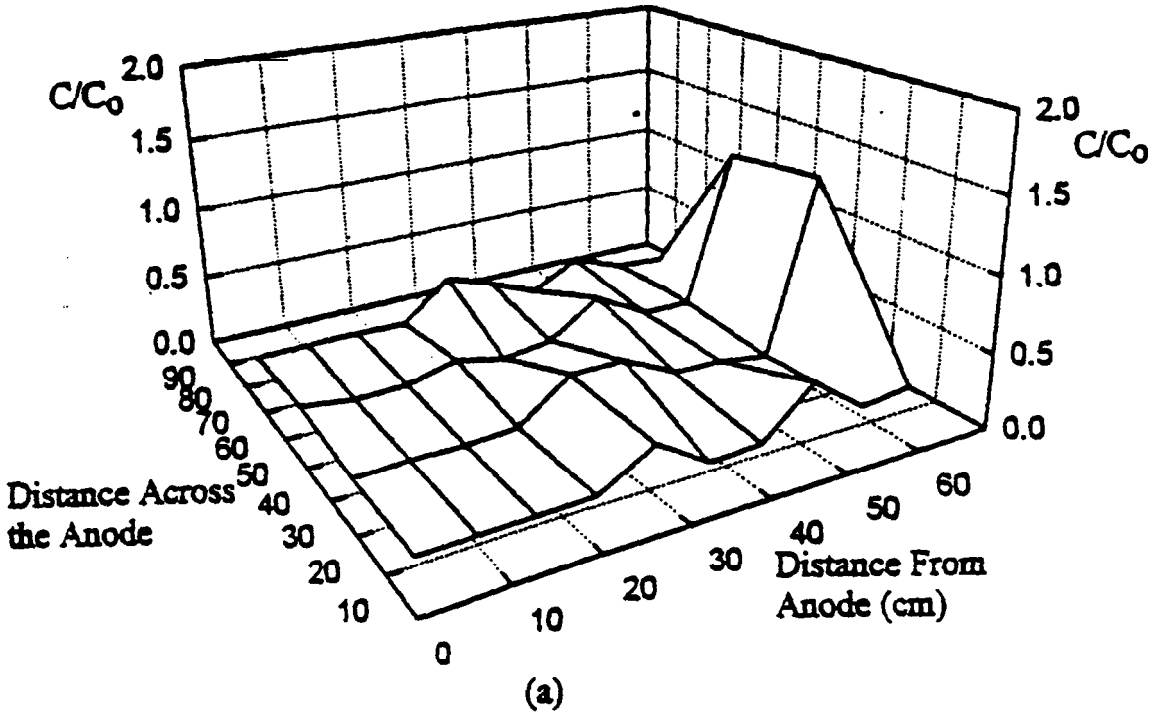

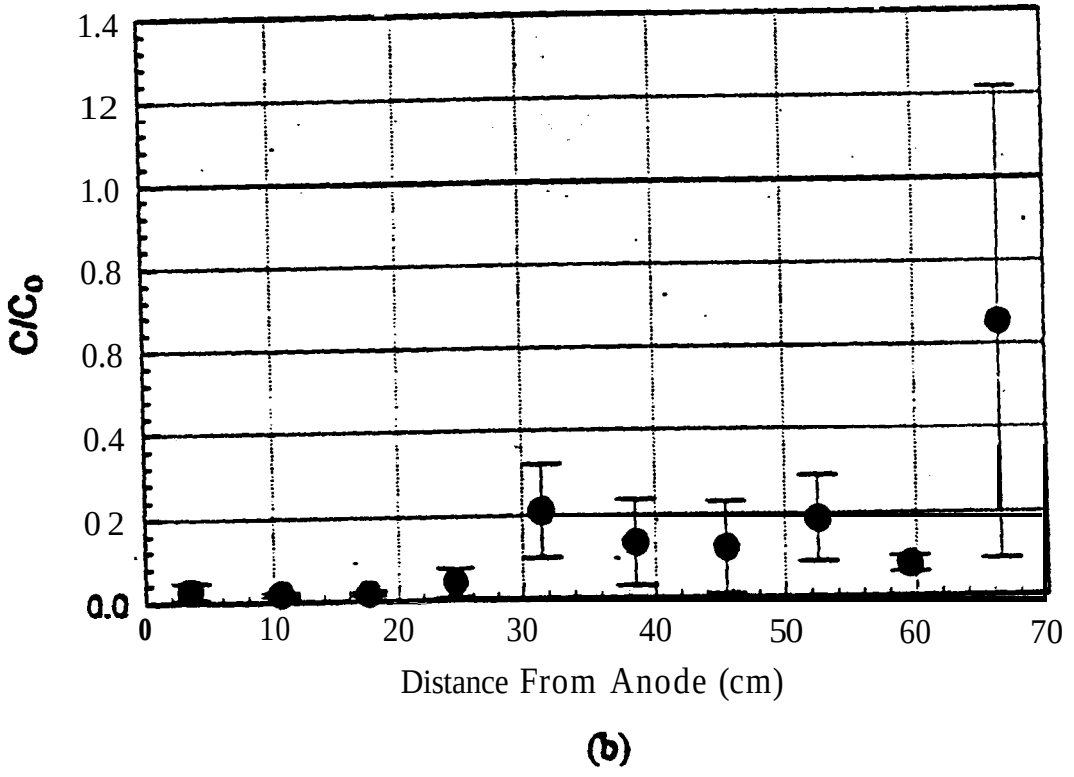

Figure 6.28: Final Lead Concentration across Cell B in the Middle Layer (Layer 3) of PST2 (a) 3-D Contour Diagram and (b) Mean and Standard Deviation

the layers. All layers in cells A and B demonstrated that most of the lead was transported to the cathode zone.

Figure 6.29 presents lead mass balances in both Cell's A and B of PST2. The two cells have shown identical and symmetrical final lead distributions, In both cells, about 80% removal was achieved in the specimen, while 90% removal was achieved in sections 1-9.50% of the lead was round in the last 2 cm near the cathode and about 15% to 20% was precipitated on the fabric separating the soil from the cathode compartments. Almost no lead was found in the cathode compartment (less than 0.01% of the initial lead was found in the catholyte and only 0.02% was precipitated and/or electrodeposited on the graphite electrodes). It was noted that the error in mass balance in Cell A and Cell B was about 17-19% of the initial lead (Figure 6.30). The size or volume of the spiked matrix was not specified. In bench-scale tests, soil mass was more under control than pilot-scale tests. The whole bench-scale specimen was divided into section and analyzed rendering high percent recovery. However in pilot-scale tests, representative samples were taken from the soil for analysis, and not the whole sample. Therefore, more error was expected in pilot-scale tests. In any case, a percent recovery of 80-85% of the initial lead was achieved, which has surpassed EPA requirements [80-120% (Simes 1989)].

The results of PST2 have shown the efficiency of the process in transport of Pb across the specimen towards the cathode. The lead input in the soil system was in the aqueous phase since the initial soil pH is about 4-5. This facilitated transport of lead. Although lead adsorption on the soil particles was expected to retard its transport, the results have shown that adsorption did not have any significance on lead removal. The final lead concentration in most parts of the specimen was found to be less than 150 µg/g which was much below the cation exchange capacity of the soil.

Soil type, pore fluid chemistry, and pH were the major factors that affected lead sorption and retardation. As presented in Table (2.2), lead was highly retarded and adsorbed on clay minerals. Kaolinite was the mineral used and it has low sorption capacity compared to other minerals (such as montmorillonite or illite). The cation exchange capacity for Georgia kaolinite was 1.06 mcq/l00 gm of dry soil (Table 5.2); which was much less than that for other minerals (80-150 meq/100 gm for montmorillonite and 10-40 meq/100 for illite). Therefore, Georgia kaolinite was not expected to show significant retardation to lead transport. The presence of illite and montmorillonite in natural deposits was expected to cause a more significant retardation of lead transport. Furthermore, the soil pH was initially around 4 and decreased to less than 2 (especially

Mass Balance For PST2
Initial Concentration = 6401 mg/kg
Total Lead = 803.4 g

	Cell A		Cell B	
Section Name	Lead (g)	% of Lead	Lead (g)	% of Lead
Sections 1 to 9	69.86	8.69	66.7	8.30
Section 10	96.04	11.95	86.52	10.77
Last 2 cm	398.4	49.57	353.70	44.01
Fabric	119.2	14.83	154.20	19.19
Electrode	1.62	0.20	1.39	0.17
Effluent	.02	0.00	0.08	0.01
Total (g)	685.14	85.25	662.59	82.45
Error		-14.75		-17.55

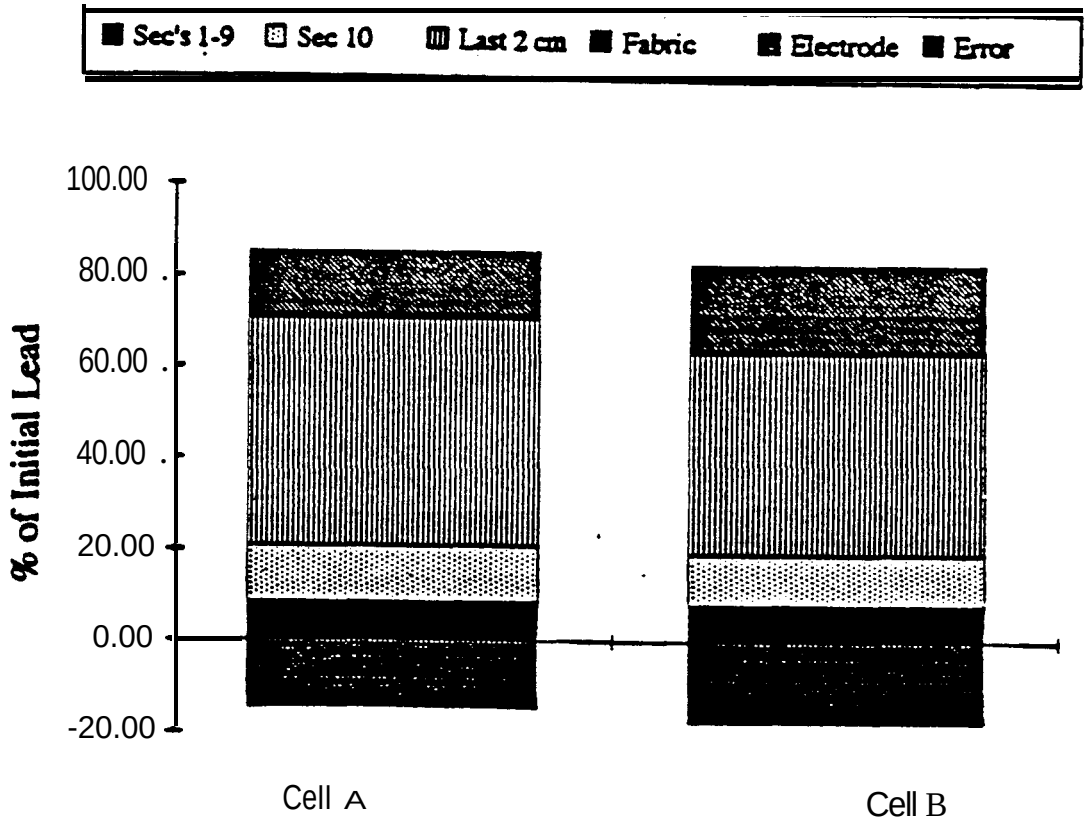

Figure 6.29: Mass Balance for Cells A and B in PST2 (Duration=2950 h, Current Density= I_r= I33 $\mu A/cm^2$)

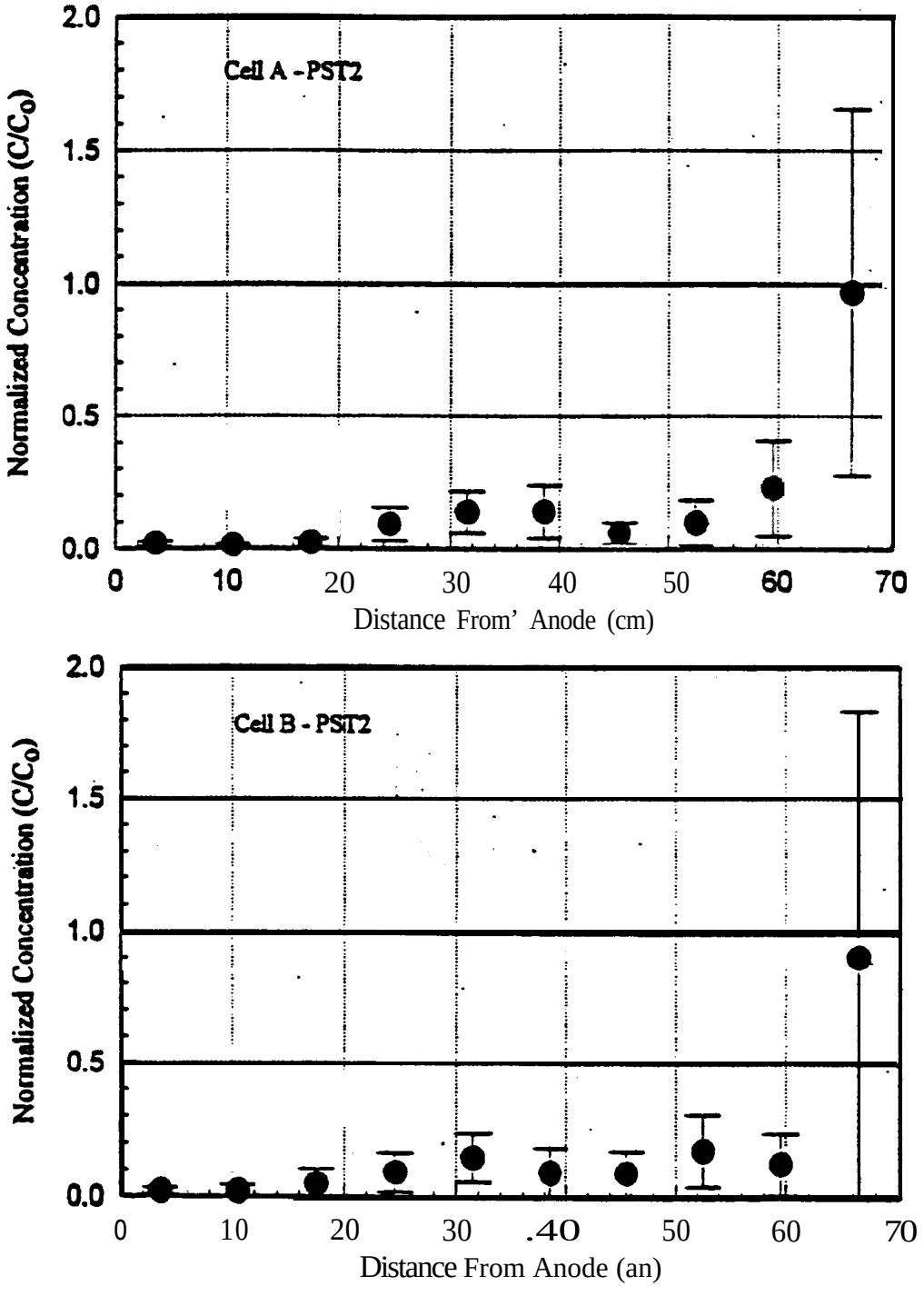

Figure 6.30: Mean and Standard Deviation of Final Lead Concentration across all Layers in PST2 after 2950 h at a Current Density of $I_o = 133\ \mu A/cm^2$ (a) Cell A and (b) Cell-B

near the anode) resulting in desorption and dissolution of lead into the pore fluid. Such conditions in low sorption capacity soils and acidic conditions resulted in almost no retardation in lead transport.

PST2 displayed different results than bench-scale tests in the mass of lead precipitated and/or electrodeposited at the electrodes. In PST2 about half of the initial lead was precipitated in the last 2 cm near the cathode, with almost no lead found on the cathode, whereas in BST2 most of the initial lead was found at the cathode. The differences between these tests were related to the differences in placement of electrodes. In pilot-scale tests, the electrodes are placed in compartments filled with water and separated from the soil with a fabric. This differs from bench-scale tests where the electrodes were separated from the soil by only a filter paper that was in direct contact with the soil and the electrodes. Lead precipitation within the last section near the cathode in PST2 was due to the high pH within that region. This section was in direct contact with the cathode compartment that had a pH of 11. It was necessary that the lead be dissolved in order to transport into the catholyte which necessitated a very high or low pH in the catholyte. Research ongoing at LSU and Electrokinetics Inc. is investigating the use of different enhancements techniques to eliminate the problem of heavy metal precipitation at the cathode (Acar et al. 1993).

Results of the pilot-scale tests demonstrated the efficiency of using the process for the transport of heavy metals from pilot-scale kaolinite samples. Specimens with high initial concentrations of lead (above the cation exchange capacity) displayed a more uniform removal than samples loaded at an initial concentration below the cation exchange capacity.

The results of the pilot-scale studies conducted demonstrate the feasibility of electrokinetic soil remediation. However, the effects of other factors, such as soil inhomogeneities, presence of a multicomponent electrolyte, and the presence of a variety of heavy metal salt at high concentrations should be further investigated.

6.11 **Energy Expenditure and Cost**

Evaluation of energy expenditure was an important component in evaluation of the total cost of the process. Energy expenditure is evaluated per unit volume of the soil treated in kWh/m^3.

A small increase in energy expenditure to about 3kh/m^3 occurred in thc first 100 h of processing BSTI and BST2 (Figurc 6.31). Subscqucntly, energy increased linearly with time to about 60 **kWh/m^3** in BSTl after 169 h and to 330 **kWh/m^3** in BST2 after 598 h. Differences betwcen the total energy expenditures in BSTl and BST2 were related to differences in processing periods. Processing time for BST2 was about 3.5 times that of BSTI. Both tests displayed similar behavior in energy expenditure because they shared the same current density and initial concentration.

Energy expenditures in PSTl, PST2, and PST3 increased slightly with time within the first 500 h of processing to about 50 **kWh/m^3** (Figure 6.32). Subsequent to the nonlinear segment **of** the first 500 h, energy expenditure increased linearly with time to about 325 **kWh/m^3** in PST1 after 1300h, 700**kWh/m^3** in PST2 after 2950 h, and 700 **kWh/m^3** in PST3 after 2500 h of processing. Figure 6.32 implies that the steady state conditions with respect to energy expenditure were realized within the first 500 h for PST1 and PST2, and within the first 700 h for PST3. Both bench-scale tests and pilot-scale tests have shown similar trends in energy expenditure. In all cases, energy increased at a low rate at early stages (100 h in bench-scale tests and 500-700 h in pilot-scale tests), then the rates increased and remained constant. Energy expenditure was directly related to the corresponding electric potentials. The nonlinear changes in energy expenditure realized early in the process were associatcd with the increase in the total voltage applied within the first 100 h in bench-scale tests and within the first 1000 h in pilot-scale tests.

The electric power per unit volume, P, evaluated the rate of increase in energy expenditure with time,

$$P = \frac{E I_t}{A L} = I_r \, i_e \qquad (6.9)$$

Figures 6.33 and 6.34 display time changes in the electric power in bench-scale specimens and pilot-scale specimens, respectively. Generally, the results displayed that the eletric power increased linearly with time until it reached a constant value (or steady state condition). In bench-scale tests, the electric power increased within the first 100 to 150 hours and reached a constant value of about 600 watt/m^3 For pilot-scale tests, 800 to 1000 hours were required for the power to reach a constant value of 250-350 **watt/m^3**. It was noted that, at steady state conditions, the electric power per unit volume of the soil in bench-scale tests was about twice that of pilot-scale tests.

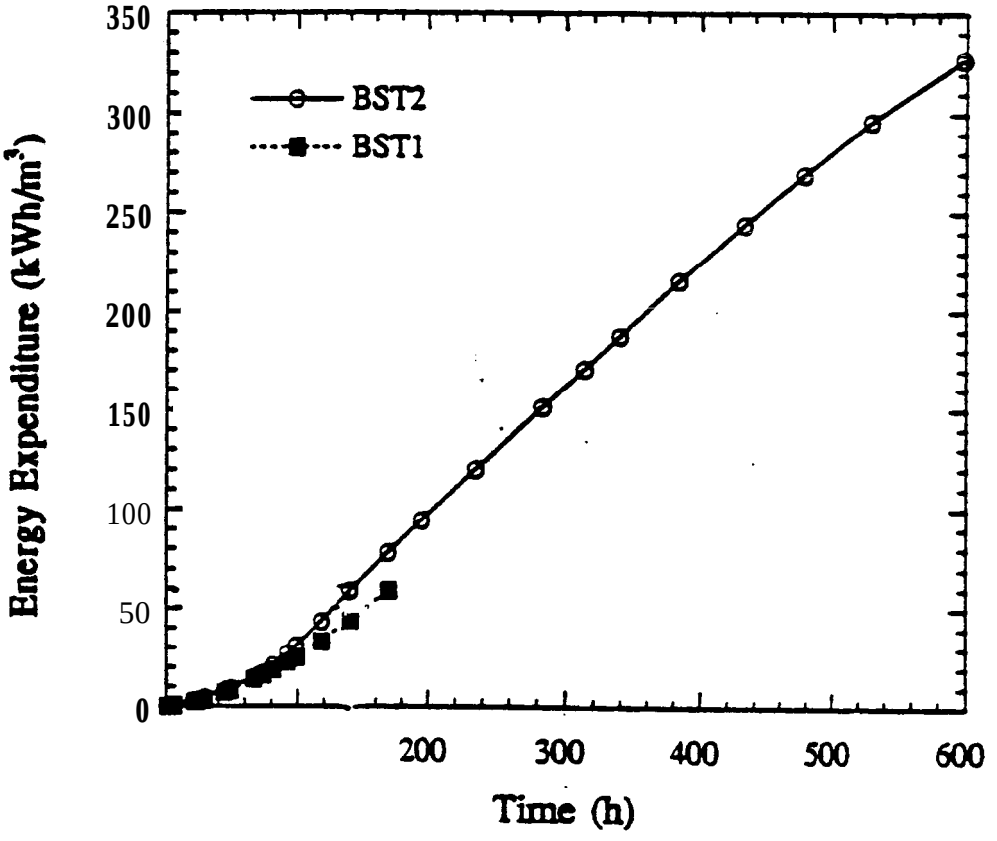

Figure 6.31: Energy Consumption in Bench-Scale Tests

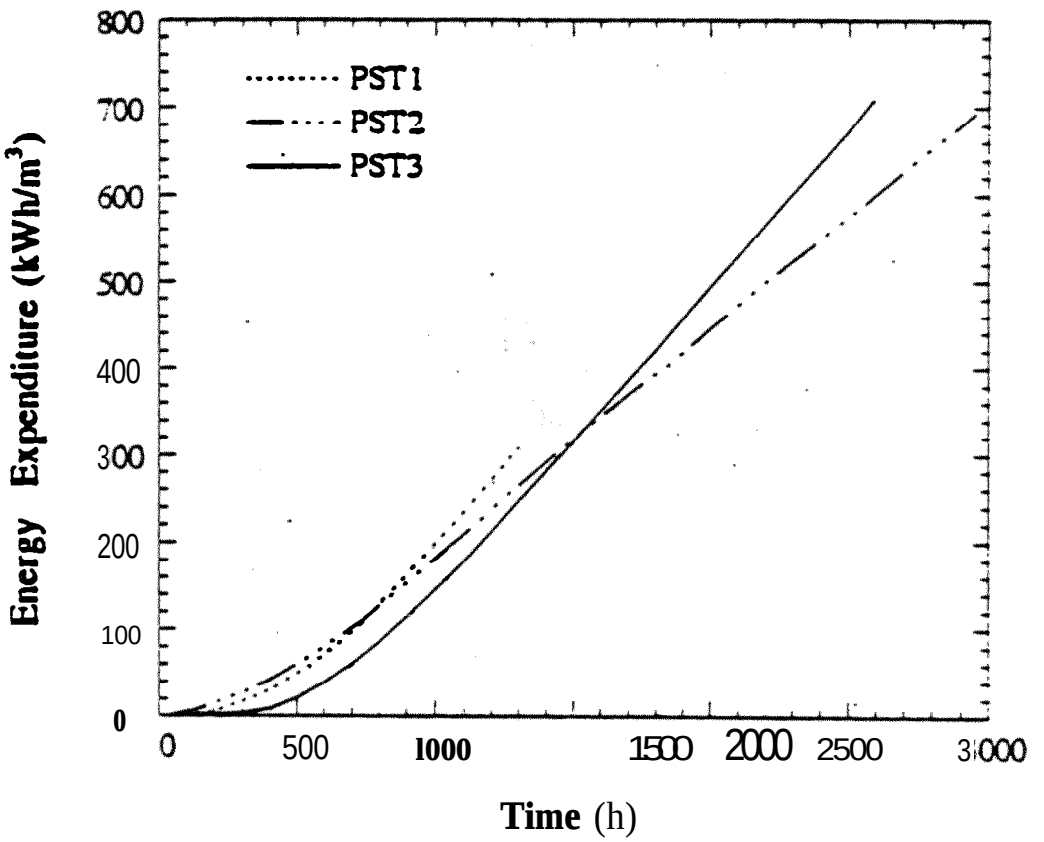

Figure 6.32: Energy Consumption in PST1, PST2, and PST3

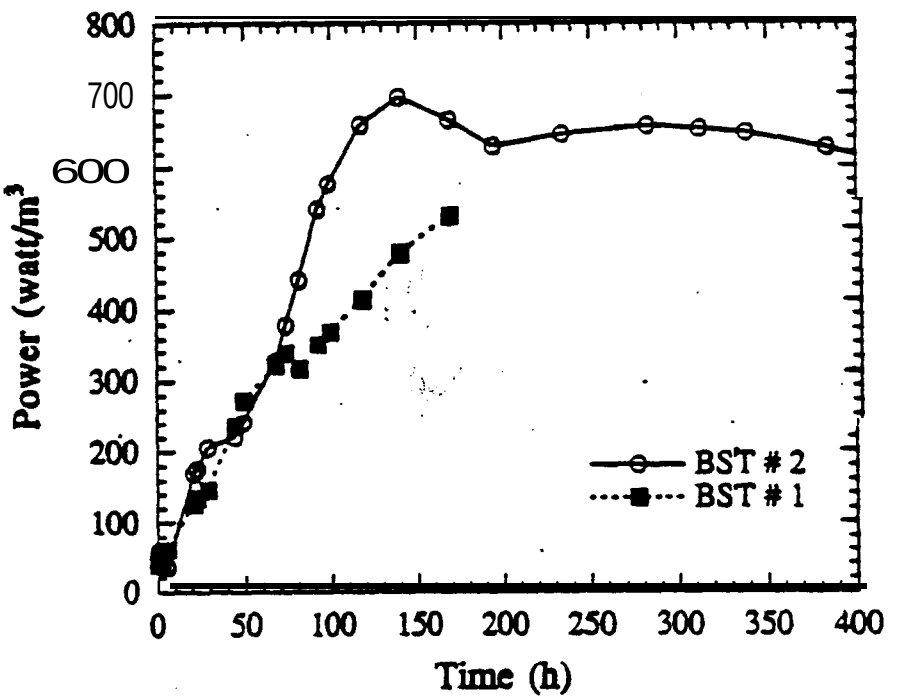

Figure 6.33: Changes in the Electric Power in Bench-Scale Tests

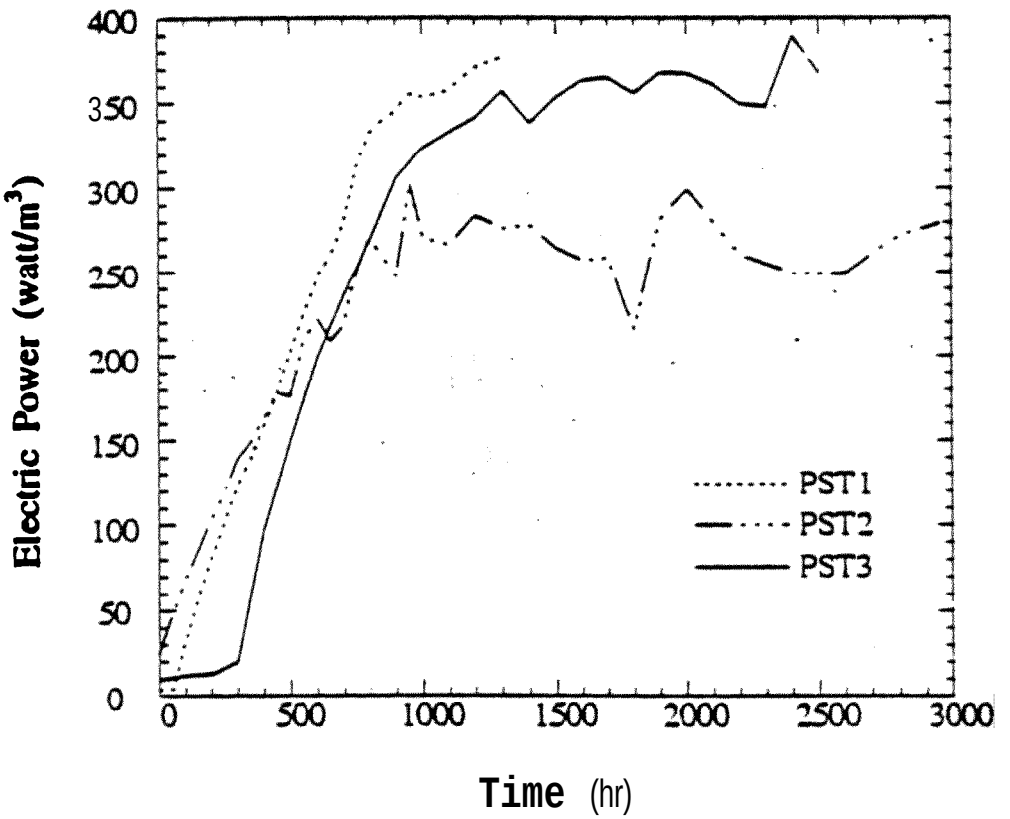

Figure 6.34: Changes in the Electric Power in Pilot-Scale Tests

Equation 6.9 shows that the electric power was equal to the current density times the voltage gradient. For all bench-scale and pilot-scale tests, the current density was the same and therefore, changes in the power and energy expenditure were due to changes in the voltage gradient. Comparing the bench-scale and pilot-scale tests, the final electric gradients across the samples were about 5 V/cm in bench-scale tests and 2-3 V/cm in pilot-scale tests as discussed in previous sections. Table 62 summarizes the differences between the electric properties and energy consumption of bench-scale and pilot-scale specimens at the end of processing.

6.12 Pore Fluid Chemistry

Figure 6.35 shows the distribution of the free anions in the soil pore fluid at the end of processing PST2. Free anions concentrations were determined by mixing 2.0 g of dry soil with 40.0 ml of deionized water. The results displayed a uniform distribution of these anions across the soil between the electrodes. Metals' distributions at the end of the processing of PST2 are shown in Figure 6.36. Distribution of AI was shown in a separate figure because it was present at concentrations significantly higher than the other cations. Ca and Na showed almost a uniform distribution across the sample. Fe had the same uniform distribution but with an increase at the last section near the cathode. This increase in Fe concentration might have been related to precipitation of its hydroxides at their solubitity limit in the zone of high pH near the cathode.

Both Al and Si displayed concentration profiles different than the other metals. Their concentrations at the anode zone were significantly less than those at the cathode zone. Their distribution was similar in shape to the final pH across the specimen. The acid generated at the anode resulted in dissolution of the clay mineral releasing A1 and Si which were then transported under the electric gradient to the cathode. This may have been a reasonable explanation of reduction in the source concentration of these species at the anode. On the other hand, at the cathode the pH did not drop to a value that could have caused mineral dissolution. The effect of pH changes across the soil on mineral dissolution would also affect the electroosmotic flow and the sorption capacity of the clay. Such effects on the efficiency of the process were not investigated.

Table 6.2: Measurement Units Used for Variables Identified in EK-REM

Parameter	BSTl	BST2	PST1	PST2
Final Electric Gradient *(V/cm)*	4.2	4.2	2.9	2.0
Final Electric Conductivity *(μS/cm)*	30	30	50	70
Final Electric Power *(watt/m³)*	520	650	380	270
Energy Expenditure *(kWh/m³)*	60	330	325	700
Processing Time	69	596	1300	2950
Energy cost=*($/m³)*	3.0	16.5	16.3	35.0

. =0.05$/$m^3$

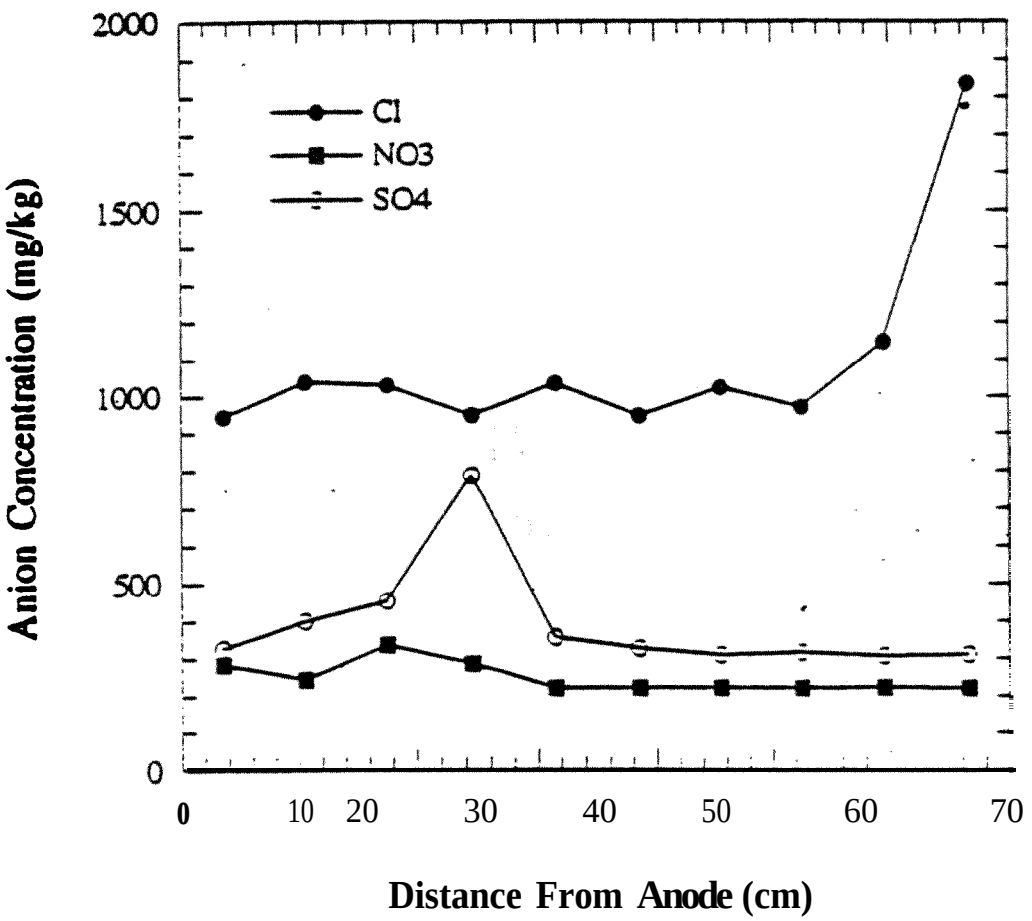

Figure 6.35: Final Anion Concentration in the Soil Pore Fluid in PST2

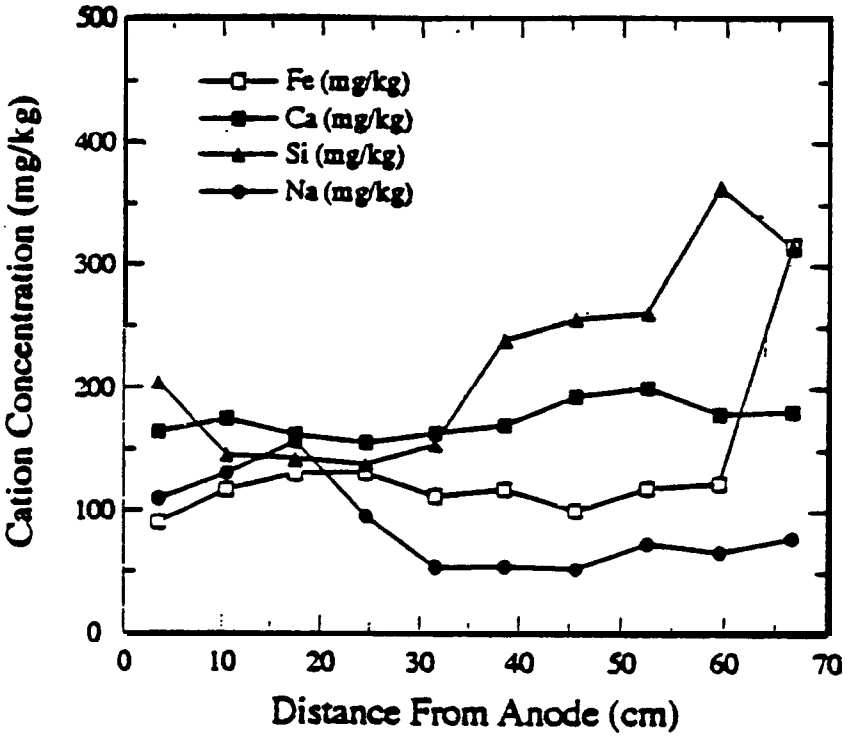

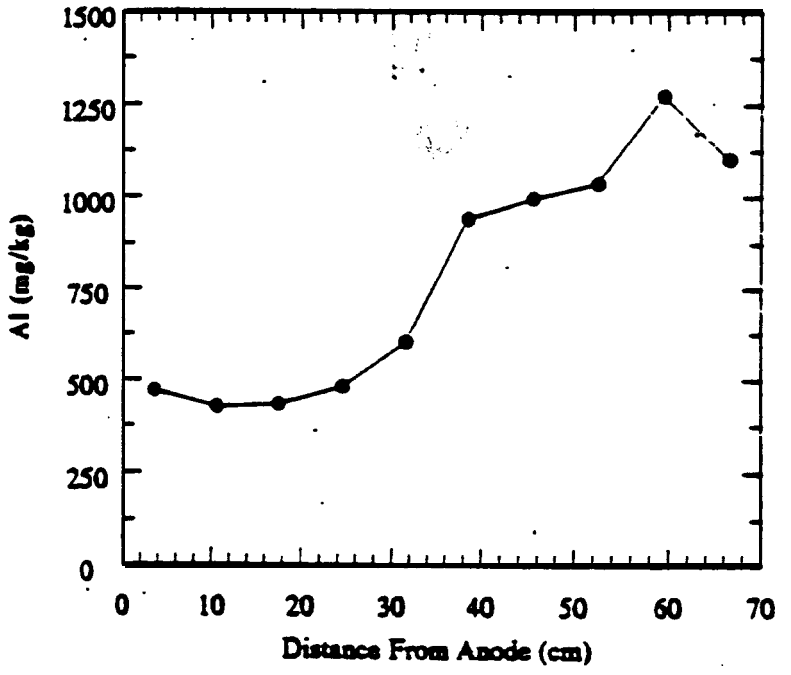

Figure 6.36: (a) Find Cation Distribution across the Soil Specimen in PST2 (b) Final **A1** Distribution across the Soil Specimen in PST2

6.13 Temperature Changes

Thermocouples were used to monitor temperature changes across the soil specimen and at the electrodes. Figure 6.37 displays these changes for PST2. Data for temperature changes in this test are presented in Appendix D. Four thermocouples were used in this test; one in the cathode compartment (catholyte), one in the anode compartment (anolyte), one in the soil at the anode region, and the fourth one is placed in the soil at the cathode region (Figure 5.9). The thermocouple placed in the anode region failed and rendered unrealistic temperature values. Reliable measurements were obtained from the other three thermocouples.

In PST2, the original temperature before processing the sample was 23° C. The results demonstrated an increase in the temperature at different rates across the soil specimen and at the electrode compartments. Soil sections near the cathode experienced the highest increase in temperature (23° C to 42° C) while the anolyte experienced the lowest increase in temperature (23^0 C to 35° C). The heat flux due to electrical gradients was a function of the electrical potential gradient and heat conductivity of the medium under electric fields. The electrolyte concentration was again expected to have a significant role in generation of heat. When the pore fluid conductivity was high, the resistance to current should have been low, and energy loss due to heat should have been relatively low. On the other hand, the zone of high electric resistance near the cathode resulted in higher voltage drop and energy loss.

Most of the temperature increase occurred in the first 1000 h of processing, which was the same time that showed most of the increase in the voltage across the soil. Differences in temperature changes between the soil and the electrode compartments were related to the voltage distribution. Most of the voltage drop was developed at the cathode region resulting in a higher increase in temperature at that zone.

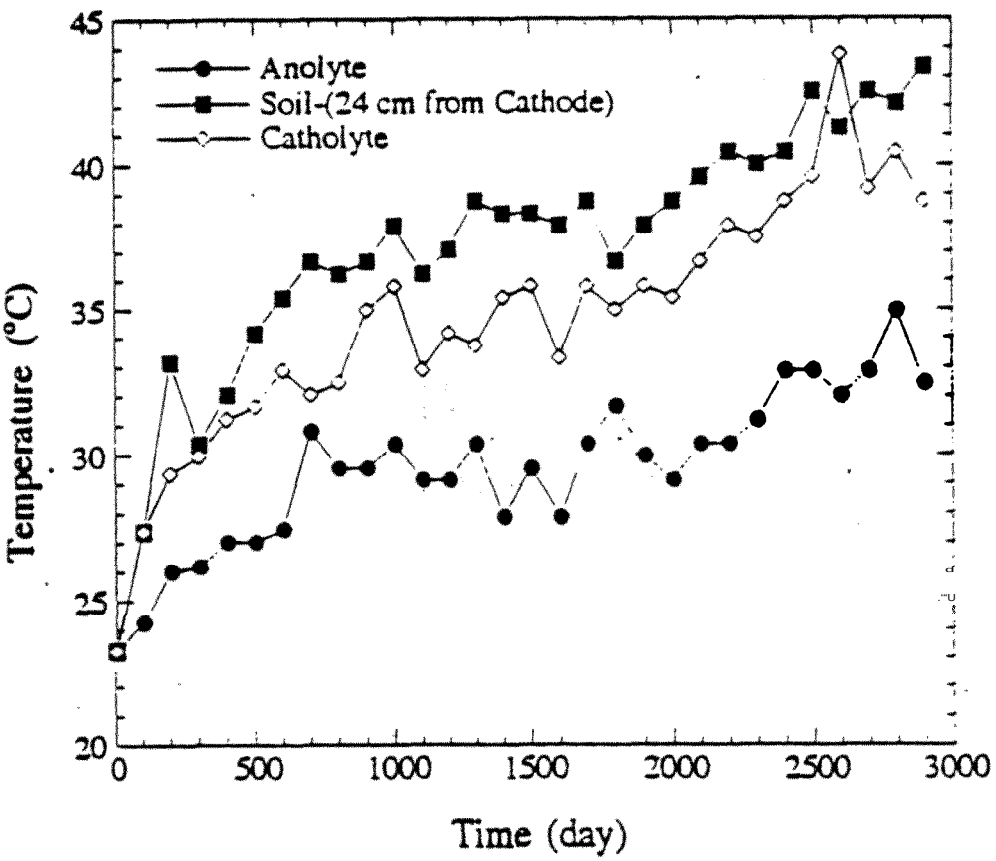

Figure 6.37: Temperature Changes in PST2

6.14 Data Quality

Precision, completeness, acuracy method detection limit, and mass balance were the data quality indicators used in this study. Procedures and relations used for evaluation of these indicators are presented in Appendix F.

Precision: Duplicate measurements were taken for 20% of the samples. Precision was expressed as relative percent difference (RPD). Table 6.3 shows the results and precision calculations for the second layer in PST2. In all duplicate samples, the RPD was less than 40, which was specified as the maximum allowed value in the QA/QC Project Plan. Accordingly, all these measurements are considered valid with 100% completeness (%C).

Accuracy : Accuracy of data can be expressed as percent recovery (%R) from laboratory matrix spikes. Table 6.4 shows sample results used for accuracy evaluation. Three spikes with initial lead concentration of 10, 50, and 90 mg/kg and blank samples were analyzed for lead content. Percent recovery in all samples was greater than 95%. Two of the samples had percent recovery greater than 99%.

Initial lead concentrations were measured after mixing and compaction. The measured concentrations were then compared with the targeted concentration as described in Section 5.12. Table 6.5 compares targeted values to measured values. The results show that the target concentration were not identically achieved, but they fell within a standard deviation of the measured values. It is noted that measured lead concentrations in the pilot-scale tests were higher than the target concentrations, while the opposite is true for bench-scale tests. It was possible to employ a stricter control in the bench-scale tests rather than the pilot-scale tests. In any case, percent recovery in these measurements were between 95% and 107%.

Mass balance: Mass balance calculations are presented in Figures 6.23, 6.26, and 6.29. In all tests, the error was less than 20%. This error is not expected to significantly affect the quality of data collected. The error could be to related human, instrumental, and/or procedural error. In the pilot-scale tests, each sample is representative of about 3 kg of soil. Although, care was taken in homogenizing and mixing each sample, minor variations in the concentration could affect the results. In any case, an error of less than 20% in mass balance calculations was expected and the results meet the QA/QC project plan objectives of a maximum mass balance error of 20%.

Table 6.3 Sample Precision Calculations for the Second Layer in PST2

Section	X (cm)	Y (cm)	C1 (mg/kg)	C2 (mg/kg)	RPD (%)
A2 - A1	3.5	11.25	30.48	23.4	26.28
A2 - A2	10.5	11.25	18.28	17.74	3.00
A2 - A3	17.5	11.25	15.94	14.54	9.19
A2 - A4	24.5	11.25	89.36	71.28	22.51
A2 - A5	31.5	11.25	283.00	227.40	21.79
A2 - A6	38.5	11.25	146.50	168.36	13.89
A2 - A7	45.5	II.25	25.86	33.64	26.15
A2 - A8	52.5	11.25	274.40	197.38	32.65
A2-A9	59.5	11.25	95.78	115.4	18.58
A2 - A10	66.5	11.25	1959.60	1670.60	15.92

Table 6.4 Sample Accuracy (% Recovery) calculation for Lead Spiked Samples

Sam ple Number	Actual Conc. (mg/kg)	Measured Spiked Conc. (mg/kg)	Measured Unspiked Conc. (mg/kg)	% Recovery
Sample 1	10.00	10.06	0.53	95.30 %
Sample 2	50.00	50.18	0.54	99.28 %
Sample 3	90.00	90.26	0.54	99.69%

Table 6.5 Target and Measured Lead Concentrations in Bench-Scale and Pilot-Scale Tests

Test	Target Concentration (mg/kg)	Measured Concentration (mg/kg)	Standard Deviation of Measd. Conc. (mg/kg)	% Recovery
BST1 & BST2	1,500	1,439	79	95.9
PST1	850	856	54	100.1
PST2	1,500	1,533	63	102.2
PST3	5,000	5,322	417	106.4

Section 7

MODEL PREDICTIONS AND COMPARISONS WITH PILOT-SCALE TEST RESULTS

7.1 Introduction

The principles of modeling coupled-reactive **multicomponent** species transport under an electric field in a saturated soil results in a system of differential/algebraic equations. These are presented in Section **3. The** partial differential equations describe fluid, charge, and species transport while algebraic equations describe the chemical reactions in the soil pore fluid. Section 4 presents the numerical scheme used to solve the developed system. The computer code EK-REM (ELECTROKINETIC REMEDIATION) is written using Fortran on an IBM **RS/6000** cluster running with the Unix operating system. A list of the program and the input and output pertinent to the pilot-scale study are given in Appendices A and B. A summary of the subroutines is presented below.

7.2 Flow Chart for EK-REM

Figure 7.1 presents the flow chart of EK-REM. The main program opens the files where the input and output of the numerical calculations are saved. EK-REM also reads the time step (DT), number of nodal points (NUMNP), elements (NUMEL), species (NCONT), and cycles (NCYCLE) from the input file before calling subroutine INPUT.

Figure 7.2 describes a flow chart for subroutine INPUT which reads the initial parameters and initial conditions pertaining to the system. At each node, INPUT requires the coordinates, boundary condition codes together with the initial potentials and species concentrations in the pore fluid. Initial soil parameters such as the hydraulic conductivity, coefficient of electroosmotic permeability, tortuosity, porosity and total length of the specimen are defined in INPUT. Diffusion coefficients and electric charges of the chemical species are also input in this subroutine. Finally, INPUT reads the boundary conditions for each element and specifies the concentration or

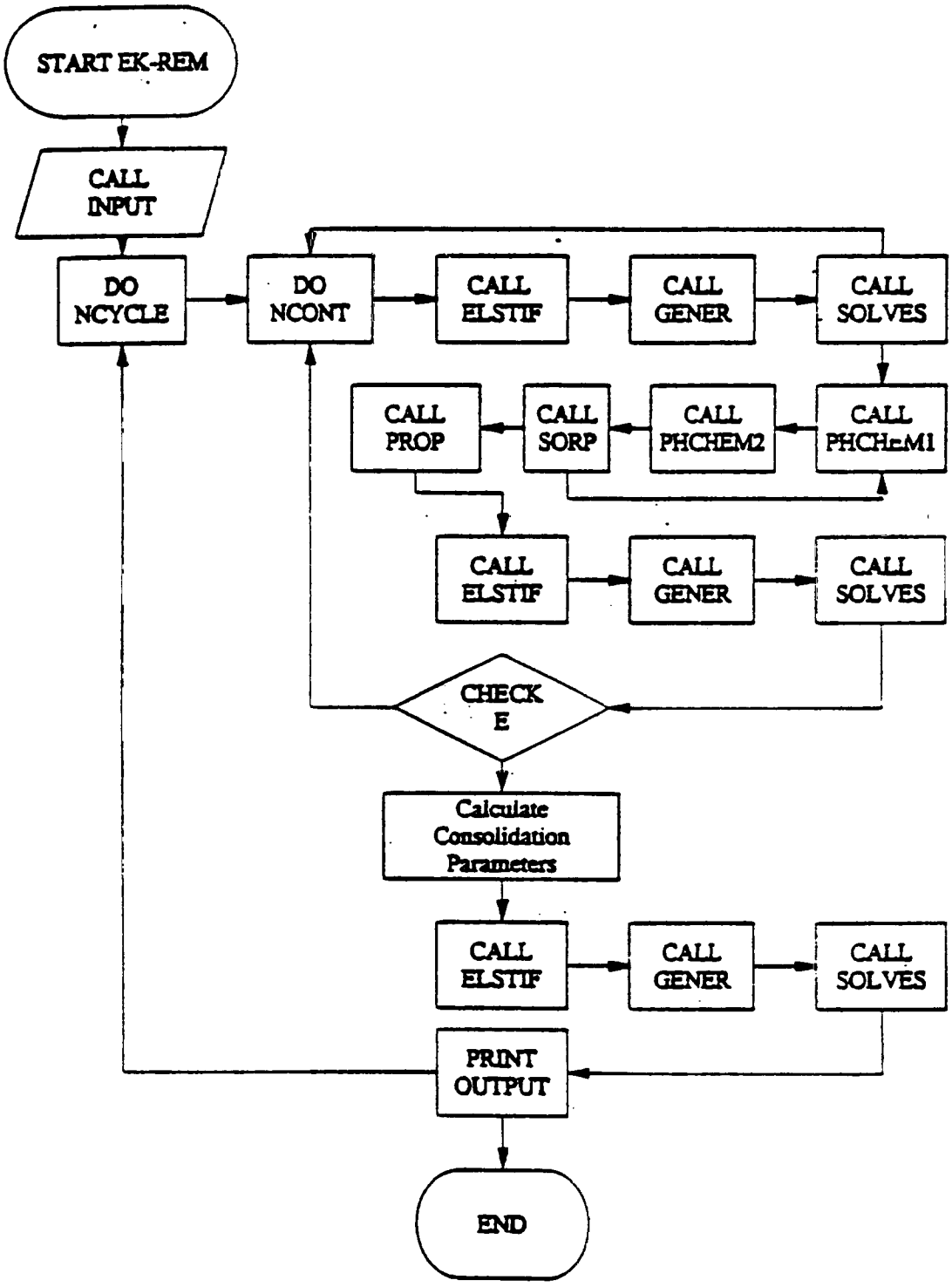

Figure 7.1: Flow Chart for EK-REM

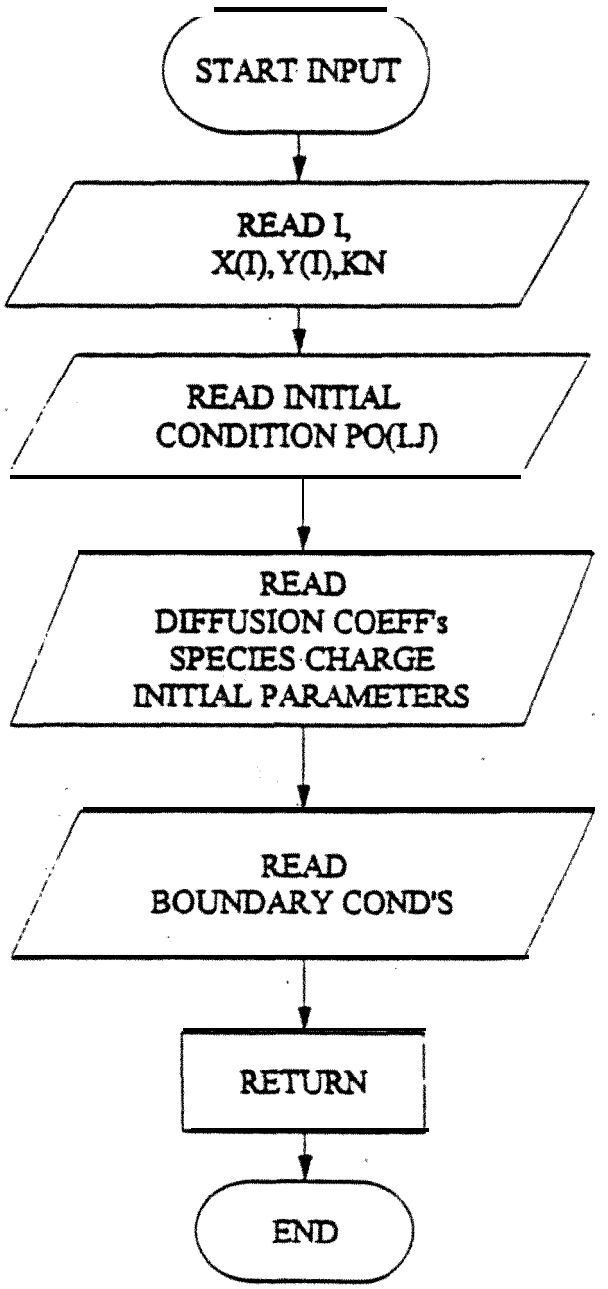

Figure 7.2: Flow Chart for Subroutine INPUT

flux of each species at these boundries. EK-REM employs the data fed in INPUT to calculate the effective parameters of the differential and algebraic equations (such as the effective diffusion coefficient and effective ionic mobility). Calculations for the first time step start with solving the differential equations describing species transport. For every species, EK-REM calls subroutine ELSTIF, subroutine GENER and then subroutine SOLVES to evaluate their concentration across the soil mass. Subroutine ELSTIF calls subroutine FORMBM which calculates the shape functions, their first and second derivatives, and the Jacobian matrix for each elenent. ELSTIF uses these values to form [SKf], [VL] [AK], [VB] [E], {QQ}, and {F} matrices defined by equations 4.144-4.148. This operation is carried out for each species and at every element. ELSTIF first uses the initial distributions of the electric and hydraulic potential (time =0) in evaluation of members of these stiffness matrices. Figure 7.3 shows the flow chart for ELSTIF.

Subroutine GENER uses the matrices evaluated in ELSTIF to generate the master stiffness matrix A to calculate the column vector b for each dependent variable at every timestep. Subroutine SOLVES sends A and b to subroutine CHOLES which uses Choleski decomposition to invert the **A matrix** and multiply it with b vector in evaluation of the concentrations at the first time step.

Subroutines PHCHEMI, PHCHEM2, and SORP are then called. These subroutines evaluate the concentration of the chemical species when subjected to the chemical reactions described by the algebraic equations.

EK-REM then calls subroutine PROP which evaluates the first and second derivatives of the concentration of each species at every element to determine the parameters to be used for the charge and water transport equations. PROP uses the shape functions and their derivatives (evaluated in FORMBM) to determine the first and second derivatives of species concentrations. The parameters that will be used in the charge conservation equation are then evaluated. These parameters include the effective electric conductivity and its gradient and the component of diffusional charge flux. EK-REM calls ELSTIF, GENER, and SOLVES to provide the solution for the differential equation describing variation of the electric potential across the electrodes.

The newly calculated electric potential distribution is then compared with the initial values at each node. If the difference is more than 0.5V at any node, then EK-REM loops over these steps taking the newly calculated potential distribution as the initial profile.

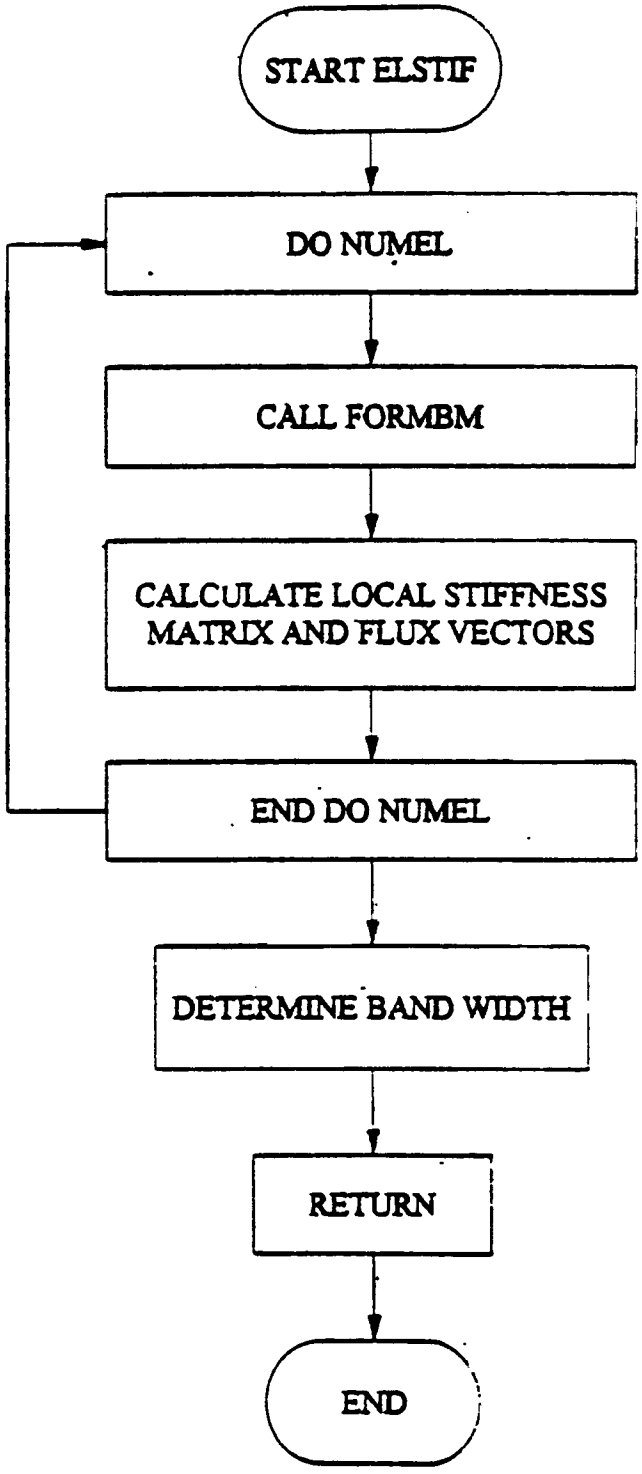

Figure 7.3: Flow Chart for Subroutine ELSTIF

When the concentration and electric potential distributions across the specimen are evaluated, the second derivative of the electric potential is calculated and the differential equation describing the electroosmotic consolidation is solved by calling subroutines ELSTTF, GENER, and SOLVES. EK-REM then calculates other variables such as electrooosmotic flux and energy consumption. At this point, the results for this time step are saved in the output files. A second step in time is then taken.

7.3 Modeling Lead Transport and Removal

The initial conditions for PST3 are used in the computer program developed for transport and removal of lead. Soil parameters and constitutive relations are evaluated, either through laboratory tests conducted on soil specimens retrieved from the pilot-scale cell, or approximated from data presented in the iterature. since several variables with different measurement units are used in this model, non-nomalized parameters are used. Table 7.1 summarizes the measurement units chosen. The input and output data in EK-REM are listed in these units.

7.3.1 Soil Parameters and Constitutive Relations

Accurate estimates of soil parameters and proportionality constants in the constitutive relations are a substantial component for accurate predictions using the model. Different parameters are identified and required in modeling coupled reactive multicomponent species transport under electric fields. Table 7.2 summarizes the values of the parameters and proportionality constants used in modeling PST3.

The principal objective of comparing the predictions of the theoretical model with the pilot-scale test results is to assess whether or not the theoretical formalism presented reasonably predicts the mechanics and chemistry of multispecies transport under an electric field. Therefore, it is not necesary to use acurate measurements of all soil parameters.

Table 7. 1 : Measurement Units Used for variabIcs Identified in EK-REM

Variable	unit
Length	cm
Time	day
Concentration	
Pore Fluid	*mole/L*
Soil Mass	mg/kg
Electric Potential	*V*
Current	A
Hydraulic Head	cm
Diffusion Coefficient	cm^2/day
Ionic Mobility	cm^2/day - V
Hydraulic Conductivity	cm/day
Coefficient Electroosmotic Permeability	cm^2/day – V
Faraday's Constant	Coulomb/mole

Table 7.2: Paramenters and Relations Used in Modeling Lead Removal from Kaolinite by Electrokinetics

Parameter	Value
D_H	8,05 cm^2/day
D_{OH}	4.57 cm^2/day
D_{Pb}	0.82 cm^2/day
D_{NO3}	1.64 cm^2/day
D_{Na}	1.15 an^2/day
D_{Cl}	1.76 cm^2/day
k_e	$8.64x10^{-1}$ $cm^2/day - V$
k_h	$5.87x10^{-3}$ *cm/day*
L	70 cm
n	0.56
τ	0.44
$m_w\gamma_w$	$0.1x10^{-5}$ /cm

7.3.1.1 Diffusion Coefficients and Ionic Mobilities

Diffusion coefficients and ionic mobilities of species of concern at infinite dilution are presented in Tables 3.3 and 3.4 and the values are taken directly from these tables.

7.3.1.2 Tortuosity Factor

Table 3.2 demonstrates that the tortuosity factor, π, for kaolinite varies over a range of 0.12 to 0.50. Alshawabkeh and Acar (1994) and Acar et al. (1989) use a tortuosity factor of 0.35 for kaolinite and show that reasonable predictions of acid/base transport are obtained. Shapiro et al. (1989) and Shapiro and Probstein (1993) use a different definition for the tortuosity, which is equivalent to a factor of $(1/1.24)^2$ or a tortuosity factor equivalent to 0.65 for kaolinite. Eykholt (1992) uses a term similar to that of Shapiro and Probstein (1993), a value equivalent to a tortuosity factor of $(1/1.5)^2=0.44$ is used for kaolinite. The tortuosity factor for kaolinite specimens is not evaluated by separate tests. A value of 0.45 is used in the model.

7.3.1.3 Coefficient of Electroosmotic Permeability

The coefficient of electroosmotic permeability varies over a wide range (10^{-4} to 10^{-7}); the higher values are those for lower activity clays at higher water contents. Ballou (1955) reported k_e values up to 1.1×10^{-4} cm^2/Vs for a sodium-kaolinite sample at 92% water content. Experiments at Louisiana State University rendered maximum k_e values of 10^{-5} cm^2/Vs in lead-, cadmium-, or chromium-spiked kaolinite specimens (Hamed et al. 1991; Acar et al. 1994; Acar et al. 1990; Hamed 1990).

Earlier attempts to model the electrokinetic process have used k_e values in the order of 10^{-5} cm^2/Vs. Alshawabkeh and Acar (1992) used a coefficient of electroosmotic permeability of 1×10^{-5} cm^2/Vs for kaolinite, Yeung (1990) and Mitchell and Yeung (1991) used a value of 2×10^{-5} cm^2/Vs for the coefficient of electroosmotic permeability for an illitie Altamont clay. Shapiro and Probstein (1993) evaluated the electroosmotic flow using zeta potential. Eykholt (1992) also evaluated the

electrooosmotic flow as a function of zeta potential and used a zeta potential that is dependent upon the soil pH. A constant k_e value of $1x10^{-5}$ cm^2/Vs is used in this study.

An electroosmotic flow was not measured in PST2 or PST3. However, this does not necessarily imply that there was not any electroosmotic flow. As discussed, boundary conditions may be the fundamental reason why a flow was not recorded. Furthermore, it is not well established what the meaning of the k_e value would be with the continuously changing chemistry and electric potential gradient across the electrodes. Consequently it is decided to use a constant k_e value of $1x10^{-5}$ cm^2/Vs for this specimen. This value is reported for the first 100h to 200h of processing of most kaolinite specimens tested by Hamed (1990). It **seems** reasonable while it is not an accurate value. It is essential to provide better experimental measurements to obtain the values of coefficient **of** electroosmotic permeability with less physical and chemical inhomogeneities.

7.3.1.4 Coefficient **of Volume Compressibility**

Two soil blocks, each of 30cm by 30cm dimensions, are extracted from the middle part of PST2. Two horizontal soil samples, one for consolidation and one for hydraulic conductivity measurement, are taken from one block while two vertical samples are taken for the same purpose from the other block. Consolidation samples are extracted from these soil blocks using consolidometer rings each of 5.0cm diameter and 2.0cm length. Two consolidation tests are conducted on these samples. Coefficient of volume compressibility (mv) is calculated for each specimen using the square root time method at 8kg and 16kg loadings (40 kPa and 80 kPa stress).

7.3.1.5 **Hydraulic Conductivity**

Two hydraulic conductivity tests are conducted, one on the sample extracted horizontally and the other on the sample extracted vertically. Each of these samples is 10.2cm in diameter and 5.2cm in length. Constant rate of flow test (ASTM D5084 method D) is used for hydraulic conductivity measurement. Figure 7.4 shows measurement of hydraulic conductivity of the sample retrieved horizontally from the pilot-scale cell (Gokmen 1994).

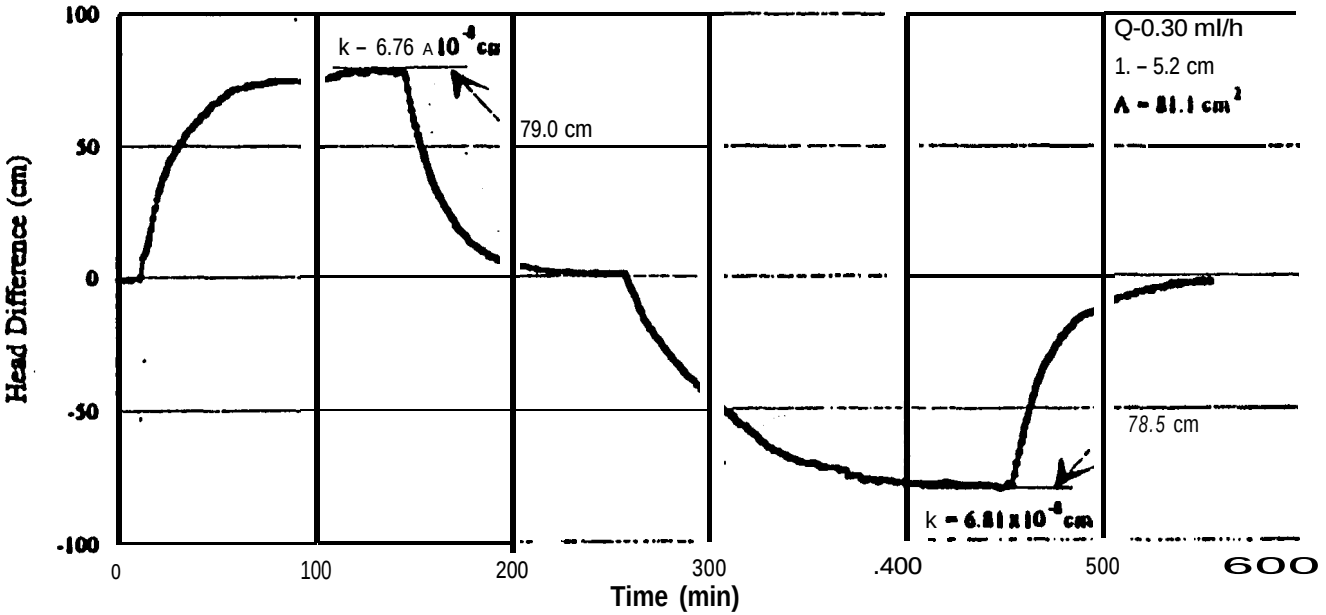

Figure 7.4: Hydraulic Conductivity Measurement of the Horizontal Sample (Gokmen 1994)

7.3.1.6 Lead Sorption

Lead sorption at different pH and concentration levels is described by an empirical relation that is discussed in more detail in Section **3.7. The** parameters of this relation are **determined using** the results of the study by Yong et al. (1990). Figure 3.7 presents a comparison of the experimental data of Yong et al. (1990) and the relation used for modeling lead sorption during processing. It is noted that the relation describes complete sorption of the pore fluid lead at higher pH values. Studies on the effect of pH on heavy metal sorption demonstrate that higher pH values ($\geq$ 7) result in complete retardation of the pore fluid metals (Maguire et al. 1981; Harter 1983; Yong 1990). However, when the pore fluid is basic, soil may display a different sorption behavior. Any attempt is not made to assess and rationalize adsorption at high pH values.

7.3.1.7 Hydrogen Retardation

Georgia kaolinite has a low cation exchange capacity (1.06 meq / 100 g) and low buffering capacity. Yong et al. (1990) has reported that kaolinite does not show major resistance to changes in the pH due to its low buffering capacity. This indicates that significant retardation in the transport of H+ may not be encountered in kaolinite. However, it is noted that the values used for the effective ionic mobility of H + (using the molecular value, soil porosity and tortuosity) do not provide reasonable predictions of the rate of advance of H +. In all cases, the predicted profiles show much faster advance rates for H + than the measured profiles (up to 10 times). Differences between the theoretical and experimental effective ionic mobility (and diffusion coefficient) are related to either the tortuosity factor or the value of the molecular mobility. Tortuosity factor for kaolinite does not vary significantly with a change in fabric (0. 1 to 0.5). Variation of the tortuosity within that range will effect transport rates. The presence of other species in the pore fluid and the effect of multicomponent mobilities also will affect the effective values, rendering lower experimental values. It is esssential to estimate **a** retardation factor for H+ transport. Such a factor can either be obtained from batch adsorption tests **or from** bench-scale tests; Both experiments have their difficulties in providing an accurate retardation factor for H+. The surface charge density and adsorption behavior of kaolinite changes with decreasing pH making it quite difficult to formalize the kaolinite-H+ adsorptive behavior. Special experimentation is necessary to evaluate

the ionic migration of H+ in soils under an electric fidd Therefore it seems reasonable to estimate **a retardation** factor using the results of the pilot-scale study.

Figure 6.8 shows the relation between the distance from the anode and the time required to reach a pH of 3 in PST3. The rate of advance of the acid front estimated in this test is 1.0cm/d. The molecular ionic mobility of H+ at infinite dilution **is** 313 cm^2/Vd (Table 3.3). When an average tortuosity of 0.45 and a porosity of 0.56 are used, the theoretical value of effective ionic mobility is 79 cm^2/Vd. Voltage gradients in the anode zone are about 0.01 to 0. 1 V/cm, rendering a rate of advance of the acid front of 0.8 cm/d to 8.0 cm/d. If an average rate of 4.6 cm / d is taken, a retardation factor of 4.6 is obtained when the calculated rate is divided by that evaluated from the experiment. It is noted that this value will significantly affect the predictions of transport of the acid/base profile, the extent of the prediction zone, the magnitude and distribution of the electric potential, its gradient as well as the location and magnitude of the pore water pressure developed across the electrodes.

7.3.2 **Initial and** Boundary **Conditions**

Four differential equations are used to describe the transport of 4 chemical species in the soil pore fluid; Pb^{2+}, H+, OH-, and NO^-_3. The differential equation describing conservation of charge together with the differential equation describing electrooosmotic consolidation bring the total number of differential equations to 6. Four algebraic equations are used in addition to describe chemical reactions of lead in the soil pore fluid. For one dimensional applications, the partial differential equations require 6 initial conditions and 12 boundary conditions. However, the algebraic equation describing preservation of electrical neutrality replaces one differential equation, decreasing the number of differential equations to 5, and boundary conditions to 10.

Table 7.3 summarizes the initial and boundary conditions for the differential equations used in the numerical simulation of PST3 (refer to Section **3.7** for definitions and development of these parameters). Initial H+ and OH- concentrations are taken as $1.0x10^{-4}M$ and $1.0x10^{-10}M$ because the initial soil pH is 4. The total initial lead concentration is 5,322 $\mu g/g$ or 0.0825 M. The initial hydraulic head is zero and initial electric potential gradient is assumed to be **0.1 V/cm** all across the

Table 7.3: Initial and Boundary Conditions Used in EK-REM

Variable	LC.	Boundary Condition $\|_{x=0}$	Boundary Condition $\|_{x=1}$
c_H	$10^{-4}M$	$J_H\|_{x=0} = c_H^e J_w + (I/F)$	$J_H\|_{x=1} = c_H^e J_w$
c_{OH}	$10^{-10}M$	$J_{OH}\|_{x=0} = c_{OH}^e J_w$	$J_{OH}\|_{x=1} = c_{OH}^e J_w - (I/F)$
c_{Pb}	0.0825M	$J_{Pb}\|_{x=0} = 0.0$	$J_{Pb}\|_{x=1} = 0.0$
E	$\frac{\partial E}{\partial x} = 0.1$	$I\|_{x=0} = I$	*0.0*
h	'0.0	0.0	*0.0*

I=130x10^{-6} A/cm^2

F=96,485 C/mol

soil. Boundary conditions for the equations describing species transport equations are evaluated using electrolysis reactions at the electrodes as described in Section 3.

The code is devdoped far two-dimensional applications, therefore it is necessary provide a two-dimensional mesh even for a one-dimensional problem. Forty elements are used each of 1.75 c m width x1.75cm length, with a total of 203 nodal points. It was not found necessary to increase the number of elements as the 8-nodal element is a higher order element. Figure 7.5 presents the one dimensional mesh with 40 elements to demonstrate the procedure used in coding each element and node. Appendix B presents the input data file and node connectivity used for the case of 40 elements. The output for the first time step is also presented.

It is essential to achieve a stable and convergent finite element solution. Element sizes and time steps are varied to achieve acceptable values. The time step required for a stable finite element solution for a specific element size depends on the parameters of the differential equation. In general, stability of the Galerkin finite element method is not considered to be a major problem, specially if the parameters are independent of time [(numerical oscilllation may occur, but the Galerkin method is never unstable (Reddy 1985)]. In this case, however, species concentrations in the pore fluid, pH, and electric conductivity change dramatically with time. Since the time step required for a stable solution depends on these parameters, the range of time increments that render a stable solution changes in time due to dramatic changes in parameters (specifically the electric conductivity, and the first and second gradients of species concentrations). There is no method yet specified to choose the required time step and element size for a stable solution of a system of differential equations with such changes.

Different trials are made using different time steps until a stable solution is achieved for a specific element size. This approach is first used in verifying the finite element solution with the existing analytical solutions. It is noted that the numerical solution changes if the time step is changed; however, in each case and for a specific time step range, a convergent and stable solution is achieved. The finite element solution for this range is shown to compare well with the analytical solution. Appendix C provides comparisons between the two solutions.

The sharp fronts developed in the electric conductivity and concentration gradient profiles lead to computational problems after 50 days of processing. It was not possible to achieve a convergent solution for the system at that time. Since the objectives of this study are achieved

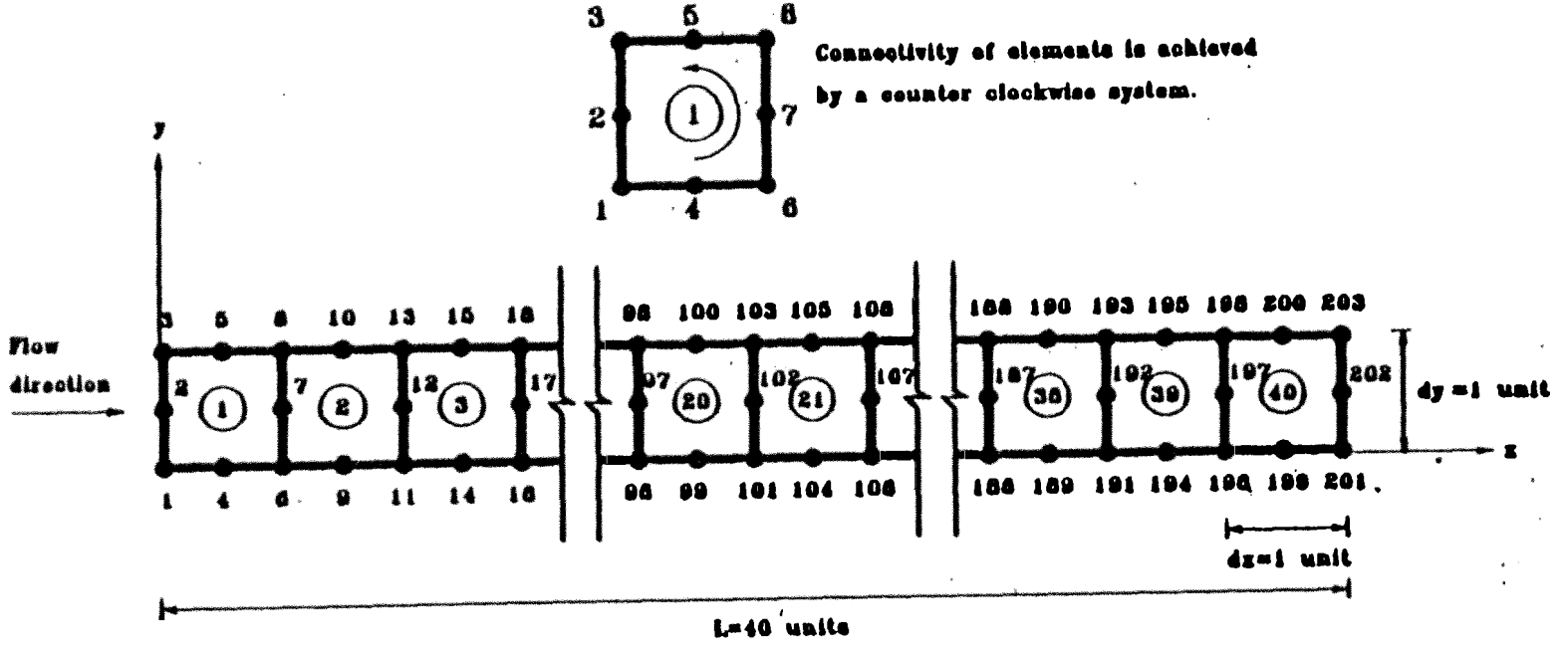

Note: Flow is one dimensional, and in x direction.

Figure 7.5: Finite Element Mesh of 40 Elements

through comparisons of the model predictions and the experimental results within the first 50 days, it is decided to stop and report the results while there exists the need to overcome the instability subsequent to 50 days.

7.4 Results and Analysis

7.4.1 Soil pH

The mass flux of OH+ at the cothode increases the pH of the soil within that zone to about 7, while the flux of H+ at the anode decreases the pH at the anode to less than 2 (Figure 7.6). The initial concentration of H+ in the pore fluid is 10^{-4} M which is six orders of magnitude higher than that of OH- (10^{-10} M). These differences in the initial concentrations are primarily responsible for the differences in the rate of change of pH at the cathode and the anode regions. The mass **of** OH- pumped into the cathode region is orders of magnitude greater than the initial concentration of OH- resulting in an immediate increase in the pH. At the anode region, the increase in H+ concentration relative to its initial value is less than the increase of OH- in the cathode relative to its initial value. Consequently, the rate of decrease in pH at the anode is less than the rate of increase in pH at the cathode (Figure 7.6).

Bench-scale and pilot-scale experiments demonstrate that the cathode compartment shows an increase in the pH to about 10-l1. The pH in the soil pore fluid close to the cathode increases only to a value of around 7 in Figure 7.6. The increase in the pH close to the cathode is known to be due to the mass flux of OH- generated by electrolysis reactions while the pH in the catholyte rises to values in excess of I0-11. The increase in the soil pH is restrained by the ongoing water autoionization reaction and the precipitation reaction.

Lead hydroxide precipitation at the cathode region depends upon the available concentrations **of** OH- and Pb+2 and the solubility product constant. The law **of** mass action applied to lead hydroxide precipitation requires (Equation 3.121)

$$c_{OH} \leq \left| \sqrt{\frac{K^{sp}}{c_{Pb}}} \right| \qquad (7.1)$$

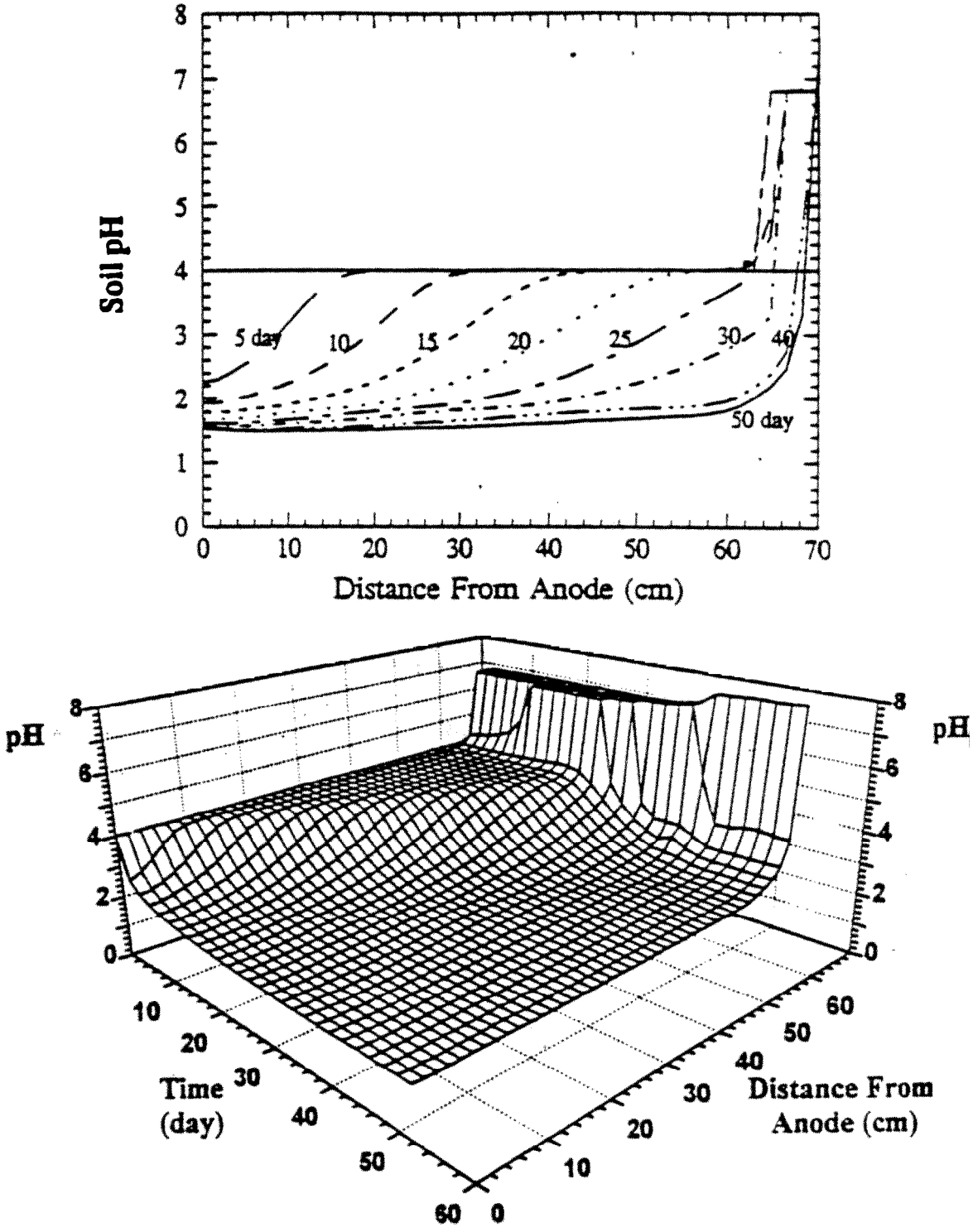

Figure 7.6: Predicted Changes in Soil pH Across the Soil Specimen in Time

where K_{sp} for lead hydroxide precipitation is $2.8*10^{-16}$. For PST3, the initial lead concentration in the soil is relatively high (0.0825 M, or 5322 μg/g) and most of the generated OH- at the cathode will be consumed in precipitation of $Pb(OH)_2$. Consequently, the concentration of OH- evaluated by Equation 7.1 will be within the range of $1.7*107$ M to $5.3*10^{-8}$ M if the dissolved lead concentration in the soil pore fluid stays in the range of 0.1 M to 0.01 M (the case for PST3). Furthermore, initial soil pH is about 4 and the some of the mass of OH- generated by electrolysis reactions will react with the high initial concentration of H- (10^{-4}M) to produce water. As a result of the two reactions, the predicted pH at the cathode zone increases only to about 7.

The rate of advance of the acid front towards the cathode is faster than that of the advance of the base front towards the anode. The predicted pH profile across the specimen shows that the acid front meets the base in the last 10 to 15 cm of the soil specimen within the first 25 days of processsing (near the cathode). Consequently, the acid front drives the base back to the last 2 cm of the specimen after 37 days of processing. At this time, the pH profile reaches steady state. The generated H+ at the anode and OH- at the cathode react to produce water at the front within the last 2 cm of the specimen

Comparisons between the predicted and experimental pH profiles after 8,15, and 22 days are depicted in Figures 7.7 and 7.8. A reasonable agreement is obtained with the experimental results. The advance of the predicted acid front is faster than those recorded in the experiment.

7.4.2 Electric **Conductivity**

Figure 7.9 displays the predicted changes in electric conductivity across the soil specimen. The electric conductivity is evaluated from concentrations of charged species in the pore fluid. There are high initial concentrations of H+, Pb2+, OH-, and NO_3^-, in the pore fluid. The initial conductivity is higher than 20 mS/cm. The increase in the soil pH near the cathode to about 7 and the prevailing decrease in the dissolved lead concentration result in **a gradual** decrease in the conductivity to about 15 mS/cm within the first 37 days of processing. At the anode zone; however, the advance of the acid front increases H+ concentration and the dissolved lead concentration in the pore fluid decreases due to transport under electric field. The change in the

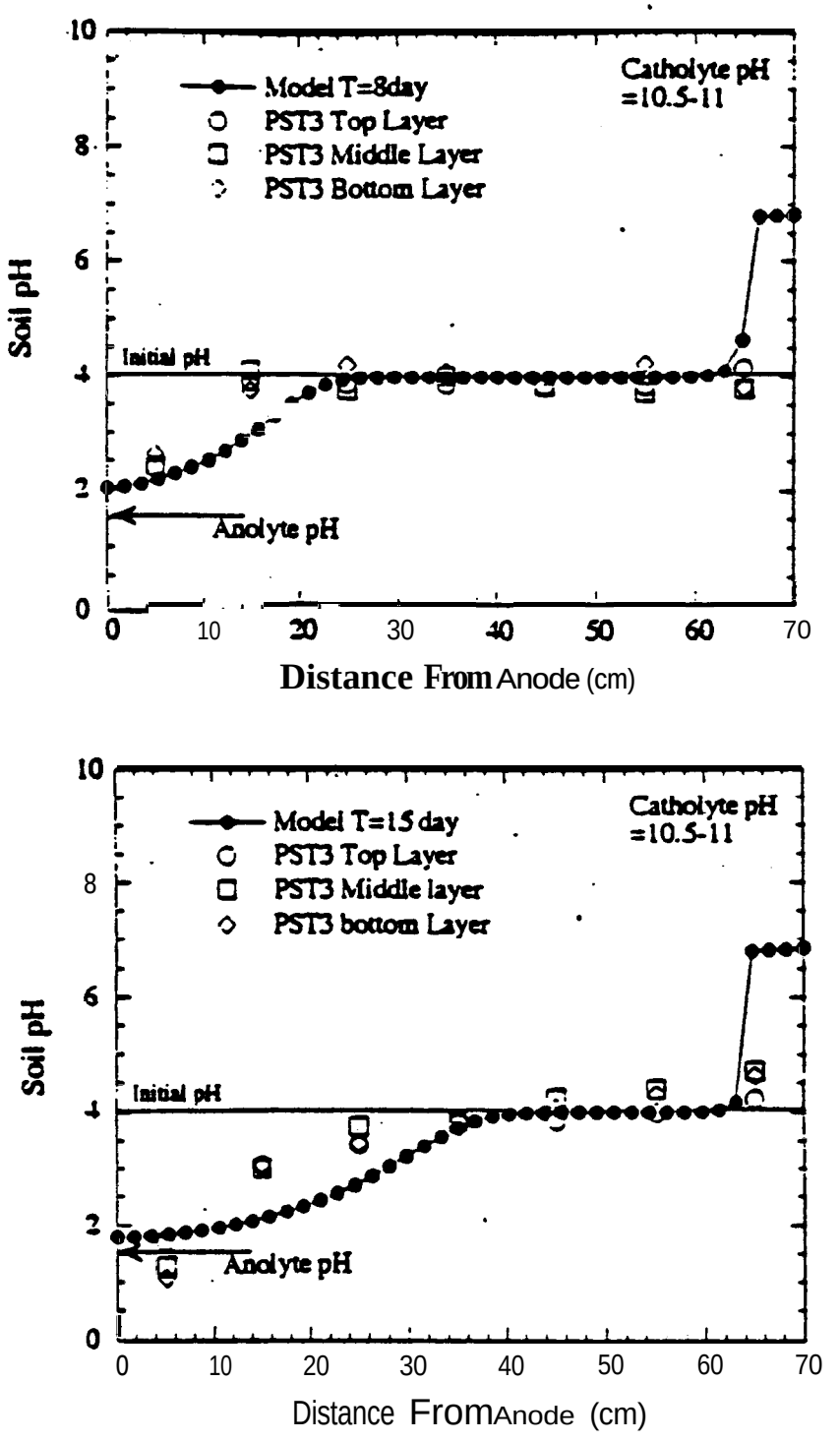

Figure 7.7: Comparison Between Predicted and Experiment pH Profiles after 8 days and I5 days of Processing

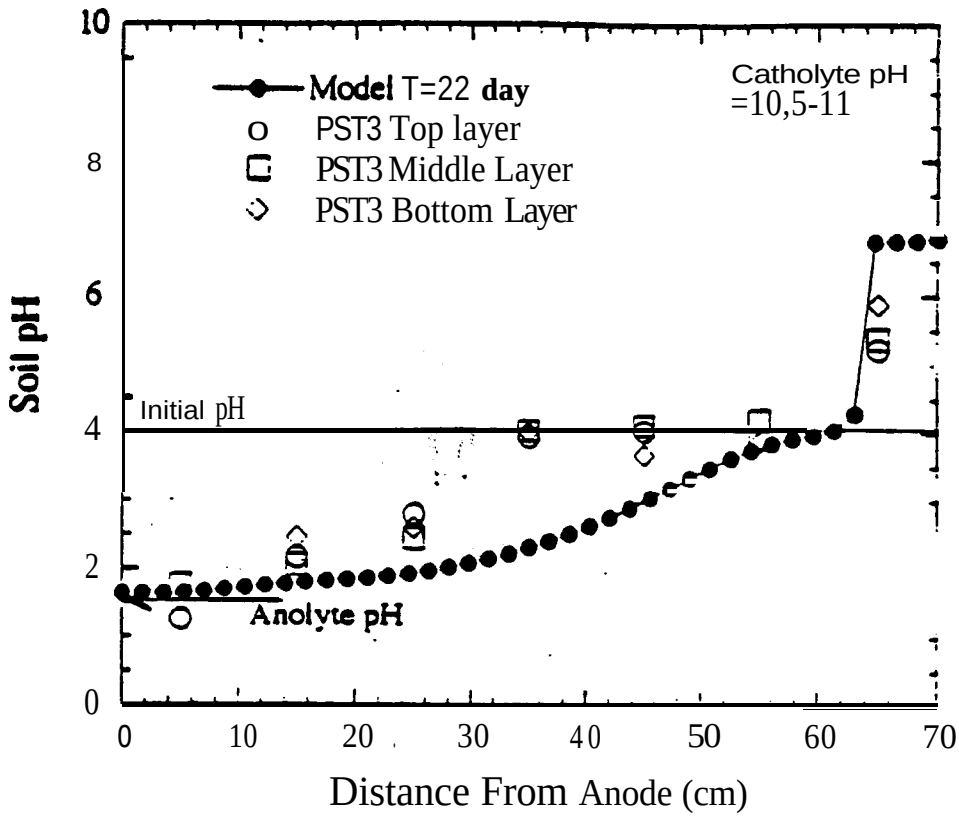

Figure 7.8: Comparison Between Predicted and Experiment pH Profiles After 22 days of Processing

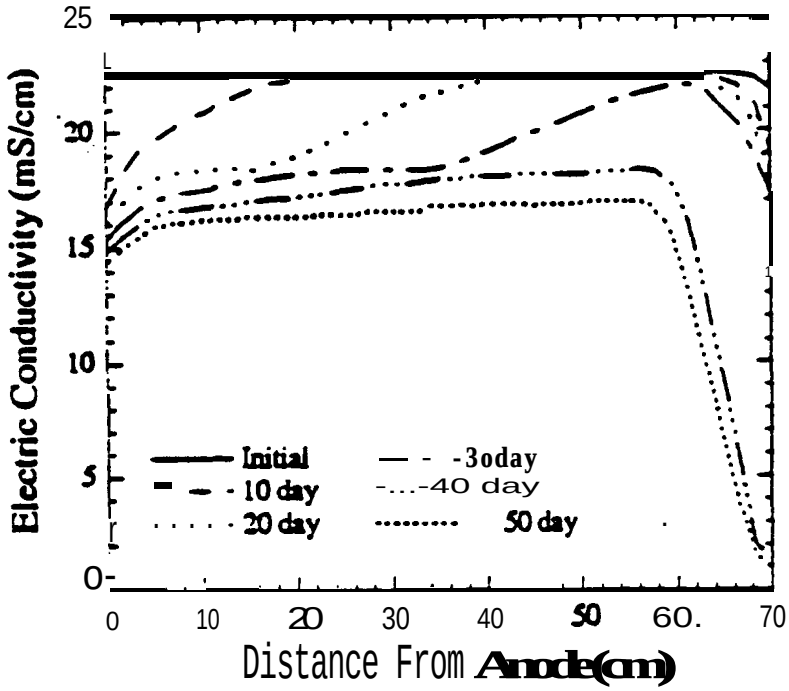

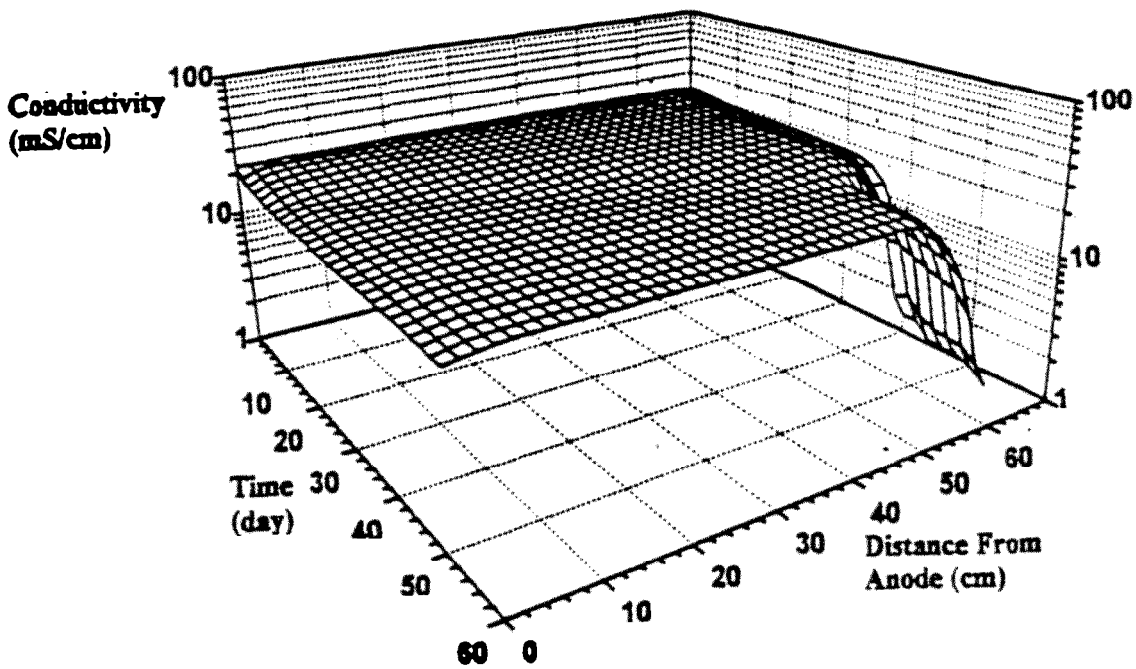

Figure 7.9: Predicted Electric Conductivity Distribution **Across the** Pilot-Scale Test Specimen

electric conductivity is dependent on the relative change in Pb^{2+} concentration with respect to H+ concentration. If the rate of decrease in the ionic strength due to transport lead is higher than the rate of increase in the ionic stregth due to the advance of H+ then the electric conductivity will decrease. Theoretically, the conductivity could go either way. The major factors affecting the rate of change of the conductivity would be the initial chemistry of the specimen, the electric current (or the rate of generation of H^+ at the anode) and the transport number of each species. The transport number is a function of the ionic mobility and concentration; higher the mobility and higher the concentration of a particulate ion, higher would be its transport number. In this case, the H+ ionic mobility is about 5 times that of Pb^{2+}; however the initial Pb^{2+} concentration is about 800 times the initial H^+ concentration. As a result, the rate of decrease in the ionic strength of the pore fluid due to lead removal is more significant than the rate of increase in the ionic strength due to the decrese in the pH. A decrease in the electric near the anode to less about 14 mS/cm in 30 days is a consequence.

A zone of very low electric conductivity is developed near the cathode after 37 days of processing. After 50 days of processing, Figure 7.9 displays a decrease in the electric conductivity to less than 800 S/cm in the last I0cm Of the specimen near the cathode. Changes in the electric conductivity across the specimen will result in a nonlinear electric potential distribution as long as the electric current applied is kept constant across the electrodes.

Figure 7.10 displays a comparison of the voltage distribution after 100 h and 300 h of processing. A good agreement is observed between the predicted and experimental values. A relatively linear distribution is depicted due to the relatively uniform electric conductivity distribution across the soil. Although prediction of the electric potential is significant in measurement of the energy required, the rate of species transport under electric fields depends on the electric gradient profile across the soil and not on the absolute value of the electric potential. Therefore, it is essential that the distribution of electrical potential gradient compare well with experimental results for accurate prediction of species transport. Figure 7.11 presents comparisons between the electric gradient in the model and the experiment after 100 h, and 300 h of processing. A good agreement is obtained. A uniform electric gradient of about 0.06 to 0.07 V/cm develops in the model while the experiment displays an electric gradient of about 0.01 to 0.1 V/cm.

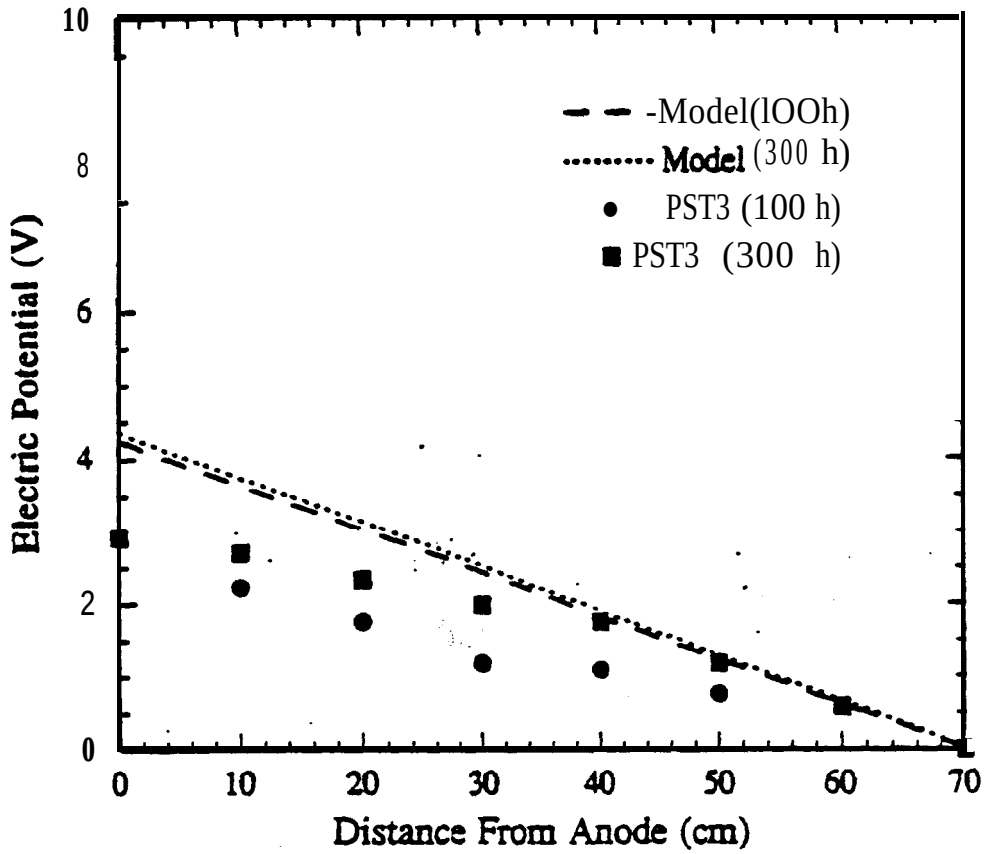

Figure 7.10: Predicted and Experimental Electric Potential Distributions After 100 h and 300 h of Processing PST3

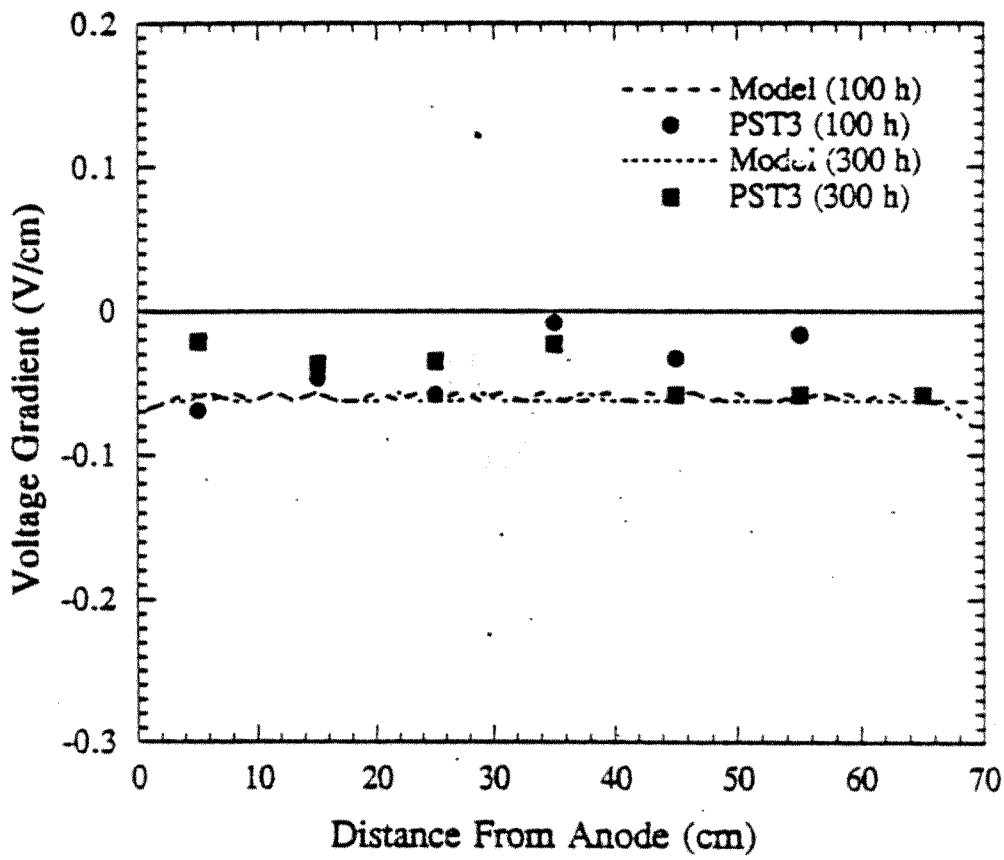

Figure 7.11: Model and Experimental Results of the Electric Gradient Distributions After 100 h and 300 h of Processing PST3

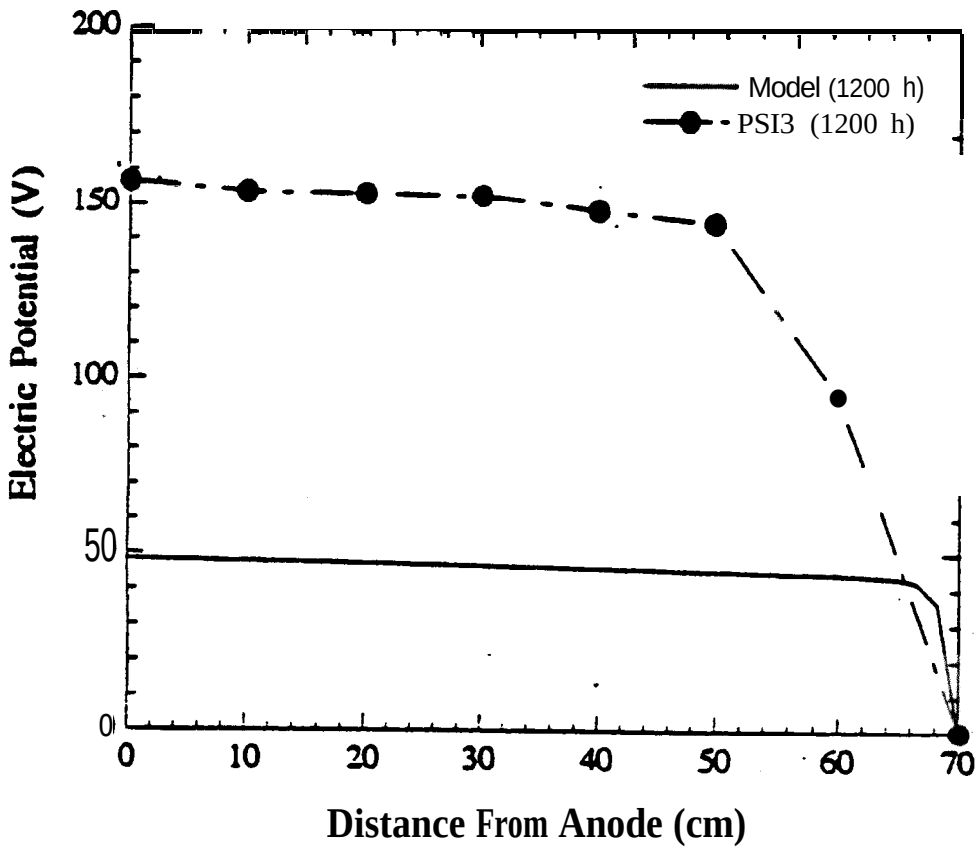

Figure 7.12: Comparison of Eletric Potential Disaibution **After** 1200 h of Processing PST3

Later in the process (600 h), the zone of low electric conductivity near the cathode results in a nonlinear electric potential distribution as depicted in Figure 7.12. The electric potential profile is similar in the experiment and the model; however, the model predicts a significantly lower potential difference than the pilot-scale study (60 V versus 150 V). A comparison between the predicted and the experimental electrical gradient demontrates quite good agreement, except for the last 15 cm near the cathode (Figure 7.13). The voltage gradient across the specimen is less than 0.1 V/cm; however, in the model it increases to more than 20V/cm in the cathode and remains at 10 v/cm in the experiment.

The disagreement in the absolute value of electric potential at later stages is due to the differences in the extent of the zone of low electric conductivity near the cathode. In the experiment, the zone of low electric conductivity advances farther into the soil specimen than in the model. This is also depicted in the pH profiles. A wider low electric conductivity zone results in a higher voltage drop across the specimen.

7.4.3 **Total Pore Fluid Flow and Pressure**

Figure 7.14 displays that at early stages of the process (the first 30 days), the predicted rate of pore fluid flow is almost constant across the specimen and it is in the order of 0.001 ml/cm^2d. Since a constant value **of the** coefficient of electroosmotic permeability is assumed, the hydraulic head is kept zero at the electrodes, and a uniform electric gradient is depicted across the specimen (Figure 7.1 I), the pore fluid flow is uniform across the specimen at this time. After 37 days; however, the nonlinearity in the electric potential across the specimen leads to a predicted, nonlinear electroosmotic flow rate across the specimen. The highest flow rate (up to 0.2 ml/cm^2d) is depicted close to the cathode and the lowest flow rate (0.001 ml/cm^2d) is depicted close to the anode (Figure 7.14). Since the hydraulic conductivity of the soil is low (less than 10^{-7} cm/s), pore fluid flow across the specimen is insufficient to balance that required near the cathode. A negative pore water pressure develops to balance the demand in pore fluid.

PST3 did not show any significant change in the pore water pressure within the first 37 days. **Figure 7.15** shows comparisons between the measured pore water pressure in two tensiometers, located at a distance of **14 cm** and 42 cm from the cathode, with predicted pore

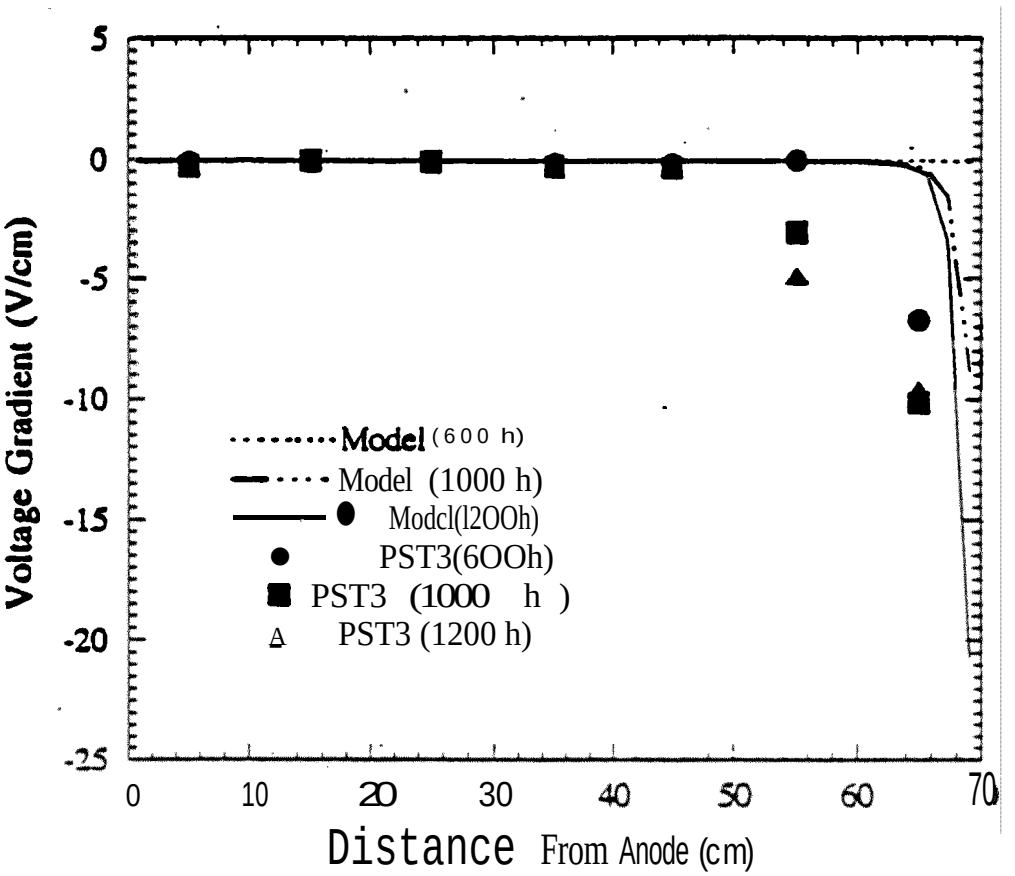

Figure 7.13: Comparison of the Electric Gradient Distributions in PST3

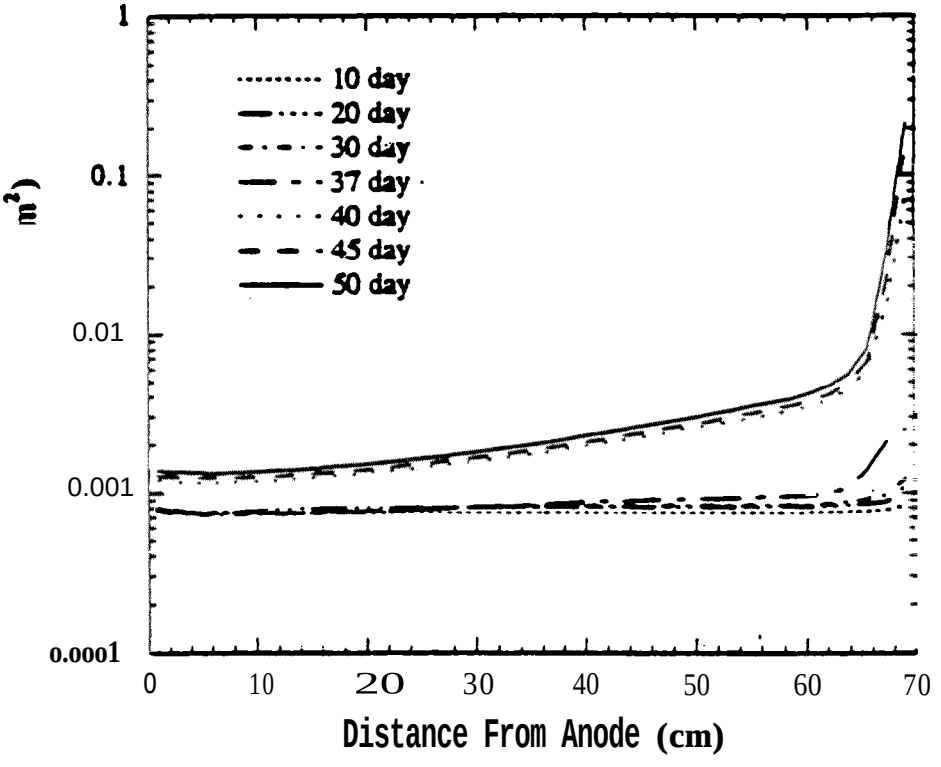

Figure 7.14: Predicted Pore Fluid Flow Rates Across the Specimen

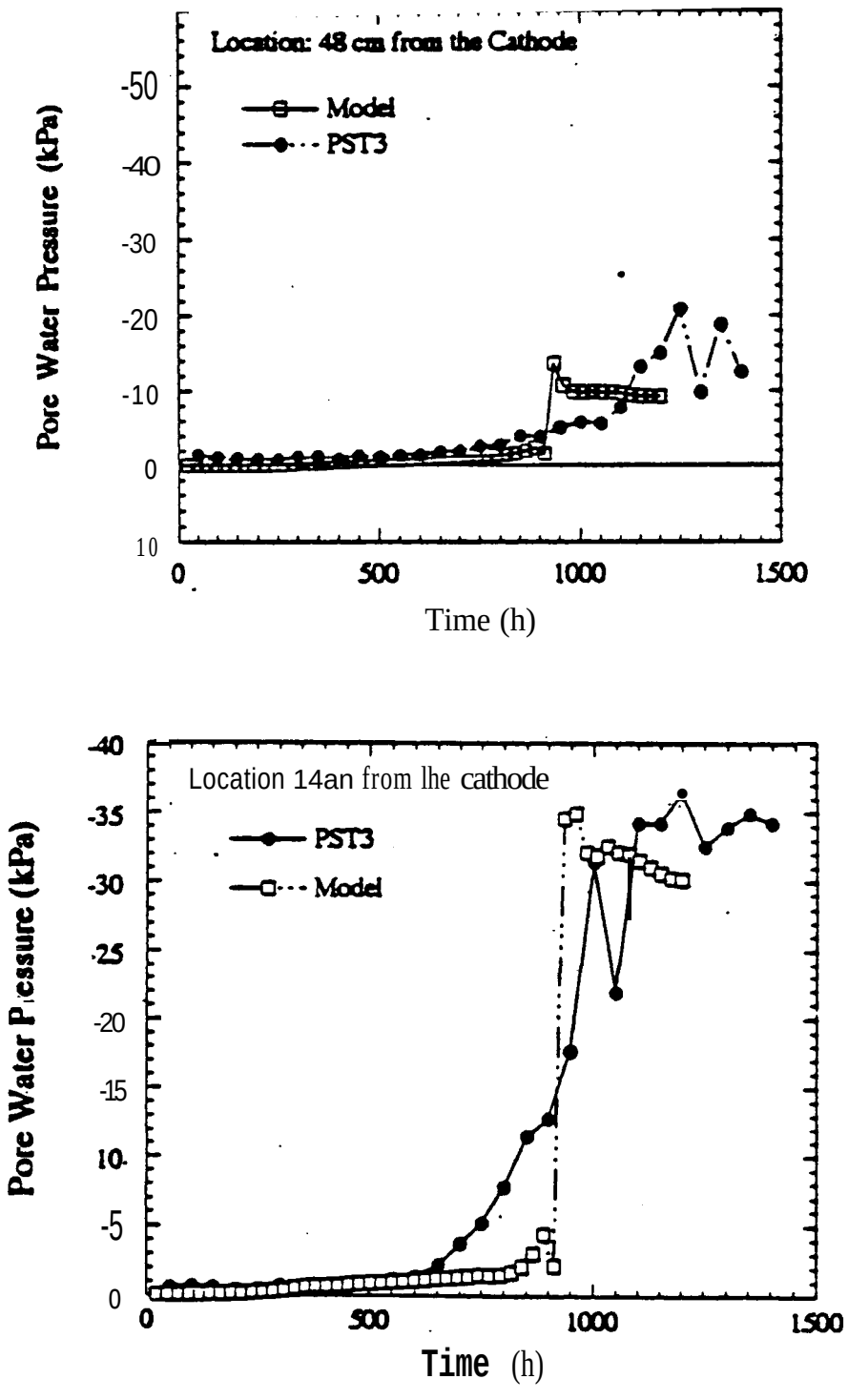

Figure 7.15: Predicted and Measured Pore Water Pressure in Tensiometers Located at a Distance of 14 cm and 42 cm from the Cathode

water pressure in the same locations. Data from other tensioneters are presented in Appendix D. Predicted and measured pore pressure in these locations display development of negative pore water pressure (matrix suction) after 800 h -1000 h (34 to 40 days). It is noted that both the model and the measured values exhibit good agreement. However, the model predictions indicate instantaneous increase in the suction after 900 h (≈ 37 days) to about -35 kPa and -15 kPa in these locations, the higher suction is nearest to the cathode. A sudden drop in the predicted electric conductivity and increase in the electric gradient near the cathode at that time (after 37 days) is the reason for the sudden increase in suction at that time.

Comparisons between the predicted and measured suction profiles across the electrodes at 37,40,45, and 50 days are shown in Figures 7.16 and Figure 7.17. Pore pressure distributions demonstrate development of a suction of up to -10 kPa in the experiment and up to -6 kPa in the model after 37 days. In both cases, most of the suction is developed near the cathode zone and gradually decreases towards the anode. The predicted suction displays an increase of up to -50 kPa near the cathode after 40,45, and 50 days. The experimental results for the same times show an increase in the suction of up to -30 kPa. Predicted and experimental results at 40,45, and 50 days exhibit similar patterns in the suction profiles across the specimen; both show an increase near the cathode tailed by a decrease towards the anode. Suction in the experiment favorably agrees with model results; however, the model Predicts higher values and closer to the cathode. The experimental values are more skewed towards midsections of the specimen.

The distributions of suction predicted across the soil after 37 days show that suction is generated at a location where most of the changes in the pore fluid flow rate occur (last 6 cm near the cathode). Furthermore, the highest electrical gradient across the soil specimen after37 days is developed within the last 6cm near the cathode. The results reveal that the nonlinearity in the electric potential distribution due to the development of a zone of low electric conductivity near the cathode results in a higher electric gradient and electroosmotic flow near the cathode and initiation of suction at the interface between the zone with the high electric gradient and that of low electric gradient. This is a direct consequence of the fact that second derivative of electrical potential develops the suction in the mass balance equation (Equation 3.62).

Bench-scaIe tests reported by Hamed (1990) show that the rate of electroosmotic flow decreases and ceases at later stages of the process. The coefficient of electroosmotic permeability is conceived to be a function of zeta potential which is highly dependent on the chemistry of the

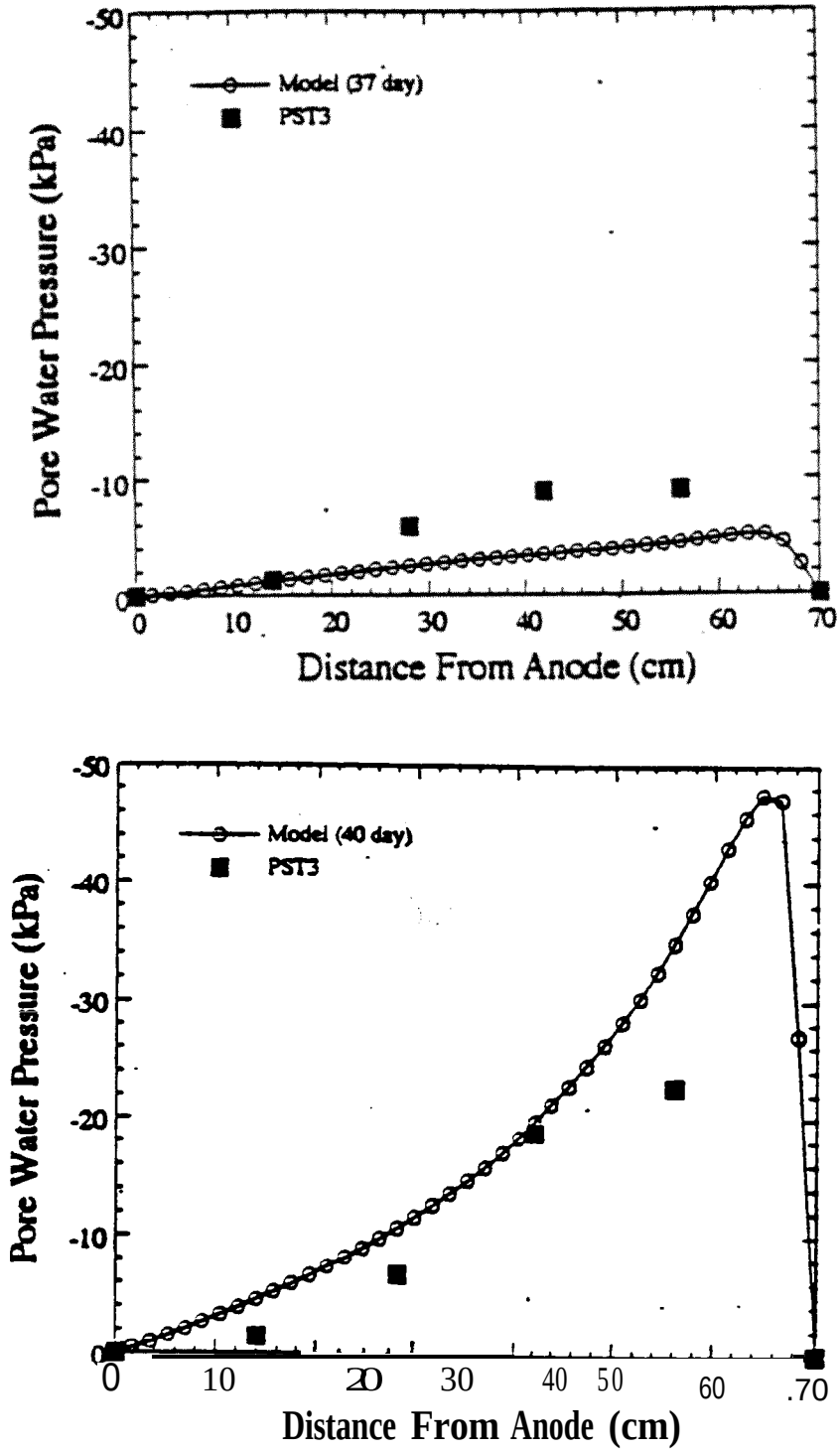

Figure 7.16: Comparison Between Suction Generated in the Model and in the Experiment After 37 and 40 days of processing

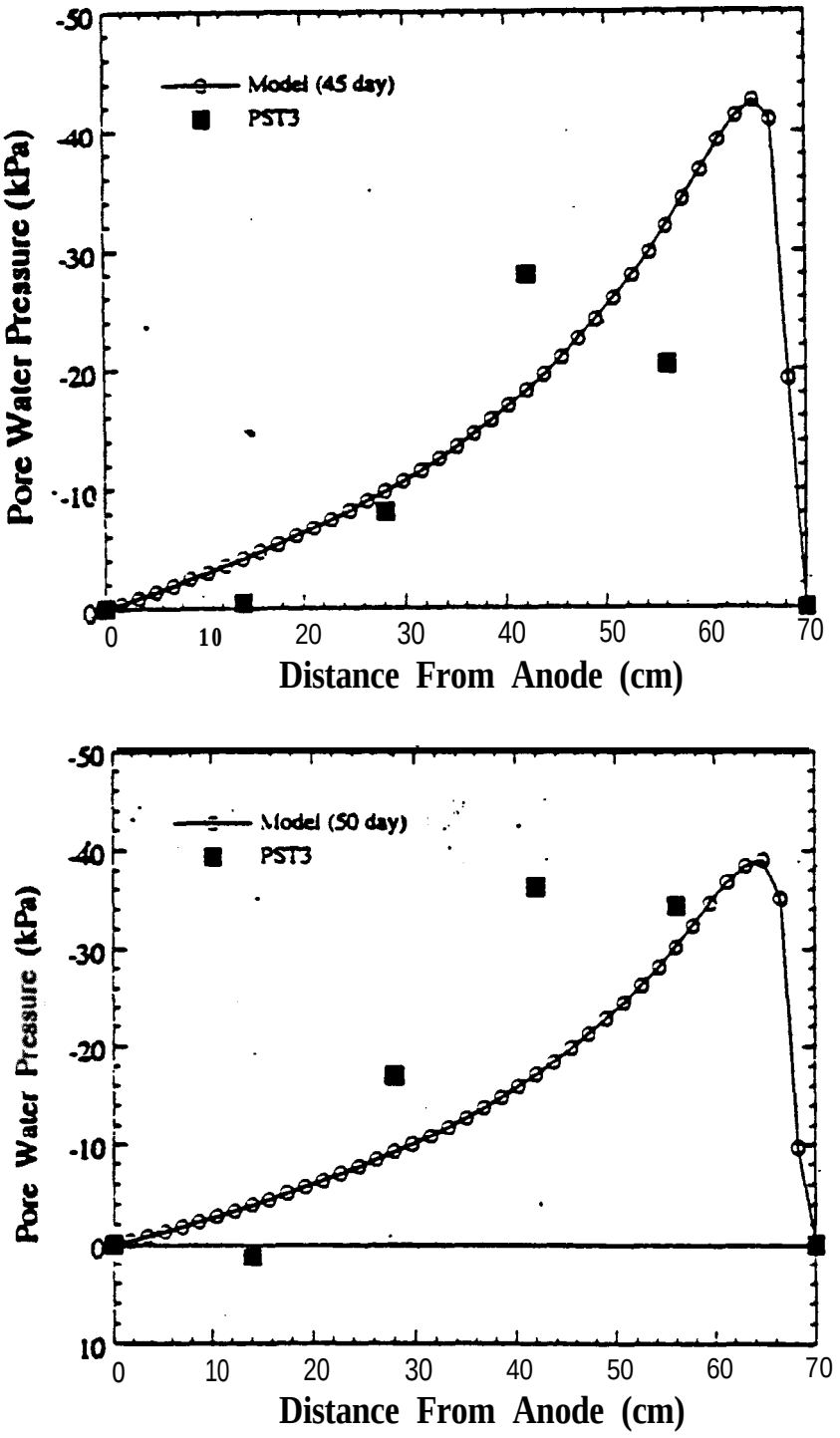

Figure 7.17: Comparison Between Suction Generated in the Model and in the Experiment After 45 and 50 days of Processing

soil specimen. Decrease in the soil pH and surface charge across the specimen will decrease the zeta potential and the coefficient of electroosmotic permeability and hinder the electroosmotic flow at later stages of the process. In this model, a constant k_e, value is assumed throughout the process that is independent of the soil chemistry or pH. As a result there will always be an electroosmotic flow as long as there is an electric gradient across the soil. It is not expected to see the time-dependent changes in k_e and flow rate reported by Hamed (1990) since the experiments are on a relative shorter time frame.

7.4.4 Lead Transport and Removal

The model predicts changes in different forms of lead in the soil; dissolved lead in the pore fluid in mole/l, lead precipitated as hydroxide in mg/kg, lead adsorbed on the clay surface in mg/kg, and total lead in the soil in mg/kg. Three dimensional contour diagrams are presented to describe the changes in space and time. As each form of lead affects the total lead profile separately, the figures provide a sense of the contribution of each. It is noted that transport occurs only when lead dissolves in the pore fluid and the adsorbed and precipitated lead remain immobilized in the soil.

Dissolved lead in the pore fluid is continuously transported from the anode zone towards the cathode (Figure 7.18). The concentration of dissolved lead near the cathode shows a decrease in time mainly due to consumption of the ionic lead as lead hydroxide precipitation. At later stages (after 30 days), the high electric gradient zone near the cathode leads to an increased transport rate in lead due to advection and migration, further decreasing the dissolved lead concentration. Figure 7.18 shows that a hump is developed in the dissolved lead profile in the soil pore fluid at the acid/base interface. This hump is located at a distance of 55cm to 60cm from the anode (15 cm to 10 cm from the cathode). The high pH zone in the last 10 cm near the cathode results in precipitation and sorption of most the lead at that zone. On the other hand, low pH across the soil (less than 2) results in dissolution, desorption, and transport of the lead into the soil pore fluid. Consequently, the differences in species transport rates at these locations result in the depicted hump in the dissolved lead profile.

A decrease in adsorbed lead concentration is not observed for about the first 10 days (Figure 7.19). Desorption occurs as a result of either a decrease in the soil pH or a decrease in lead

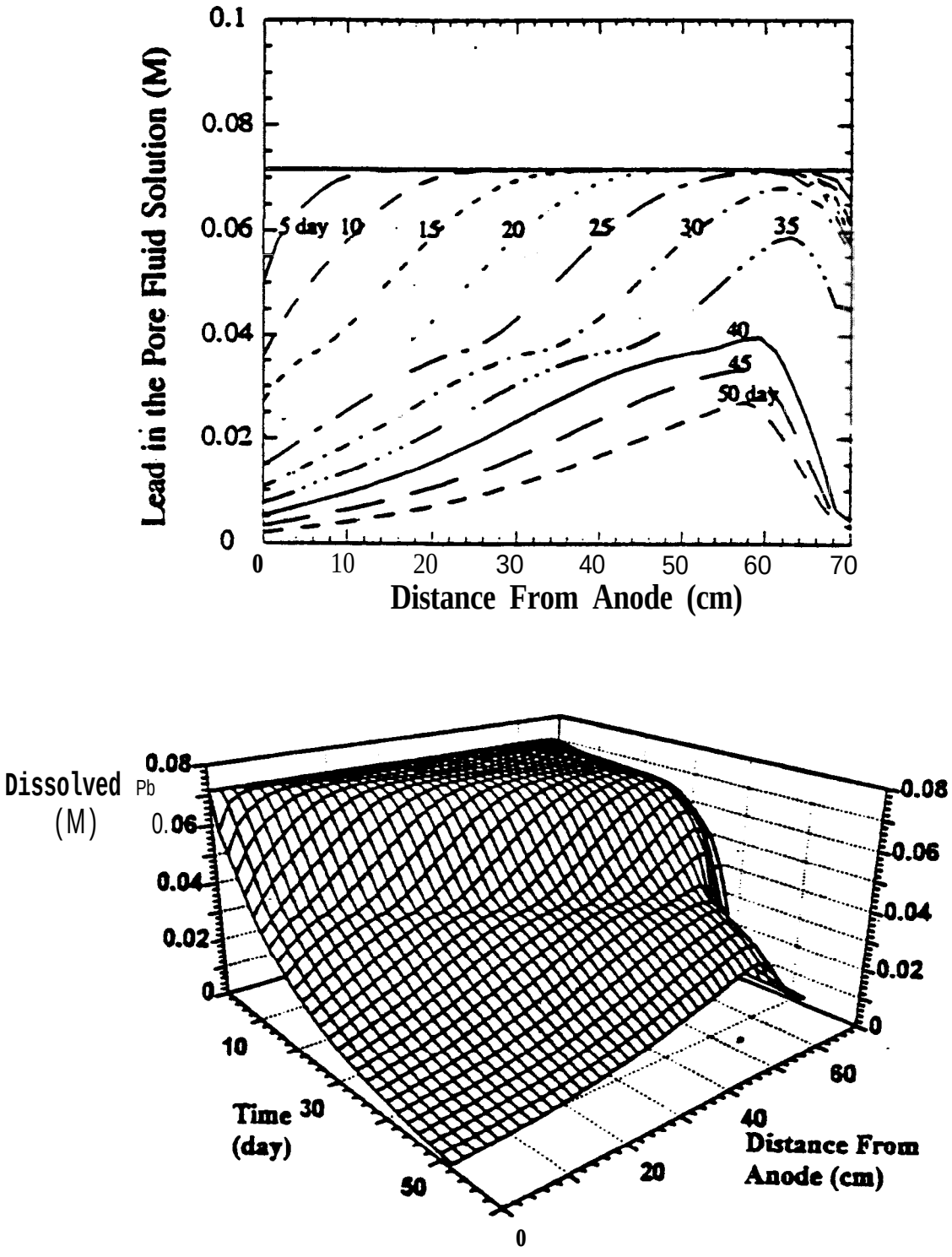

Figure 7.18: Predicted Dissolved Lead Concentration in the Pore Fluid

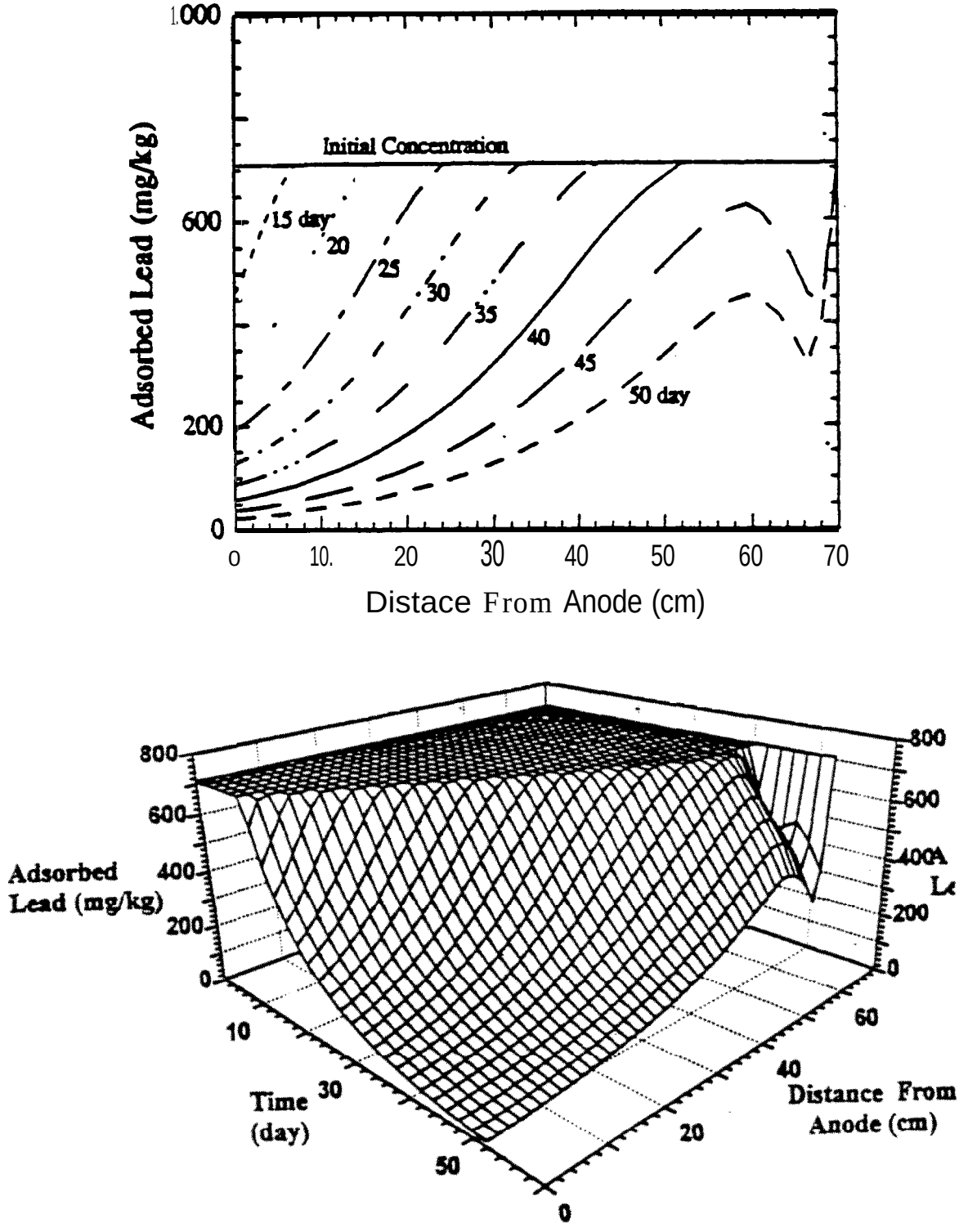

Figure 7.19: Predicted Adsorbed Lead Profile

concentration in the pore fluid. Soil pH decreases within the first 10 days to about 2 near the anode; however, the high concentration of ionic lead in the pore fluid delays any lead desorption until that time. Subsequent to that period, desorption occurs at almost a constant rate decreasing the total lead concentration.

Two fronts are developed when lead desorption is initiated after 10 days (Figure 7.20); one close to the anode and another to the cathode. The difference in the rate of transport of lead at these fronts is due to the replacement of the transported ionic lead in the pore fluid with those desorbed from the soil surface. The increase in the pH at the cathode *zone results* in precipitation of lead hydroxide. Precipitation starts almost immediately after starting the process because of the immediate increase in the pH at the cathode (Figure 7.20). Precipitation retards lead transport and at the same time decreases the concentration of ionic lead in the pore fluid. The zone of high precipitation and high pH near the cathode is the zone of low electrical conductivity across the soil. Since steady state pH distribution (Figure 7.6) shows no breakthrough of the acid across the specimen, lead precipitation and total lead concentration will both continue to increase within that zone. Enhancement techniques which prevent such precipitation are currently being investigated at LSU (1993).

The total lead profiles predicted by the model are shown in Figure 7.21. Decrease in total lead concentration is depicted at the anode region. The last 5 cm near the cathode show an increase in total lead to more than 10,000 ug/g as a result of lead hydroxide precipitation. At later stages of the process (after 30 days) a hump in concentration is developed at about 60 cm from the anode similar to that developed in the ionic lead profile.

Nitric acid extraction technique of the soil samples retrieved from PST3 gives the total lead in the soil. These experimental results are compared with model predictions in further assessment of the performance of the model. Comparisons at 8,15,22, 37, and 50 days are presented in Figures 7.22-7.24. Total lead distribution across the specimen in PST3 is evaluated at three different elevations (top, middle, and bottom layers). Experimental data for PST3 are presented in Appendix D.

After 8 days of processing, both the model and the experimental results in PST3 demonstrate similar lead distributions (Figure 7.22). A decrease in lead concentration at the anode zone (up to a distance of 10 cm to 15 cm from the anode) and an increase in lead concentration

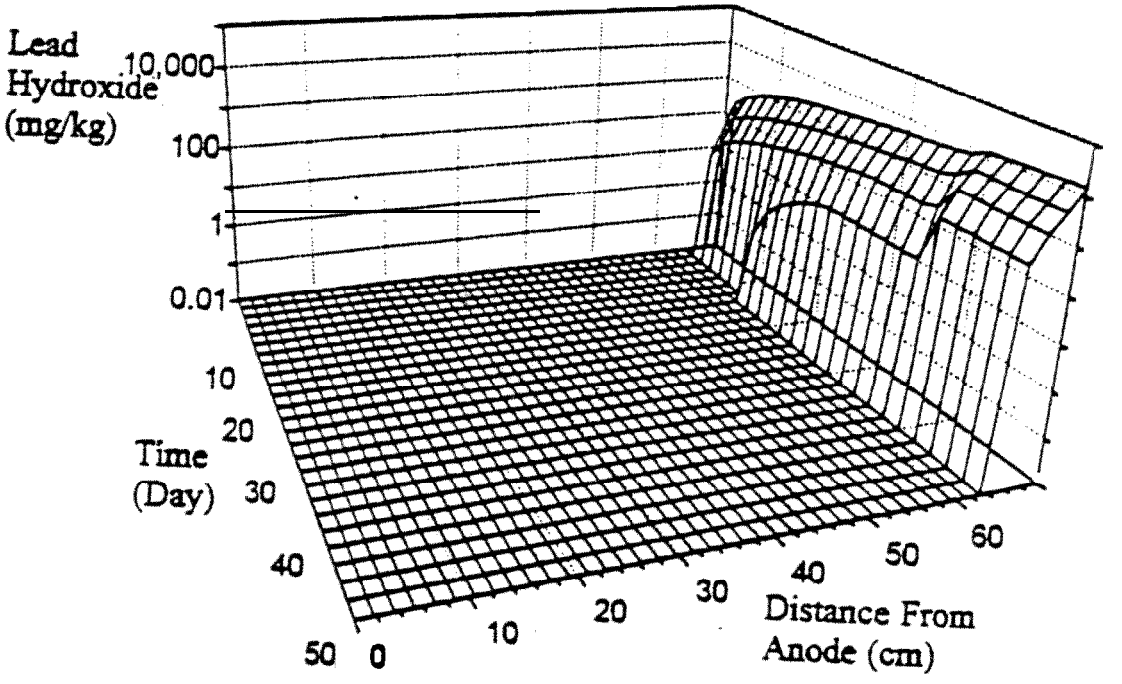

Figure 7.20: Predicted Precipitated Lead Hydroxide Profile

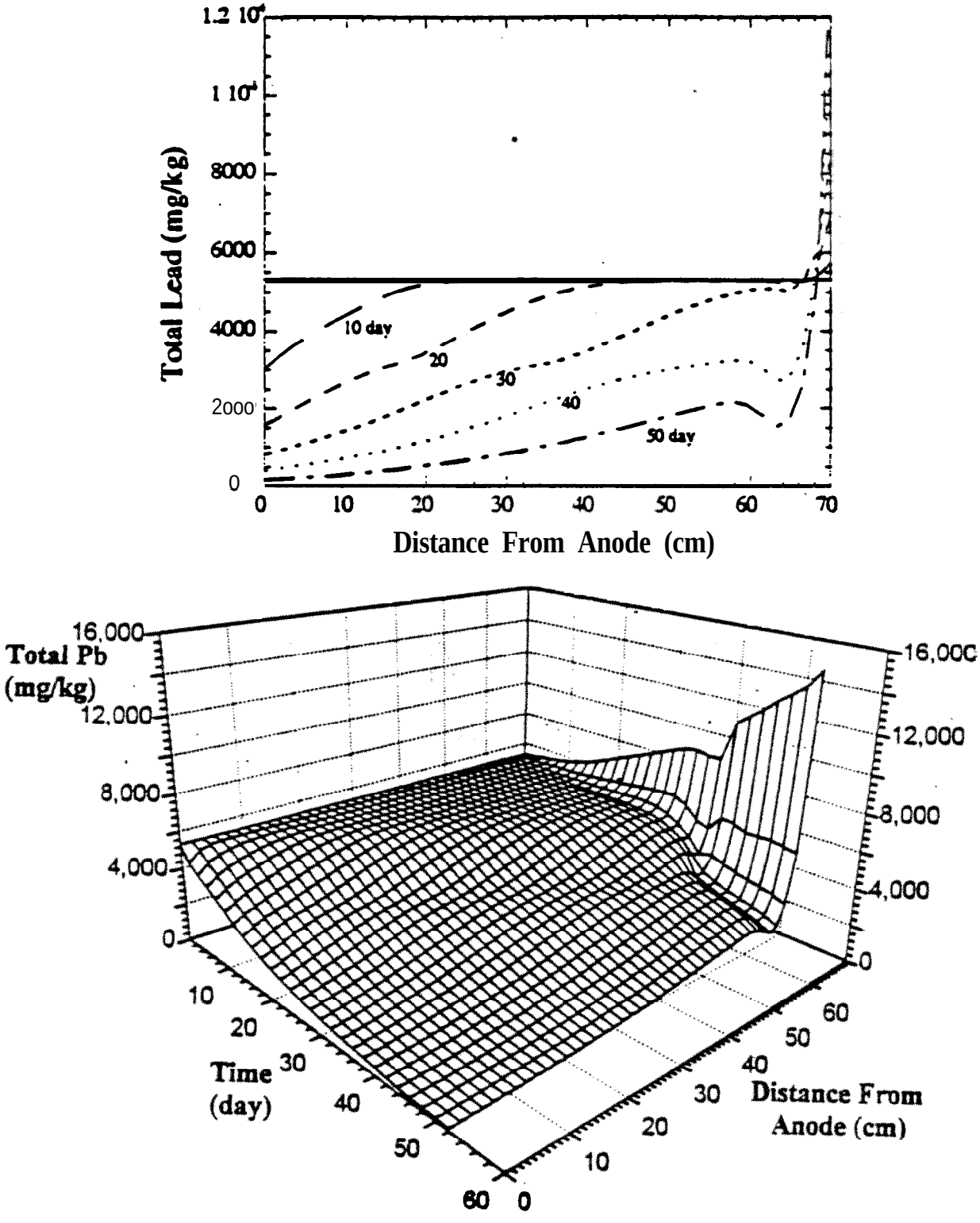

Figure 7.21: Predicted Total Lead Profile

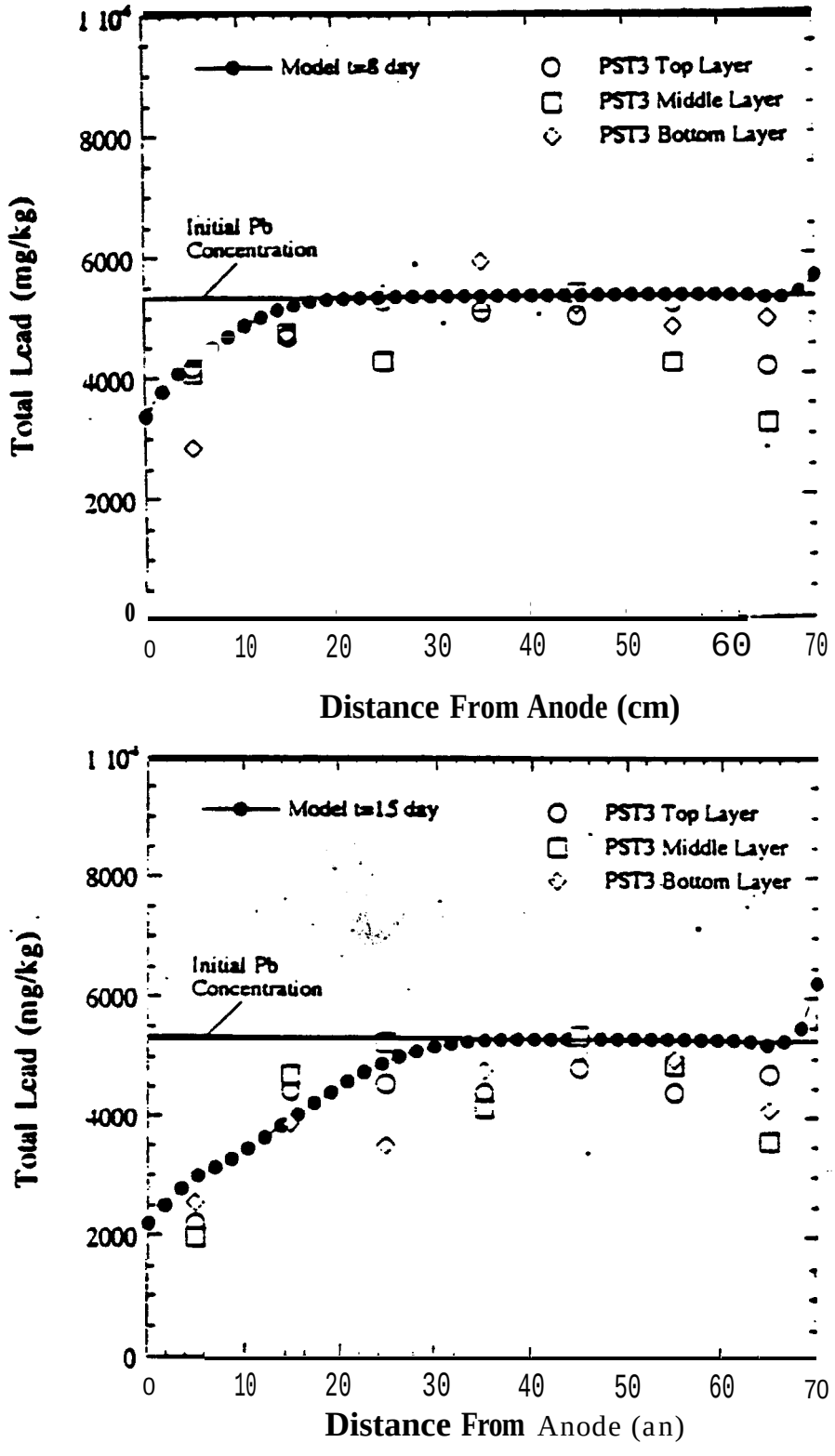

Figure 7.22: A Comparison of Pilot-Scale Test Results and Predicted Total Lead Concentration After 8 and 15 days

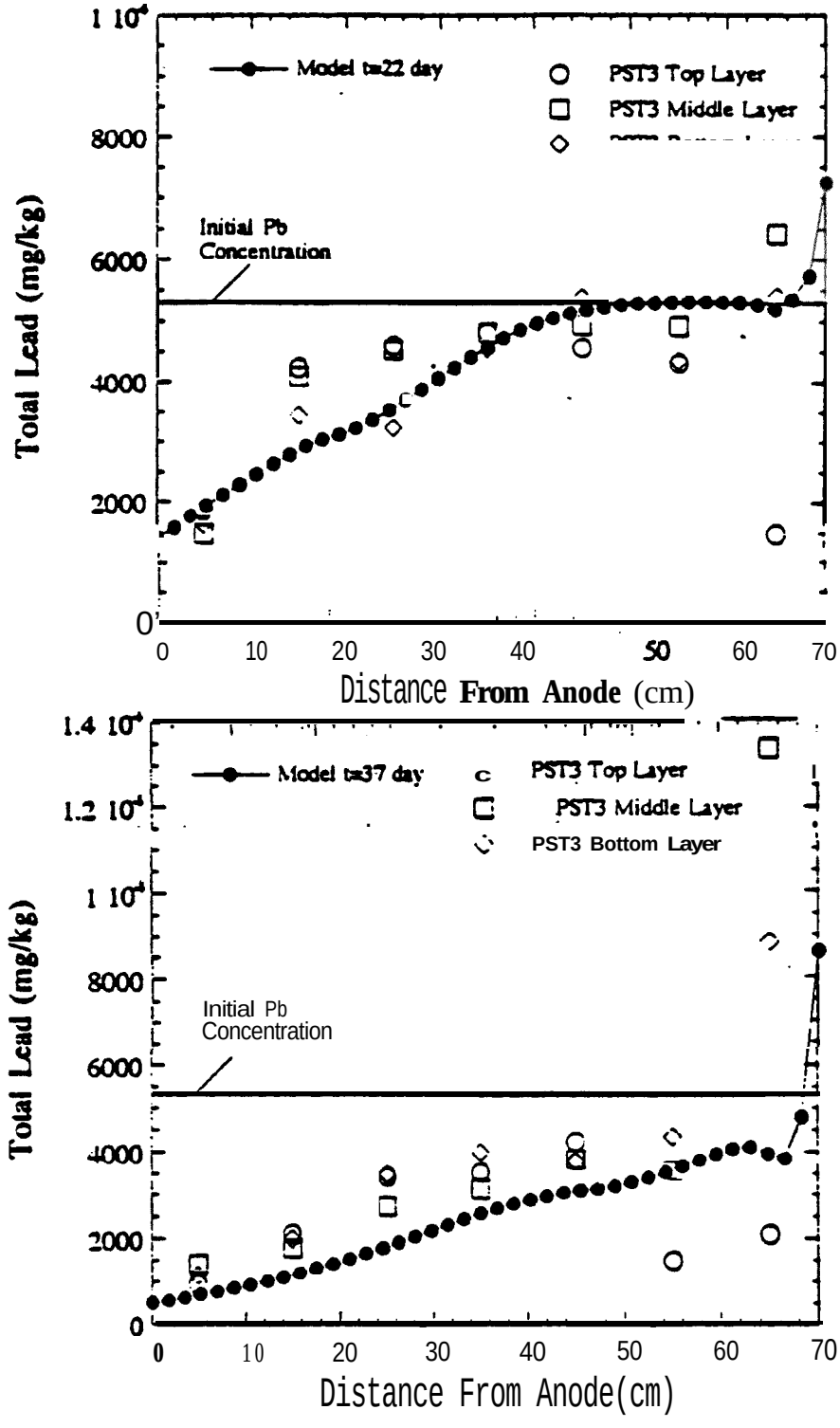

Figure 7.23: A Comparison of Pilot-Scale Test Results and Modeled Total Lead Concentration After 22 and 37 days

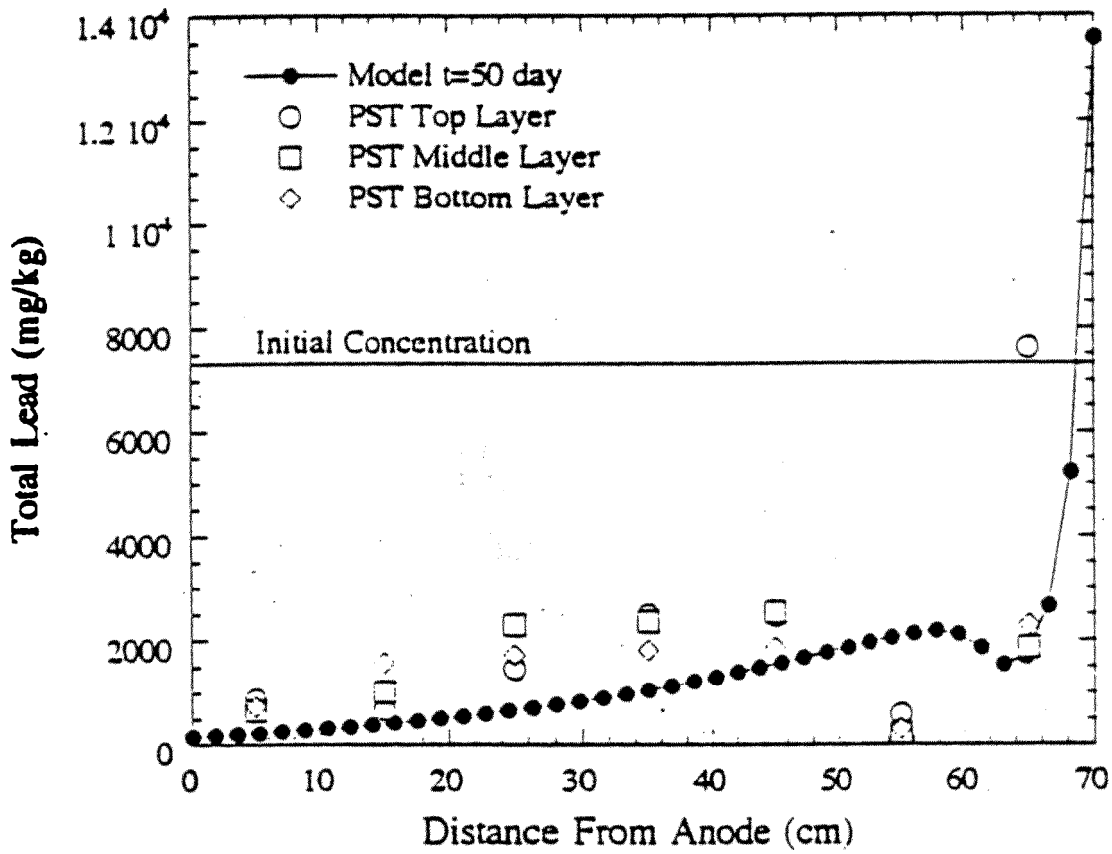

Figure 7.24: A Comparison of Pilot-Scale Test Results and Modeled Total Lead Concentration After 50 days

near the cathode (last 5 cm near the cathode) are depicted in the model results. An increase is not observed in lead concentration near the cathode in the experiment. There are several reasons for this discrepancy. One-dimensional application of the model might be one of these reasons. The surface of the specimen in the experiment was only covered by a clear plastic cover which might have resulted in a two dimensional effect and consequently different behavior than the model. The effect of high pH near the cathode on sorption characteristics and negative lead complexation is not employed in the model. Different sorption behavior or formulation of negatively charged complexes of lead at the zone of high pH are expected to influence the concentration profiles of lead.

After 15 days of processing, lead concentration is decreased at the anode but the profile is still similar to that of 8 days. A decrease in lead concentration to about 20 cm from the anode due to transport of the dissolved lead towards the cathode, and an increase in total lead concentration in the fast 10 cm near the cathode due to lead hydroxide precipitation are apparent in Figure 7.22.

Reasonable qualitative and quantitative agreements are achieved in lead profiles after 8 and 15 days of processing. The experimental results, however, show a decrease in total lead in the last 15 cm of the specimen near the cathode. The two dimensional effect of the open surface of the soil specimen (covered only with clear plastic cover), high pH complexation and sorption might be the reasons for these differences.

After 22 and 37 days, a further decrease in lead concentration is noted across the specimen in both the experiment and model results. Concentration near the anode (first 10 cm) decreased to below 2,000 μg/g after 22 days and to below 1,000 μg/g after 37 days. On the other hand, the lead profile displays different behavior near the cathode. Lead concentration in the middle layer near the cathode shows an increase up to 6,500 μg/g after 22 days and up to 13,000 μg/g after 37 days. The top layer, however, displays a decrease in concentration to about 2,000 μg/g. Predicted concentrations within the last 4 cm near the cathode at 22 and 37 days show continuous increase in concentration up to 8,000 μg/g.

Variations between predicted concentrations and experimental results near the cathode are noted in most comparisons, specially after 22 and 37 days. These variations could be related to either the two dimensional effect of the soil surface or the effect of lead complexation and sorption in the zone of high pH near the cathode. Furthermore, comparisons of the measured electric

gradient profile with the predicted one displays some differences in the cathode region (Figure 7.13). The zone of low electric conductivity is further inward from the soil from the cathode than the predicted conductivity. This results in differences in the predicted and measured rates of species transport.

The effect of differences in measured and predicted electric gradient on lead transport is apparent after 50 days. Figure 7.24 shows comparison of the predicted lead profile after 50 days and the measured profile after 53 days. Both profiles display significant decrease in lead across the specimen (less than 2,000 μg/g). The predicted profile is lower than the measure done in the first 40 to 45 cm from the anode. It is interesting to note that both profiles display similar qualitative agreement near the cathode. A small hump is developed in both of them. The predicted hump is located at a distance of 60 cm from the anode at a concentration of about 2,000 μg/g. The experimental results display a similar hump at a distance of 45 to 50 cm from the anode at a concentration of 2,000 μg/g. As discussed elsewhere, the different rates of transport after and before the hump are the main reason for its development. The increase in the predicted electric gradient occurs only in the last 5 cm near the cathode. In the experiment, the zone of high electric gradient advances to about 15cm into the soil from the cathode. These differences result in differences in the predicted and measured rates of lead transport and consequently lead profiles near the cathode.

The model results and their comparisons with the pilot-scale test results demonstrate that the principles of multispecies transport under an electric field have been quite well understood and formalized. EK-REM displays excellent predictions of transport and precipitation of lead and pore pressure distribution across the electrodes. This model should be improved to develop into a design/analysis tool in electrokinetic remediation.

Section 8

SUMMARY AND CONCLUSIONS

8.1 Summary

Natural concentrations of heavy metals in soil deposits are not high; however, studies have indicated that many areas near urban complexes, metalliferous mines or major roads display abnormally high concentrations of these elenents. Soil contamination with lead, which may result from its use in petrol, paints, batteries, and pesticide, smelting of metals and mining, and disposal of lead-acid storage batteries, has been documented at concentrations that may go up to 10% to 20% by weight. Compared to other hazardous species, lead is shown to be the most frequently identified species in hazardous waste sites listed on the NPL.

A variety of options may exist to select a cleanup remedy at a site, however, the efficiency and costs of these options may vary widely. Most of the existing remediation technologies are limited to soils with high hydraulic conductivities and are not effective in removing heavy metals adsorbed on soil particles, particularly fine-grained deposits. There exists a need to introduce cost-effective, innovative, and preferably in-situ remediation technologies.

Electrokinetic soil processing is a new, innovative, and cost-effective remediation technology that employs conduction phenomena under electric currents for transport, extraction, and separation. A low level direct electric current (or electric potential difference) is applied across contaminated soil deposits through inert electrodes placed in holes or trenches in the soil filled with processing fluids. The applied electric current leads to electrolysis reactions at the electrodes generating an acidic medium at the anode and an alkaline medium at the cathode. The electric field across the contaminated soil mass leads to transport of hydrogen ion from the anode to the hydroxyl ion from the cathode to the anode. The hydrogen ion transport is faster than the base transport due to high ionic mobility of H+ further enhanced with the electroosmotic flow. The soil mass is thus acidified. This acidification facilitates desorption and dissolution of heavy metals in the soil pore fluid

Charged species present in the soil pore fluid or desorped from the soil surface are transported under electric fields towards the electrodes depending on their electric charge. The driving mechanisms for species transport are ion migration by electrical gradients, pore fluid advection by prevailing electroosmotic flow, pore fluid flow due to any externally applied or internally generated hydraulic potential differnce, and diffusion due to generated chemical gradients. As a result, cations are accumulated at the cathode an anions at the anode while there is a continuous transfer of hydrogen and hydroxyl ions across the medium. Various bench-scale studies on the feasibility of the process have shown that heavy metals and other cationic species can be removed from the soil specifically when electrolyte conditioning process enhancement techniques are employed.

The demonstrated feasibility of the process prompted the need to formalize multispecies transport under an electric field. It was necessary to assess the validity of the hypothesized principles of the process through comparisons of the predictions a theoretical model with expermental results.

A mathematical model is formulated utilizing principles of conservation of matter and energy to species transport under an electric field. Fluxes of fluid, charge, and species in a saturated soil under coupled hydraulic, electric, and chemical potential gradients together with the principles of conservation of matter and energy are used to describe multispecies transport by a set of differential equations. A set of algebraic nonlinear equations describes the chemical reactions among the species in the soil pore fluid. These equations describe sorption, precipitation/dissolution, aqueous phase, water auto-ionization, and electrolysis reactions. A model describing coupled reactive transport of lead in soils under an electric field is thus formulated by the set of differential /algebraic equations. Six differential equations four algebraic equations are used to model transport of Pb^{2+}, H^+, OH^-, NO^{3-}, the associated chemical reactions, electric potential and the hydraulic head across the electrodes.

Iterative scheme is chosen in solution. Finite EIement Method is **used** in space discretization. Finite difference technique is used for in time discretization. Two-dimensional nodal quadratic isoparametric elements are specified are employed in domain discretization. Bisection method is used in solving the algebraic equations.

Three pilot-scale tests are conducted in order to investigate the effect of up-scaling bench-scale tests and to demonstrate the feasibility and cost efficiency of electrokinetec soil remediation at **dimensions** representative of field conditions. Two of these tests are conducted on kaolinite samples spiked with lead nitrate solution at lead concentrations of 856 μg/g and 1,533 μg/g. The third test is conducted on kaolinite/sand mixture loaded with lead at a concentration of 5,322 μg/g. The samples are compacted at wet of optimum to achieve a high degree of saturation. Inert graphite electrodes are used in both anode and cathode compartments. The physicochemical changes in the soil are monitored during processing. Voltage probes are used to monitor electric potential distribution across the soil, thermocouples to monitor temperature changes, tensiometers, transducers to measure suction, and pH meters to monitor cathode and anode PH. The experiments are **connected to a data** acquisition system and **a constant current** density of 133 $\mu A/cm^2$ is applied across the soil. Two bench-scale tests are also conducted on kaolinite samples spiked with lead at a concentration of 1,439 μg/g. In these tests, a constant current density of 127 $\mu A/cm^2$ is applied.

The results of the third pilot-scale test conducted at a lead of 5,322 μg/g are used to compare the predictions of the mathematical model with pilot-scale results. Species concentration, electric potential, and hydraulic potential profiles in space and time are compared. Distributions of pH, different forms of lead (pore fluid, precipitated, adsorbed, and total), pore water pressure, electric potential, and electric potential gradient are evaluated within the predictions of the model. Pilot-scale tests also demonstrated the effect of up-scaling on the efficiency of the process.

8.2 Conclusions

The following conclusions are derived from this study.

* In unenhanced electrokinetic processing, pH values attained by electrolysis reactions at the electrodes in pilot-scale tests are no different than the bench-scale tests. The catholyte pH rises to about 11 and the anolyte pH drops to less than 2. Most pH changes at the electrode compartments occur within the first 100 h **of** processing. These changes are perfectly explicable by Faradic reactions.

* The first pilot-scale test demonstrated development of cracks at the cathode zone. A nonuniform final lead distribution is developed in this test due to sections of high

lead accumulation in the cracks. Pilot-scale tests conducted at initial concentration of 1,533 µg/g and 5,322 µg/g resulted in higher removal efficiencies than the first test. These tests displayed significant lead removal from the soil specimen. More than 90% (up to 98% in most parts) removal is achieved across the second-pilot test except the last 7 cm near the cathode. High concentration **of lead** is encountered near the cathode in all tests due to lead hydroxide precipitation in the high **pH** environment. Almost no lead is found in the effluent or on the electrodes. The result indicate that placement of the cathode, in direct contact with the soil or at a distance from the soil greatly influences the amount of lead precipitated or electro deposited at the cathode.

- A zone of low electric conductivity develops near the cathode. Though final electric gradients across the specimen are 2-3 V/cm in **bench-scale** tests and 4-4.5 in pilot-scale tests, most of the electric potential drop occurs in the last section near the cathode (last l0 cm in pilot-scale tests). The effective electrical gradient in species transport across most parts of the soil is only 0.01 to 0. I V/cm. The electric **gradient** near the cathode may go up to 20 V/cm; however, this gradient is ineffective in lead transport because lead hydroxide precipitation within that zone substantially decreases the ionic lead concentration in the pore fluid.

* The nonlinear electric potential distribution resulted in development of suction profile across the soil; even when open electro deconfiguration is used at both the anode and the cathode. A decrease in water content occurred in midsection indicating soil consolidation. An increase of water content at near the anode is observed as a result of swelling and dispersion of clay particles into the catholyte and anolyte.

* Temperature changes are measured only in the pilot-scale test conducted at an initial concentration of 1,533 µg/g, a current density of 33 µg/g and an electrical gradient of 2-4v/cm. Temperature increase is about 19°C in the soil near the cathode, 17°C in the cathode compartment and about 12°C in the anode compartment. Temperature profile is similar to that of the voltage profile across the specimen; sections with higher temperatures are located at sections of higher voltage drop. The effect of temperature increase on the process is not investigated.

- No electroosmotic flow is measured in pilot-scale tests at concentrations of 1,533 μg/g 5,322 μg/g. Ionic migration is the major species transport mechanism in these tests. The results provide another testimony to the fact that ionic migration is the most significant charged species transport mechanism in a low-permeability saturated soil.

- Energy expenditure varies over a range from 325 to 700 kWh/m^3 in pilot-scale tests and from 60 to 330 kWh/m^3 in bench-scale tests. Variation among the pilot-scale tests is due to differences in processing periods. The reason for the increase in energy expenditure is the development of the zone of low electric conductivity near the cathode. Enhancement techniques may be necessary to avoid precipitation within the cathode zone and consequently to decrease energy expenditure. The steady state electric power is similar in pilot-scale tests and in the range of 300 $watt/m^3$. Steady state electric power in pilot-scale tests is about half that in bench-scale tests (around 600 kWh/m^3).

- The predicted pH distribution show a decrease at the anode to about 2 and an increase at the cathode to around 7. The rate of advance of the acid towards the cathode is higher than the rate of advance of the base towards the anode. Predicted Steady state pH distribution does not show a breakthrough of the acid at the cathode. Steady state acid/base interface is located in the last 2 cm near the cathode. Predicted pH profiles at 8,15, and 22 days demonstrate reasonable agreement with the experiment. However, though a retardation factor of 4.6 is used for H+ transport, the predicted distributions show a faster rate of transport of the acid front than the experiment

- Adsorbed lead predicted by the model show desorption occurs as a result of decrease in the soil pH and decrease in the pore fluid lead concentration. In the pilot-scale test with 5,322 μg/g, desorption is delayed for about 10 days because of the high initial concentration in the pore fluid. The model demonstrates precipitation of lead hydroxides to about 16,000 μg/g) near the cathode as a result of the increase in soil pH. Predicted total lead distribution after 8, 15, 22, 37, and

50 days of processing demonstrate good agreement with the result of the pilot-scale test conducted.

- Electrical gradient distributions predicted by the model display agreement with those of the experiment except for sections near the cathode. The zone of low electric conductivity at the cathode is further advanced towards midsections of the specimen in the experiment than the model resulting in lower total voltage distribution across the specimen in the model than the experiment

- Development of a zone of low electric conductivity near the cathode at later stages of electrokinetic soil processing results in sharp fronts in concentration and pH profiles. These fronts cause numerical difficulties and require special treatment in space and time discritization.

- **The** model predictions demonstrate that multispecies transport under an electric field is quite well understood and rationalized. Ionic migration is the dominant transport mechanism for heavy metals under an electric field specifically when the coefficient of electroosmotic is less than 10^{-5} cm^2/Vs. Advective transport undereIectric gradient (or electroosmosis) depends on the soil type; however, even when the coefficient of electroosmotic permeability is in the order of 10^{-4} cm^2/V-s (lower activity days at high water contents), mass flux of H+ and OH- is at least 10 fold by ion migration. At these flow rates, mass flux of other species, however, is of the same order of magnitude. Advection under **a hydraulic** head difference is significant for soils with hydraulic conductivities that are higher than 10^{-5} cm/s. Diffusion is significant only at concentration and pH fronts because of the high concentration gradients.

8.3 Considerations for In-situ Implementation

- Bench-scale and pilot-scale studies show that there are no major restrictions on the soil type, ranging from clay to fine sand deposits. **Generally,** high water content and low activity soils will result in most efficient conditions for the process (Acar and Hamed 1991). High activity soils will display high retardation for heavy metals

transport and high buffering capacities for pH changes. Excessive acid generation will be required for such cases in order to facilitate desorption of heavy metals.

- The results of the pilot-scale tests conducted in this study together with the results of Lageman (1989) and (1993) demonstrate the feasibility of electrokinetic soil remediation in full field applications. Precipitation of heavy metals within the cathode region due to the alkaline environment is expected to decrease the efficiency of the process and increase energy expenditure. Enhancement techniques such as controlling the chemistry at the cathode may be necessary to increase the efficiency of removal. Acar et al: (1993b) discuss techniques to depolarize the cathode reaction with acetic acid.

- The process could be used with other remediation technologies, depending on the soil and contaminant type, to achieve more efficient and cost-effective in-situ clean-up. The electrokinetic process could be used together with soil-washing in soil deposits with relatively high hydraulic conductivities to accelerate species transport and removal. Combined use of bioremediation and electrokinetics is an area that is gaining attention for removing organics from soil deposits.

- The process could be used for a wide range of species. The results of pilot-scale tests demonstrate that the process could be used for removal of ionic lead from soils. Other bench-scale data indicate the feasibility of removal of various charged species including heavy metals, radionuclides, and selected organics. Removal of free phase non-polar organics is envisioned to be possible with the use of surfactants to form micells (Acar and Alshawabkeh 1993).

- Higher initial concentrations of contaminants do not have any major limitations on the process. Existing data show successful removal of Cu^{2+} up to levels of 10,000 µg/g and Pb^{2+} up to 5,000 µg/g. The results of pilot-scale tests demonstrate that lead at high concentrations (5,000 µg/g) could be efficiently removed deposits with low hydraulic conductivity (10^{-7} cm/s).

The results presented by Lageman (1989) and (1993) indicate that the process could work for a mixture of heavy metals and their salts. The acid generated at the anode

is necessary to cause dissolution of salts present into ionic species and the removal efficiency will be affected by the mobility of each ion and its concentration.

- The current levels reported are in the order of milliamps per square cm of electrode area. Although high current levels generate more acid that will work for the process, it increases the total ionic concentration that will decrease the overall electroosmotic flow. Furthermore, the transport numbers of other species may decrease as a result. A current density of 0.13 mA/cm^2 is efficiently used for this study.

- Precipitation of heavy metals within the cathode region due to the alkaline medium will decrease the efficiency of the process and increase energy expenditure. Controlling the chemistry at the cathode may be necessary to increase the efficiency of removal. Acar et al. (1993b) discuss techniques to depolarize the cathode reaction with acetic acid

- Inert anodes such as graphite, carbon-or platinum should be used in order to avoid introduction of secondary corrosion products. Any conductive material that will not corrrode in the basic enviroment may be use as cathode.

- Open electode corifiguration is essential for the process. The electrodes can be placed horizontally or vertically. One-dimensional flow conditions or a hexagonal network of electrodes with radial flow towards a central cathode may be used. When two dimensional electrode layout is employed, it is necessary to assess the effect of coupling between the electrical gradients.

- Spacing will depend upon the type and level of contaminants, selected current, voltage and enhancement regime. A substantial decrease in efficiency of the process may result due to increases in temperature when higher electric potentials are generated. Increasing Spacing between the electrodes may require longer processing periods. However, increasing electrode spacing is expected to result in less electric power expenditure per unit volume ($watt/m^3$). Furthermore, a substantial decrease in energy expenditure is expected if enhancement techniques are used. Accordingly, spacing should be designed for each case independently.

However, in the case of unenhanced application, **a spacing** of 1.5 m seems to be a suitable choice.

8.4 Recommendations for Future Studies

The following are studies recommended:

- Precipitation near the cathode result in immobilization of species transport and increase in energy expenditure. Bench-scale and pilot-scale studies are already ongoing on enhancement techniques for the process. It is essential to formalize these techniques in the model and assess its predictions.

- The presence of a complex of species, salts, or organics in the soil will affect the species transport. Lead and lead hydroxides are included in this study. It is recommended that assess the effect of complexation and salts on efficiency.

- Presence of carbonate and carbonate minerals, their dissolution, and their transport is expected to greatly influence the transport of species. They may significantly affect efficiency of the process and should be investigated.

- The numerecal model developed accounts only for lead hydroxide precipitation, water autoionization, and sorption. The model should be modified for other chemical reactions of other species and dissolution reactions. Chemical reactions described in the model should be generalized for several chemical species.

- Conventional theoretical models on electroosmotic consolidation of soft soils disregard the effect of chemistry changes on the electric potential distribution. Future research on this area should account for the nonlinearity in the electric potential distribution.

- Work is initiated at LSU on electrokinetic enhancement of bioremediation. This area seems to offer significant promise. Species transport under an electric field may well be one area that would render bioremediation efficient and cost-effective.

REFERENCES

- Acar, Y. B. and Gale, R J. (1986) "Decontamination of Soils-Using Electroosmosis," Proposal submitted to the ***Board of Regents of the Stare of Louisiana,*** LEQSF Research Development Program office of Research Coordination, Louisiana State University, Baton Rouge, La

- Acar, Y. B. and Olivieri, I (1989) "Pore Fluid Effect on the Fabric and Hydraulic Conductivity of laboratory Compacted Clay," ***Transportation Research Record, No.*** 1219, pp. 144-159.

- Acar, Y. B. and Gale, R J. (1992) "EIectrochemical Decontamination of Soils and Sturries," US ***Patent*** 5137608, 11 August.

- Acar, Y. B. and Hamed, J. (1992) "Electrokinetic soil Processing in Remediation/ Treatment; Synthesis of Available Data," Bulletin of the ***Transportation Research Record, No.*** 1312, Soils Geology and Foundations, Geotechnical Engineering.

- Acar, Y. B. and Alshawabkeh, A N. (1993) "Principles of Electrokinetic Remediation," ***Environmental*** *Science* ***and Technology,*** Vol. 27, No. 13, pp. 2638-2647.

- Acar, Y. B.. and Alshawabkeh, A N. (1994) "Modeling Conduction Phenomena in Soils Under an EIectric Current," ***Proceedings of XIII International Conference on Soil Mechanics and Foundation Engineering (ICSMFE), Oxford*** and IBM Publishing, New Delhi, India, V. 2, pp. 662-669.

- Acar, Y. B., Gale, R., Putnam, G., Hamed, J. and-Juran, I. (1988) "Determination of pH Gradients in Electro-Chemical Processing of Soils," Report presented to the ***Board of Regents of Louisiana,*** Civil Engineering Department, LSU, July 1988, 119p.

- **Acar,** Y. B., Gale, R J., Putnam, G. and Hamed, J. (1989) "Electrochemical Processing of Soils: Its Potential Use in Environmental Geotechnology and Significance of pH Gradients," 2nd ***International Symposium on Environmental Geotechnology;*** Shanghai, China, May 14-17, Envo Publishing, Bethlehem, PA, Vol. 1, pp. 25-38.

- Acar, Y. B.,Gale, R J., Hamed, J. and Putnam, G. (1990) "Electrochemical Processing of Soils: Theory of pH Gradient Development by Diffusion and Linear Convection," Journal ***of Environmental*** *Science and* ***Health,*** Part (a); EnvironmentaI Science and Engineering, Vol. 25, No. 6, pp. 687.714.

- Acar, Y. B., Hamed, J., Gale, R J. and Putnam, G. (1991) "Acid/Base Distributions in Electroosmosis," ***Transportation Research Record, No.*** 1288, Soils Geology and Foundations, Geotechnical Engineering, 1990, pp. 23-34.

- Acar, Y. B., Alshawabkeh, A N., and Gale, R J. (1992a) "A Review of fundamentals of Removing Contaminants by Electrokinetic Soil Processing," ***Proceedings of*** *the* ***Mediterranean Conference on Environmental Geotechnology,*** edited by Usmen, M. and Acar Y., Cesme, Turkey, May 1992, pp. 321-330.

Acar, Y. B., Li, H. and ,Gale, R J. (1992b) "Phenol Removal From Kaolinite by Electrokinetics," ASCE, Journal ***of Geotechnical Engineering*** Vo. 118, No. 11, pp. 18370-1852.

Acar, Y. B., Gale, R J., Ugaz, A, and Puppala, S. (1992c) "Feasibility of Removing Uranium, Thorium, and Radium from Kaolinite by Electrochemical Soil Processing" Report prepared by Electrokinetics, Inc. for Office of Research and. Development, *Risk* ***Reduction Engineering Laboratory, USEPA,*** Report No. EK-BR-OO9-0292,243 p.

Acar, Y. B., Alshawabkeh, A. N., and Gale, R (1993a) "Fundamentals of Extracting Species from Soils by Electrokinetics", Waste ***Management,*** Pregamon Press, London, Vol. 12, No. 3, pp. 141-151.

Acar, Y. B., Puppala, S., Marks, R, Gale R J., and Bricka, M. (1993b) "An Investigation of Selected Enhancement Techniques in Electrokinetic Remediation," Report presented to **US Amy** ***Waterways Experiment*** **Station,** Electrokinetics Inc., Baton Rouge, Louisiana, 230p.

Acar, Y. B., Hamed, J., Alshawabkeh, **A. N.,** and Gale, R (1994a) "Cd(II) Removal From Saturated Kaolinite by Application of EIectrical Current" ***Geotechnique,*** June 1994 (in press).

Acar, Y. B., Gale, R J., Alshawabkeh, A N., Marks, R, Bricka, M., and Parker, R (1994b) '"Electrokinetic Remediation: Basics and Technology Transfer," Journal *of* ***Hazardous Waste Management (in press).***

Alloway, B. J. (:1990) "Heavy Metals in Soils," John Wiley & Sons Inc., New York 339p.

Alshawabkeh, A. and Acar, Y. (1992) "Removal **of** Contaminants from Soils by Electrokinetics: A Theoretical Treatise," Journal ***of Environmental*** *Science and Health,* A27(7), pp. 1835-1861.

Alshawabkeh, A and Acar, Y. (1993) "Discussion on (A New Apparatus for the Evaluation of Electrokinetic Processes in Hazardous Waste Management) by Yeung, A T., Sadek, M. S., and Mitchell, J. K." *ASTM* ***Geotechnical Testing Journal,*** 16(3), pp. 397-398.

Amba, S. A, Chilingar, *G.* V. and Beeson, C. M. (1964) "Use of Direct EIectrical Current for Increasing the Flow Rate of Reservoir Fluids During Petroleum Recovery," Journal ***of*** ***Canadian Petroleum Technology,*** Spring 1964, pp. 6-14.

Arbuckle, J., Bosco, *M.*, *Case*, D., Laws, E., Martin, J., Miller, A, Randle, R., Stolli R, Sullivan, T., Vanderver, T., and Wilson, P. (1989) "Environmental Law Handbook" Tenth Edition, ***Government Institutes, Inc.,*** Rockville, MD, 664p.

Austin, Teresa (1993) "Superfund: New Leadership, Old Problems" ASCE, CiviI Engineering, V. 63, No. 3, March 1993, pp. 46-49.

Ballou, E. V. (1955) "Electroosmotic Flow in Homoionic Kaolinite," ***Journal of*** *Colloid Science,* Vol. 10, No. 5, pp. 450-460.

Banerjee, S.; Horng, J., Ferguson, J., and Nelson, P. (1990) "Field Scale Feasibility of Electrokinetic Remediation" Report presented to USEPA, Land ***pollution Control Division, PREL,*** CR 811762-01,122p.

Banerjee, S. and Mitchell, J. K. (1980a) "In-Situ Volume-Change Properties by Electra-Osmosis - Theory," **ASCE Journal** ***of Geotechnicai*** *Engineering* ***Division,*** Vol. 106. No. GT4, pp. 347-365.

Banejee, S. and Mitchell, J. K. (1980b) "In-Situ Volume-Change Properties by EIectro-Osmosis - Evaluation," **ASCE** ***journal of Geotechnical Engineering Division,*** Vol. 106, No. GT4, pp. 367-841.

Bathe, K. and Wilson, E (1976) "Numerical Methods in Finite Element Analysis" Prentice-Hall, Inc., 528 p.

Bear, J. (1972) "Dynamics of Fluids in Porous Media," American Elsevier, New York, 764 p.

Bruch, J. C. (1976) "Electro-Osmosis in Ground Water Pollution Control," PB-273 377 Report, National Science ***Foundation, UCSB-ME-76-***1,80 p.

Bruell, C., Segal, B., and Walsh, H (1992) ***"Electroosmotic*** Removal of Gasoline Hydrocarbons and TCE from Clay," ASCE, ***Journal of Environmental Engineering,*** Vol. 118, No. 1, pp- 68-83.

Burnett D. S. (1987) "Finite Element Analysis: From Concepts to Applications" Addison-Wesley Publishing Company, 844 p.

By, T. (1992) "Hydraulic Fracture and Conductor Installation: Effect on load Carrying Capacity. of Neighboring Piles," Report NGI Report 521660, Oslo, Norway.

Casagrande, L. (1952) "EIectroosmotic Stabilization of Soils," ***Journal of Boston*** *Society* ***of Civil Engineers,*** Vol. 39, No. 1, pp. 51-83.

Casagrande, L. (1983) "Stabilization of Soils by Means of Electroosmosis: State of the Art," ***Journal of Boston*** *Society* ***of Civil Engineering,*** ASCE, 69(2), pp. 255-302.

Corapcioglu, M. Y. (1991) "Formulation of EIectro-Chemico-osmotic Processes in Soils," ***Transport in*** Porous **Media,** ***No.*** 6, pp. 435-444.

Dahab, M., Kelly, W., and Goderya, F. (1992) "Removal of Metallic Contaminants in Unsaturated Soils Using EIectrokinetics," DOE ***Workshop on Electrokinetics,*** January 22, Atlanta, Georgia

Dean, J. **A** (1985) "Lange's Handbook of Chemistry," 14th. Edition, McGraw Hill, New York 1856p.

Esrig, M. I. (1968) "Pore Pressures, Consolidation, and Electrokinetics," ASCE. ***Journal of Soil Mechanics and Foundation Division,*** Vol 94, No. SM4, pp. 899-921.

Eykhols G. R (1992) "Driving and Complicating Features of the Electrokinetic treatment Of Contaminated Soils" Dissertation presented to the Faculty of the Graduate School of the University of Texas at Austin in Partial Fulfillment of the requirements for the Degree of Doctor of Philosophy, 269 p.

Finno, R J., Chung, K. Y., Yin, J., and Feldcamp, J. R (1994) "Permeability from Results of A/C Electroosmosis Experiments," Abstract submitted for the Geoenviromnent-2000, ASCE *Specialty Conference on Characterization, Containment, Remediation, and Performance in Environmental Geotechnics, New Orleans, 14-16* February, 1995.

Gilham, R W. and Cherry, J. A (1982) "Contaminant Migration in Saturated Unconsolidated Geologic Deposits," Geological *Society of America,* Special Paper 189, pp. 31-61.

Gladewell, J. K. (1965) "Practical Application of Electroosmosis," New Zealand Engineering, Vol 20, No. 2, pp. 66-72.

Gokmen, C. (1994) "Contaminant Transport and the Leachability of ChemicaI Species Through Phosphogypsum," *Maters Thesis,* Louisiana State University.

Gray, D. H and Mitchell,J K (1967) "Fundamental Aspects of Electroosmosis in Soils," ASCE, Journal of the Soil Mechanics and Foundation Division, Vol. 93, No. SM6, pp. 209-236.

Gray, D. H. and Schlocker, J. (1969) "EIectrochemical Alteration of Clay Soils," Clays and Clay *Minerals, Vol. 17,* pp. 309-322.

Gray, D. H. and Somogyi, F. (1977) "Electroosmotic Dewatering with Polarity Reversals," ASCE, *Journal of Geotechnical Engineering,* Vol. 103, No. GTI, pp. 5 l-54.

Groenevelt, P. H. and Bolt, G. H. (1969) "Non-Equilibrium Thermodynamics of the Soil-Water-System," Review Paper, *Journal of Hydrology,* Vol. 7, pp. 358-388.

Hamed, J. (1990) "Decontamination of Soil Using Electroosmosis," A *Dissertation* submitted to the Graduate School of Louisiana State University in Partial Fulfillment of the Degree of Doctor of Philosophy.

Hamed, J., Acar, Y. B. and Gale, R J. (1991) "Pb(II) Removal from Kaolinite by Electrokinetics," ASCE, *Journal of Geotechnical Engineering Division,* Vol. 117, No. 2, February 1991, pp. 241-271.

Hamnet, R (1980) "A Study of the Processes Involved in the Electro Reclamation of Contaminated Soils," *Master Thesis,* University of Manchester, England, 84p.

Harrison, R and Laxen, (198 1) "Lead PolIution Causes and Control," Chapman and Hall, 168p.

Harter, R. D. (1983) "Effect of Soil pH on Adsorption of Lead, Copper, Zinc, and Nickel," *Soil Science Society of America Journal No.* 47, pp. 47-51.

* Ho,S. V., Sheridan,. P. W., **Athmer,** *C.* J., Brodsky, P., Heitkamp, M., and Brackin, J. (1993) "Innovative Soil Remediation Technology" ***I&EC Division, ACS*** *Special symposium on Emerging Technologies in Hazardous waste Management V. Atlanta Georgia, Editor,* Tedder, W., Vol. II, pp. 73l-734.

• Holmes, P. J. (1962) "The Electrochemistry of Semconductors," Academic Press, London, 396 p.

* Hunter, R J. (1981) "Zeta Potential in Colloid Science," Academic Press, London, 386p.

• Jennings, A A, Kirkner,D. J., and Theis, L L. (1982) "Multicomponent Equilibrium Chemistry in Ground Water Quality Models," *Water Resourses Research, No.* 18(4), pp. 1089-1096.

* Johnston, L and Butterfield, R (1977) "A laboratory Investigation of Soil Consolidation by Electroosmosis," *Australian Geomechanics Journal,* Vol. G7, No. 1, pp. 21-32.

• Kirkner, D. J., Theis, I. L., and Jennings, A. A (1984) "Multicomponent Solute Transport with Sorption and Soluble Compiexation," Advances in *Water Resources, No. 7,* pp. 120-125.

* Kirkner, D. J. and Reeves, M. (1988) "Multicomponent Mass Transport with Homogeneous and Heterogeneous Chemical Reactions: Effect of the Chemistry on the choice of Numerical Algorithm, 1, Theory," *Water Resources Research,* Vol. 24, No. 1, pp. 1719-1729.

• Kirkner, D. J., Theis, 1. L., and Jennings, A. A. (1985) "Multicomponent Mass Transport with Chemical Interactions Kinetics," Journal of Hydrology, 76, pp. 107-l17.

* Koryta J. and Dvorak, J: (1987) "Principles of Electro Chemistry," John Wiley and Sons, New York; 447p.

* Kotz J. C. and Purcell, K. F. (1987) "Chemistry and Chemical Reactivity" Saunders College Publishing, 1020p.

• Kreyszig, E. (1988) "Advanced Engineering Mathematics" Sixth Edition, John Wiley and Sons, Inc., 1294p.

• Krizek, R J., Gularte, F. B., and Hununel, P. L. (1976) "Stabilization of Polluted Dredging by Electroosmosis," ASCE, **National** *Water Resources and Ocean Engineering Convention, San* Diego.

• Kruyt, H R (1952) "Colloid Science (I): Irreversible Systems," Elsevier Publishing Company, 389 p.

• Lageman, R (1993) "Eletro-Reclamation,," Journal of Environmental *Science and* Technology, V61. 27, No. 13, pp. 2648-2650.

• Lageman, R., Wieberen, P., and Seffinga, G. (1989) "Electro-Reclamation: Theory and Practice," *Chem. Industry* London, 9, pp. 585-590.

- Langmuir, D. (1987) "Overview of Coupled Processes with Emphasis on Geochemistry," in Coupled Processes Associated with Nuclear Waste Repositories, edited by Tsang, C. F., Academic Press, San Diego, Calif.
- Lewis, R W. and Humpheson, C. (1973) "Numerical Analysis of EIctro-Osmotic Flow in Soils," ASCE ***Jurnal of SoilMeckanics and Foundation Division,*** Vol. 99, No. SM8, pp. 603-616.
- Lewis, R W., Humpheson, C. and Bruch, J. (1975) "Applications of Electro Osmosis to Ground Water Flow Problems," ***Ground Water,*** Vol. 13, No. 6, pp. 484-491.
- Lewis, F. M., Voss, C. I., and Rubin, J. (1987) "Solute Transport with Equilibrium Aqueous Complexation and Either Sorption or ion Exchange Simulation Methodology and Applications," ***Journal of Hydrology, 90, pp.*** 81-115.
- Lichtner, P. c. (1985) "Continuum Model for Simultaneous Chemical Reactions and Mass Transport in Hydrothermal Systems," Geochim. Cosmochim. Acta, No. 49, pp. 779-800.
- Lindgren, E., Mattson, E., and Kozak, M. (1992) "Electrokinetic Remediation of Contaminated Soils," DOE Workshop on Electrokinetics, January 22, **Atlanta,** Georgia
- Lockhart, N. (1981) "Sedimentation and EIectroosmotic Dewatering of Coalwashery **Slimes,"** ***Fuel,*** Vol. 60, No. 10, pp. 919-923.
- Lockhast, N. (1983) "Electroosmotic Dewatering of Clays. II. Influence of Salt, Acid, and Flocculants," Colloids and Surfaces, No. 6, pp. 239-251.
- Lockhart, N. and Stickland, R (1984) " Dewatering Coal Washery Tailing Ponds by Electroosmosis," Powder ***Technology,*** Vol. 40, No. l-3, pp. 2 15-221.
- Lorenz P. B. (1969) "Surface Conductance and Eletrokinetic Properties of Kaolinite Beds," Clays and Clay Minerals, Vol. 17, pp. 223-231.
- Mangold, D. C. and Tsang, C. (1991) "A Summary of Subsurface Hydrological and Hydrochemical Models," Review of **Geophysics, 29,** l/February 1991, pp. 51-79.
- Manguire, M., Slavek, J., Vimpany, I., Higginson, F., and Pickering, W (1981) "Influence of pH on Copper and Zinc Uptake by Soil Clays," ***Australian Journal of Soil Research,*** Vol. 19, pp. 217-229.
- Miller, C. W. and Benson, L. V. (1983) "Simulation of Solute Transport in a Chemically Reactive Heterogeneous System: Model Development and Application," ***Water Resources Research,*** Vol. 19, No. 2, pp. 381-391.
- Mise, T. (1961) "EIectroosmotic Dewatering of Soil and Distribution of Pore Water Pressure," ***Preceedings of the 5th ICSMFE,*** Paris, Vol. 1, pp. 255-257.
- Mitchell, J. K. (1986) "Potential Uses of Electrokinetics for Hazardous Waste site Remediation," ***Proceedings of the USEPA - University of Washington workshop on electrokinetic treatment and its application in environmental-geotechnical engineering for hazardous waste site remediation, Seattle.***

• Mitchell, J. (1991) "Conduction Phenomena from Theory to Geotechnical Prectice," 31st. ***Rankine Lecture*** of the British ***Geotechnical Society, Geotichnique,*** Vol. XLI, No. 3, pp. 299-340.

* Mitchell, J. K. (1993) "Fundamentals of Soil Behavior," John Wiley and Sons, New York, 437 p.

• Mitchell, J. K. and Yeung, T. C. (1991) "Electrokinetic Flow Barriers in Compacted Clay," Transportation ***Research Record, No.*** 1288, Soils Geology and Foundations, Geotechnical Engineering 1990, pp. 1-10.

* Mitchell, J. K., Greenberg, J. A., and Witherspoon, P. A (1973) "Chemico-Osmotic Effects in Fine Grained Soils," ***Journal of the Soil Mechanics and Foundations Division,*** VoL 99, No. SM4, pp. 307-322.

* Morse, D. (1989) "What's Wrong with Superfunds?" Civil Engineering, April, pp. 40-43

* Nyeretse, P. (1985) "An Investigation of the Relation Between the Suction Potential and Swelling Potential of Compacted Soils" A Thesis presented to Louisiana State University in partial fulfillment of the degree Of Master of Science in Civil Engineering, 76p.

* Pamukcu, S., Khan, L., and Fang, H. (1990) "Zinc Detoxification of Soils by Electroosmosis," Electrokinetic Phenomena in Soils, Transportation Research Record, TRB, Washington, D.C.

* Pamukcu, S. and Wittle, J. K. (1992) "Electrokinetic Removal of Selected Heavy Metals from Soil," Environmental ***Progress,*** V. 11, No. 3, pp. 24 I-250.

* Pratt, P. F. (1961) "Effect of pH on the Cation Exchange Capacity," ***Journal of Soil Science Society of America,*** Vol. 25, pp. 96-98.

• Reddy, J. N. (1985) "An Introduction to the Finite Element Method" McGrawHill, Inc., 495 P.

* Rubin, J. (1983) "Transport of Reacting Solute in Porous Media; Relation Between Mathematical Nature of Problem Formulation and Chemical Nature of Reactions," ***Journal of Water Resources Research,*** 19(5), pp. 123 l-1252.

* Runnels, D. D. and Larson, J. L. (1986) **"A Laboratory** Study of Electromigration as a Possible Field Technique for the Removal of Contaminants from Ground Water," ***Ground Water Monitoring Review,*** pp. 8 l-91, Summer 1986.

* Runnels, D. D. and Wahli, C. (1993) "In Situ Electromigration as a Method for Removing Sulfate, Metals, and Other Contaminants from Groundwater," ***Ground Water Monitoring Review,*** Winter 1993, pp. 121-129.

* Segal, B. and Bruell, C. (1992) "Electroosmotic Contaminant-Removal Processes," ASCE, ***Journal of Environmental Engineering,*** Vol. 118, No. 1, pp. 84-100.

* Segal, B., O'Bannon, C., and Matthias, J. (1980) "Electro-Osmosis Chemistry and Water Quality," ASCE, ***Journal of the Geotechnical Engineering division,*** Vol. 106, No. Gt 10, Oct. 1980, pp. 1143-l147.

- **Selim,** H. M. (1992) "Modeling the Transport and Retention of Inorganics in Soils," Advances ***in Agronomy, V. 47,*** pp. 33 l-384.
- Shackelford, C. D. (1991) "Diffusion of Contaminants through Waste Contaminant Barriers, ***Transportation Research Record, No.*** 1219, pp. 169-l 82.
- Shackelford, C. D. and Daniel, D. E. (1991 a), "Diffusion in Saturated Soil (I): Background," ASCE, ***Journal of Geotechnical Engineering Division,*** Vol. 117, No. 3, March, 1991, pp. 467-484.
- Shackelford, C. D. and Daniel, D. E. (199 1 b) "Diffusion in Saturated Soil (II): Results for Compacted Clay," ASCE, ***Journal of Geotechical Engineering Division,*** Vol. 117, No. 3, March, 1991, pp. 485-506.
- Shapiro, A P. and Probstein, R. F. (1993) "Removal of Contaminants from Saturated **Clay by Electroosmosis,"** ***Environmental Science and Technology,*** Vol. 27, No. 2, pp. **283-291**.
- Shapiro, A. P., Renauld, P. and Probstein, R (1989) "Preliminary Studies on the Removal of Chemical Species from Saturated Porous Media by Electroosmosis," ***Physicochemical Hydrodynamics,*** Vol. 11, No. ***5/6, pp. 785-802.***
- Simes, G. F. (1989) "Preparation Aids for the Development of PREL, Category III, Quality Assurance Project Plans," ***USEPA Office of Research and Development, Risk Reduction Engineering Laboratory, Cincinnati OH.***
- Stumm, W. (1992) "Chemistry of the Solid-Water Interface, Processes at the Mineral-Water and Particle-Water Interface in Natural Systems," **'A** Wiley Interscience Publication, John Wiley & Sons, Inc., 428p.
- Ugaz, A, Puppala, S., Gale, R, and Acar, Y. B. (1994) "Complicating Features of Electrokinetic Remediation of Soils and Slurries: Saturation Effects and the Role of the Cathode Electrolysis," ***Communications in Chemical Engineeering, accepted*** for publication.
- Volocchi A J., Street, R L., and Roberts, P. V. (1981) "Transport of Ion Exchanging Solutes in Groundwater: Chromatographic Theory and Field Simulations," ***Journal of Water Resources Research, 17(5),*** pp. 1517-1527.
- Wan, T. and Alitchell, J. K. (1976) "Electro-Osmotic Consolidation of Soils," ASCE, ***Journal of Geotechnicai Engineering Division, Vol.*** 102, No. GTS, pp. 473-491.
- Wittle, J. K. and Pamukcu, S. (1993) "Eletrokinetic Treatment of Contaminated Soils, Sludges and Lagoons," Report ***to Argonne*** National Laboratory.
- Yeh, G. T. and Tripathi, V. S. (1989) "A Critical Evaluation of Recent Developments in Hydrogeochemical Transport Models of Reactive Multichemical Components," ***Water Resources Research,*** Vol. ***25, No. 1,*** pp- 93-108.
- Yeh, G. T. and Tripathi, V. S. (1991) "A Model for Simulating Transport of Reactive Multispecies Components: Model Development and Demonstration," ***Water Resources Research,*** Vol. ***27, No. 12,*** pp. 3075-3094.

Yeung, A (1990) "Electro-Kinetic Barrier to Contaminant Transport through Compacted Clay," Dissertation submitted in partial satisfaction of the requirements for the degree of Doctor of Philosophy in Civil Engineering in the Graduate Division of the University of California at Berkeley, 260 p.

Yeung, A (1992) "Diffuse Double Layer Equation in SI Units," Technical Note, ASCE, ***Journal of the Geotechnical Engineering Division,*** Vol. 118, No. 12, pp. 2000-2005.

Yeung, A, Chung, M., Corapcioglu, Y., and Stallard, M. (1994) "One Dimensional Experimental ***Studies On*** Electrophoresis of Clay," Abstract submitted for the ***Geoenvironment-2000, ASCE Specialty Conference on Characterization, Containment, Remediation, and Preformance in Enviromental Geotechnics, New Orleans, 14-16*** February, 1995.

Yong, R N., Warkentin, B. P. Phadungchewit, Y., and Galves, R. (1990) "Buffer Capacity and Lead Retention in Some Clay Materials," ***Journal of Water, Air, and Soil Pollution, No. 53,*** pp. 53-67.

Zwillinger, D. (1989) "Handbook of Differential Equations" Academic Press, Inc., San Diego, CA, 673p.